UNIVERSITY OF OKLAHOMA

GRADUATE COLLEGE

# TECTONIC EVOLUTION AND BASIN ANALYSIS OF THE HANOVER BLOCK IN WESTERN JAMAICA

A THESIS

SUBMITTED TO THE GRADUATE FACULTY

in partial fulfillment of the requirements for the

Degree of

MASTER OF SCIENCE

[redacted]

[redacted]

[redacted]

By

BORA YALCIN
Norman, Oklahoma
2012

Downloaded from SHAREOK. Persistent Handle URL: http://hdl.handle.net/11244/342912

UNIVERSITY OF OKLAHOMA LIBRARIES

OU
THESIS
YAL
cop.2

# TECTONIC EVOLUTION AND BASIN ANALYSIS OF THE HANOVER BLOCK IN WESTERN JAMAICA

A THESIS APPROVED FOR THE
CONOCOPHILLIPS SCHOOL OF GEOLOGY AND GEOPHYSICS

BY

[redacted]

Dr. John D. Pigott, Chair

[redacted]

Dr. Roger M. Slatt

[redacted]

Dr. G. Randy Keller

© Copyright by BORA YALCIN 2012
All Rights Reserved.

© Copyright by BORA YALCIN 2012
All Rights Reserved.

To the youngest daughter of Osman Yarar and Hayriye Yarar, my beloved mother,

Sukran Yarar

## ACKNOWLEDGEMENTS

There are a number of people who have helped me in my efforts to obtain my Master's degree. I wish to express a special thanks to my thesis advisor, Dr. John D. Pigott, for supporting me with his knowledge on scientific problems, overall supervision and hours of draft revisions. I thank Dr. Slatt for his valuable supervision and for spending time to be on my thesis committee. Great appreciation goes to Dr. Randy G. Keller for his valuable comments and for spending time to be on my thesis committee.

I would like to thank Abdullah Al-Abbad for his friendship and assistance in the field helping me with my field work. Very special thanks to Hulya Yilmaz for sharing her experiences.

I would like to thank TPAO and Dr. John D. Pigott for giving me financial support to reach my goal.

Finally, I would like to thank to my mother, Sukran Yarar, for her inspiring encouragement and valuable counsel.

## TABLE OF CONTENTS

1. INTRODUCTION ..... 1

1.1 Location and Physiography ..... 1

1.2 Problem Definition ..... 2

1.3 Strategy ..... 4

2. GENERAL SETTINGS ..... 5

2.1 General Geology of Jamaica ..... 5

2.2 Overall Structural Geology of Jamaica ..... 7

2.3 General Setting of Hanover Inlier ..... 7

2.3.1 Geology of Hanover Inlier ..... 7

2.3.2 Structural Geology of Hanover Inlier ..... 12

2.3.3 Cross-Sections in Hanover Block ..... 13

2.4 Integrated Hanover Block Geological History ..... 18

2.4.1 General Geological History of Caribbean Plate and Jamaica's Position ..... 18

2.4.2 Geological History of the Hanover Block ..... 23

2.5 Petroleum Potential of Jamaica and Hanover Block ..... 27

2.5.1 Organic Geochemistry ..... 29

3. STRATIGRAPHIC CHARACTERIZATION AND SEQUENCE STRATIGRAPHY ..... 32

3.1 Sequence Stratigraphic Setting of Deepwater Systems ..... 32

3.2 Reservoir Architecture ..... 34

3.3 Sediment Gravity Flow Processes ..... 36

3.3.1 Walker Sedimentary Gravity Flow Classification ..... 36

3.4 Gamma Ray Measurements ..... 38

3.4.1 Operation principle ..... 39

3.4.2 Calibration ..... 39

3.4.3 Spectral Gamma Ray Log ..... 39

4. FIELD STUDY AND INTERPRETATION ..... 40

4.1 Stop 1 ..... 41

4.2 Stop 2 ..... 44

4.3 Stop 3 ..... 51

4.4 Stop 4 ..... 56

4.5 Basalt Outcrop ..... 61

4.6 Sedimentary Gravity Flow Type Comparison of Outcrops ..... 63

4.7 General Stratigraphic Architecture and Relative Positions of Studied Outcrops . 64

5. GRAVITY MODELING AND BASEMENT DEFINITION ..... 67

5.1 Bouguer Anomaly ..... 67

5.2 Basement Depth Modeling Using the Bouguer Anomaly ..... 68

6. CALCITE FILLED POROSITY QUANTIFICATION ..... 73

6.1 Quantification of Porosity Reduction Owing to Calcite Cementation Using Computer Assisted Petrographic Image Study ..... 74

7. BASIN MODELING PRINCIPLES ..... 75

7.1 Introduction ..... 75

7.2 1-D (One-Dimensional) Basin Modeling Principles ..... 76

7.3 Subsidence Principles ..... 76

7.4. Heat Flow Principles ..... 79

7.5 Rifting Heat Flow ..... 81

7.6 2-D (Two-Dimensional) Basin Modeling Principles ..... 82

8. BASIN ANALYSIS AND MODEL ..... 83

8.1 Introduction ..... 83

8.2 Basin Burial History Analysis ..... 84

8.3 Calculation of Subsidence and overburden of Sediment ..... 87

8.4 Determining the Stretching Factor from Tectonic Subsidence 1-D, Thermal State, and Heat Flow ..... 88

8.5 Geovalidation and Maturity ..... 91

8.5.1 1-D Maturity ..... 94

8.5.2 2-D Maturity ..... 110

9. SUMMARY OF PETROLEUM SYSTEM ANALYSIS ..... 116

10. CONCLUSIONS ..... 118

REFERENCES CITED ..... 120

APPENDICES ..... 124

## LIST OF TABLES

**Table 2.1** Summary of Exploration Drilling in Jamaica, 1955-1982……..29

**Table 3.1** SGR Data Application Examples ……40

**Table 5.1** Jamaican Rock Density Values (After Wadge, 1992)...……..…69

**Table 8.1** The Names and Locations of eighteen Virtual Wells in the Hanover Block……...……...84

**Table 8.2** Summary of Burial History of the Hanover Block…….…....85

## LIST OF FIGURES

**Figure 1.1** Location of the Hanover Block in relation to the neighboring structural subdivisions of Jamaica ..... 2

**Figure 2.1** General Stratigraphy of Jamaica ..... 6

**Figure 2.2** General Structural Map of the Area ..... 7

**Figure 2.3** Stratigrapic Legend of Hanover Inlier ..... 11

**Figure 2.4** Hanover Inlier with the Locations of Cross Section Lines ..... 14

**Figure 2.5** Cross-section A-A`..... 15

**Figure 2.6** Cross-section B-B`..... 15

**Figure 2.7** Cross-section C-C`..... 16

**Figure 2.8** Cross-section D-D`..... 16

**Figure 2.9** Cross-section E-E..... 17

**Figure 2.10** The Caribbean Plate Reconstruction during the Middle Cretaceous (Late Albian)..... 19

**Figure 2.11** The Carribean Region and Jamaica's Position during the End of Maastrictian and Paleocene..... 20

**Figure 2.12** Caribbean Region during Late Paleocene ..... 21

**Figure 2.13** The Carribean Region during the Middle Eocene..... 22

**Figure 2.14** The Caribbean Region during the Late Miocene ..... 23

**Figure 2.15** Location of Dry Holes Drilled in Jamaica, 1955-1982. ..... 28

**Figure 2.16** Frequency Distribution of Total Organic Content in particular shale layers analyzed..... 30



UNIVERSITY OF OKLAHOMA LIBRARIES

**Figure 2.17** Source-rock Classification of Shales Sampled Based on Log-Log Plot of C15+ Extractable Hydrocarbons vs. Organic Carbon Content. ..... 31

**Figure 3.1** Single Relative Sea Level Cycle ..... 32

**Figure 3.2** Falling Stage of LST ..... 33

**Figure 3.3** Late stage of LST ..... 33

**Figure 3.4** Relative Rise in the Sea Level, Representing TST ..... 33

**Figure 3.5** HST, Deltas Prograde to Fill Accommodation Created by Sea Level Rise. 34

**Figure 3.6** Principal Architectural Elements of Deepwater Clastic Systems ..... 34

**Figure 3.7** Chart Illustrating the Sediment Transport Processes of Sediment Gravity Flows and Resulting Deposits. ..... 37

**Figure 3.8** Sediment Grain Size, Structures, Divisions, and Sediment Transport Mechanisms of a Complete Bouma Sequence. ..... 38

**Figure 4.1** The Locations of Stop 1, 2, 3, 4 and Basalt Outcrop ..... 41

**Figure 4.2** Stop 1 Panoramic Images. ..... 43

**Figure 4.3** Stop 1 Interpretations ..... 44

**Figure 4.4** Stop 2 Panoramic Images. ..... 47

**Figure 4.5** Stop 2 GR logs. ..... 48

**Figure 4.6** The East Side Station with a GR Log superposed on the outcrop ..... 49

**Figure 4.7** Stop 2, the Overall Stratigraphical Succession ..... 50

**Figure 4.8** Stop 3 Panoramic Images ..... 53

**Figure 4.9** Stop 3 Interpretations. ..... 54

**Figure 4.10** Stop 3 GR, Th, K, U logs ..... 55

**Figure 4.11** Picture showing a single Bouma cycle at Stop 4 ..... 57

**Figure 4.12** Stop 4 interpretations. ..... 58

**Figure 4.13** Stop 4 GR, K, Th, U logs. ..... 60

**Figure 4.14** Basalt outcrop and Stop 1. ..... 62

**Figure 4.15** Modified Walker Sedimentary Gravity Flow Process Classification. ..... 64

**Figure 4.16** Illustrations of the relative positions of each stop between shelf edge and the Basin Floor/Abyssal Plain. ..... 66

**Figure 5.1** Bouguer Gravity Map showing the Cross-sections locations. ..... 70

**Figure 5.2** Depth-section A`-A derived from Gym-Sys with insignificant error ..... 71

**Figure 5.3** Depth-section B`-B derived from Gym-Sys with insignificant error..... 71

**Figure 5.4** Depth-section C`-C derived from Gym-Sys with insignificant error..... 72

**Figure 5.5** Depth-section D`-D derived from Gym-Sys with insignificant error. ..... 72

**Figure 5.6** Depth-section D`-D derived from Gym-Sys with insignificant error. ..... 72

**Figure 6.1** Thin section image-3 ..... 74

**Figure 7.1** Heat flow changes accompanying rifting events..... 81

**Figure 7.2** Overview of BasinMod 2-D workflow ..... 84

**Figure 8.1** Base map showing the location of the eighteen virtual wells, five cross-sections, with the boundary of Hanover Inlier and isoreflectance lines on the map ..... 84

**Figure 8.2** Data input to BasinMod 1-D for virtual well C3 ..... 88

**Figure 8.3** Tectonic Subsidence vs. Time graph with calculated beta values. ..... 89

**Figure 8.4** Rifting Heat Flow option is chosen as the thermal option ..... 90

**Figure 8.5** Beta factors have been calculated and plotted on rifting events on BasinMod 1-D. ..... 90

**Figure 8.6** Measured Bore Hole Temperatures have been inputted.. ..... 90

**Figure 8.7** Modeled heat flow for calculated rifting events for virtual well C3. ..... 91

**Figure 8.8** Vitrinite reflectance values which are belonging to adjacent unit in Hanover Group. ..... 92

**Figure 8.9** Lowest, intermediate and highest measured vitrinite reflectance values taken from isoreflectance map ..... 93

**Figure 8.10** Maturity vs. Depth graphic with % Ro values for geovalidation. ..... 94

**Figure 8.11** Burial History of Virtual Well A1 with rifting heat flow and related oil windows. ..... 94

**Figure 8.12** Burial History of Virtual Well A2 with rifting heat flow and related oil windows. ..... 95

**Figure 8.13** Burial History of Virtual Well A3 with rifting heat flow and related oil windows. ..... 96

**Figure 8.14** Burial History of Virtual Well B1 with rifting heat flow and related oil windows. ..... 97

**Figure 8.15** Burial History of Virtual Well B3 with rifting heat flow and related oil windows. ..... 98

**Figure 8.16** Burial History of Virtual Well C1 with rifting heat flow and related oil windows. ..... 99

**Figure 8.17** Burial History of Virtual Well C2 with rifting heat flow and related oil windows. ..... 100

**Figure 8.18** Burial History of Virtual Well C3 with rifting heat flow and related oil windows. ..... 101

**Figure 8.19** Burial History of Virtual Well C4 with rifting heat flow and related oil windows..... 102

**Figure 8.20** Burial History of Virtual Well C5 with rifting heat flow and related oil windows..... 103

**Figure 8.21** Burial History of Virtual Well D2 with rifting heat flow and related oil windows..... 104

**Figure 8.22** Burial History of Virtual Well D3 with rifting heat flow and related oil windows..... 105

**Figure 8.23** Burial History of Virtual Well E1 with rifting heat flow and related oil windows..... 106

**Figure 8.24** Burial History of Virtual Well E2 with rifting heat flow and related oil windows..... 107

**Figure 8.25** Burial History of Virtual Well E3 with rifting heat flow and related oil windows..... 108

**Figure 8.26** Burial History of Virtual Well E4 with rifting heat flow and related oil windows..... 109

**Figure 8.27** Burial History of Virtual Well E5 with rifting heat flow and related oil windows..... 110

**Figure 8.28** Maturity in cross-section A`-A ..... 111

**Figure 8.29** Maturity in cross-section B`-B..... 112

**Figure 8.30** Maturity in cross-section C`-C..... 113

**Figure 8.31** Maturity in cross-section D`-D. ..... 114

**Figure 8.32** Maturity in cross-section E`-E. ..... 115

**Figure 9.1** Cumulative Hydrocarbon/TOC vs. Time graphs for virtual wells C*B and A*D ..... 117

## ABSTRACT

In order to investigate the interplay between the global changes in sea level and the local changes in deposition in the Hanover Inlier of eastern Jamaica, one dimensional (1-D) basin models were constructed along five cross-sections with eighteen virtual wells, and then two-dimensional (2-D) basin models were computed.

The Hanover Inlier exhibits one major fault mechanical tectonic subsidence period at 85.3-65 Ma with a stretching factor $\beta$ of 1.85 and one major uplift or shortening period at 65-48 Ma and with a $0.78\beta$. Incorporating these crustal extensional and shortening elements allowed the maturity of the potential source rocks to be modeled with geovalidation of published vitrinite reflectance values. The first in-situ oil in the Campanian and/or Santonian formation commenced at 77, Ma but there was no expulsion of hydrocarbon owing to the inadequate amount of TOC (0.39 %). A complete petroleum system for the Hanover Group is not present for the following reasons: poor TOC of the source rock, no proven seal and trap, and calcite filling porosity reduction of possible reservoirs.

Outcrop macroscopic observations, and Spectral Gamma Ray logs reveal distinct deep water architectural elements in the (Late Campanian) Claremont Formation. Synthesis of outcrop macroscopic observations and reservoir architectural element interpretations reveal relative sedimentary facies positions on the shelf slope and its system type. Positions of reservoir architectural elements in a deep marine system and outcrop macroscopic observations reveal the relative position of deposits on a sea level cycle as several stages of a Lowstand Systems Tract.

# 1. INTRODUCTION

Jamaica lies within the northern Caribbean plate boundary zone and has experienced an active tectonic history (Pindel, 2001). The Hanover Block of north-western Jamaica represents a Cretaceous island arc sedimentary filled basin, which was later modified following deposition of limited shelf to deep water principally sediment gravity flows (Rodrigues, 1991). In order to reconstruct the three dimensional basin evolution of the Hanover Block, an integrated investigation of outcrop investigations (spectral gamma ray analysis, macroscopic observations, sequence analysis) focused on the Lucea region with published Bouguer gravity was performed. As the tectonic evolution of Jamaica is complicated owing to its position along the northern edge of the Caribbean plate, an understanding of the Hanover Block history provide fundamental knowledge of the Cretaceous and the post Cretaceous development as well as possibly provide insight into tectonized sediment gravity flows along active plate margins elsewhere.

## 1.1 Location and Physiography

The Hanover Block is located on the west side of the NNW striking Montpelier-Newmarket belt and to the north side of the east-west trending Negril-Savanna-la-Mar belt (Fig. 1.1). The Hanover Block includes the Cretaceous sediments exposed in Jamaica and makes up the large Hanover (Lucea) Inlier, which is the subject of this study.

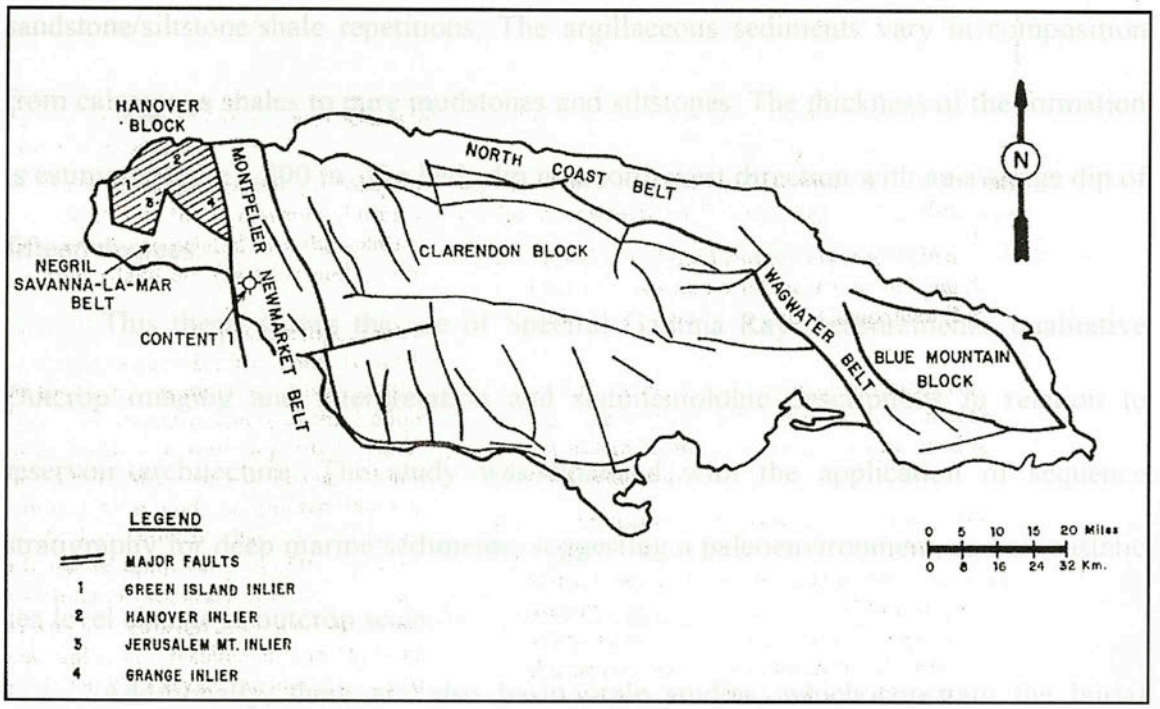


**Figure 1.1** Location of the Hanover Block in relation to the neighboring structural subdivisions of Jamaica (Rodrigues, 1991)

### 1.2 Problem Definition

In May 2010, a two-week-long field program was conducted in Western Jamaica is Negril vicinity (Fig. 1.1), which is proximal to the Hanover Block.

After focusing on outcrops in Hanover Block, basalt outcrops were discovered which have not been defined in any paper or in 1/50000 scaled geologic map of Jamaica Lucea Inlier. These basalt outcrops are important because they may indicate the source of the sediment for the late Cretaceous volcanoclastic deposits.

Literature survey also shows there is no outcrop scale reservoir characterization in that region, specifically in the Claremont Formation, where the outcrop study was conducted. The Claremont Formation is defined by Schimdt and Donovan (1987); it is composed of massive polymictic conglomerates, conglomeratic sandstones, interstarified conglomerate and sandstone beds, massive sandstones and thin

sandstone/siltstone/shale repetitions. The argillaceous sediments vary in composition from calcareous shales to pure mudstones and siltstones. The thickness of the formation is estimated to be 1,500 m. The beds dip in a north west direction with an average dip of fifteen degrees.

This thesis shows the use of Spectral Gamma Ray measurements, qualitative Outcrop imaging and interpretation and sedimentologic descriptions in relation to reservoir architecture. The study was finalized with the application of sequence stratigraphy for deep marine sediments, suggesting a paleoenvironment, and an eustatic sea level change in outcrop scale.

Additionally, there are also basin scale studies, which constrain the burial history from vitrinite reflectance in Hanover Block (Rodrigues, 1991). Kirton Rodrigues conducted a basin scale study and describes:

> By applying the Lopatin method, incorporating all available geologic data, he proposed a burial history for the Hanover Block of western Jamaica. This burial history involves deposition of 5500 m of middle Santonian to late Maastrichtian conglomerates, sandstones and shales, followed by a period of pronounced uplift and erosion of 3700 m of Cretaceous sediments in the early Tertiary. A marine transgression which began in the Early Eocene continued up to the Middle Miocene and resulted in the deposition of 900 m of limestones. Renewed uplift and erosion since the middle Miocene has continued up to the early Tertiary. TTI values derived from this reconstruction, when converted to vitrinite reflectance (Ro %), compare reasonably well with Ro values measured on field samples.

In Chapter 8, Basin Analysis and Modeling, the Ro% values from Rodrigues (1991) were used to construct the basin model. The results of Rodrigues and an alternative model are discussed and compared since his work is a one dimensional burial history model with a steady state heat flow suggestion, where this study claims are be differences throughout the whole basin, and one would not expect a homogeneous burial history throughout a volcanic island- arc complex in 3-D.

**1.3 Strategy**

In order to conduct this study, four major tasks were performed:

- Spectral Gamma Ray (SGR) outcrop readings were used as a tool for sequence stratigraphic interpretation of poorly understood platform to deepwater volcanoclastic deposition.
- Based on the SGR analysis, outcrop measurements were used to develop a sedimentological model that may be useful as a possible analog for deepwater clastic exploration.
- Thin section studies were conducted to estimate calcite filling porosity to understand decompaction required for the calculation of the burial history.
- Using gravity and geology maps to generate virtual wells, and with the help of published geochemical data such as vitrinite reflectance values, the thesis suggests a basin model was constructed in order to obtain an understanding of the tectonic evolution of the Hanover Block and possible petroleum systems.

## 2. GENERAL SETTINGS

### 2.1 General Geology of Jamaica

The General Stratigraphy of Jamaica can be conveniently described by three principal stratigraphic packages (Pigott, 2009). In ascending order they are, (Fig. 2.1):

i. The Cretaceous Basement emplacement: These rocks consist of volcanics, volcanoclastics and associated intrusive and coarse clastics (Meyerhoff and Krieg, 1977). In the Hanover Block, although coarse clastics are present, it is dominantly marine shale and silt. At the end of the Cretaceous period, the island was uplifted resulting in an unconformity marking the Cretaceous/Tertiary boundary. However, outcrop studies show a general Pleistocene reef coating on top of the Cretaceous deep marine clastics.

ii. The Wagwater-Montpelier Newmarket post Cretaceous deposition: Accompanying the east north east faulting and results in the formation of the Wagwater and Montpelier-Newmarket troughs. All Wagwater equivalent sedimentary or volcanic trough sediments that may have existed in the Montpelier-Newmarket Trough were completely covered by Tertiary limestones (Meyerhoff and Krieg, 1977).

iii. The Cenozoic White and Yellow Limestones unconformably overlie the Cretaceous basement complex of the crustal blocks forming the highlands, and conformably overlie the post Cretaceous trough sediments. Intrusive activity was confined largely to the late Mesozoic and early Cenozoic, with major deformation occurring during the Paleocene and post Miocene (Mitchell, S. F., 2003).

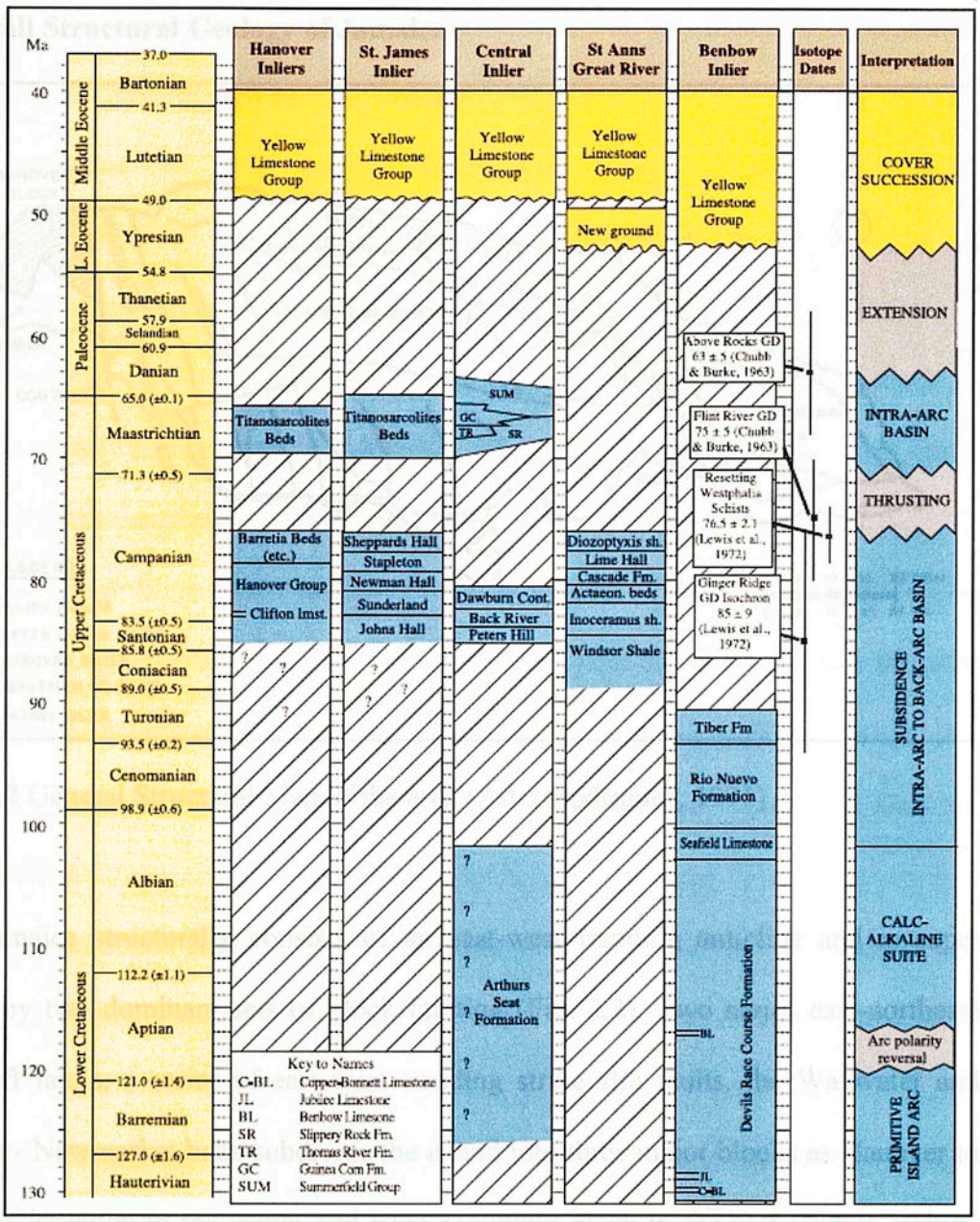


**Figure 2.1** General Stratigraphy of Jamaica focused on Hanover Block and Upper Cretaceous. The stratigraphic column shows that owing to uplift and erosion, there is no or very little record of upper sections except for Late Cretaceous formations. In the field study there are only Cretaceous deep marine clastics overlain by Pleistocene carbonate reefs unconformably (From Mitchell, 2003).

## 2.2 Overall Structural Geology of Jamaica

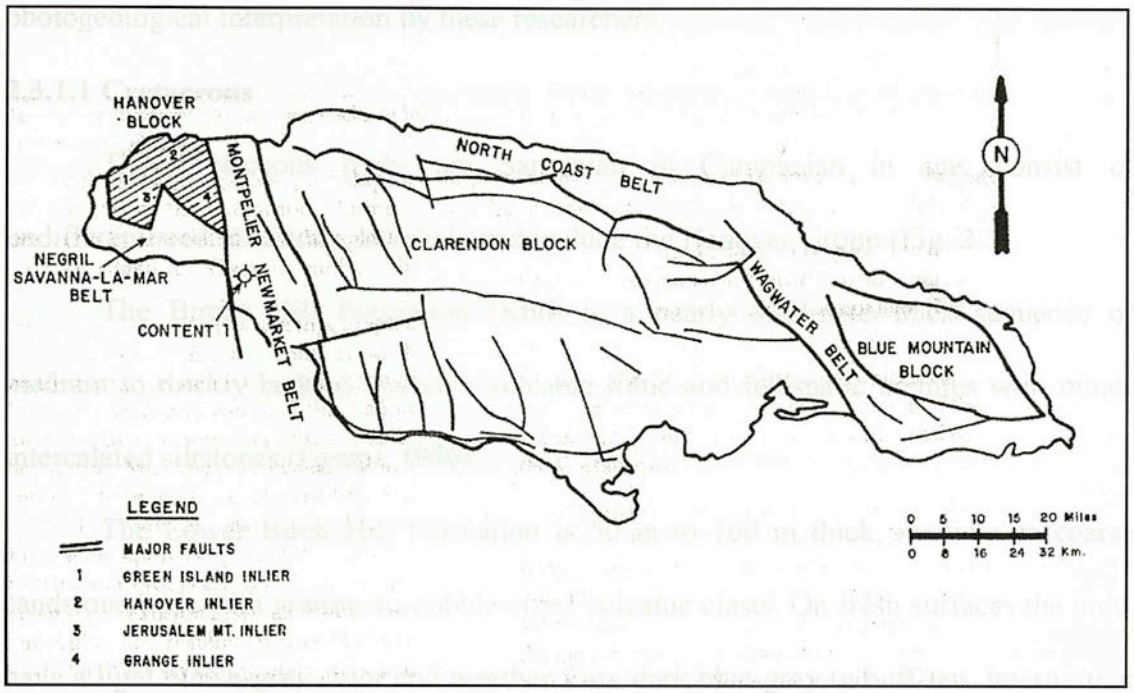


**Figure 2.2** General Structural Map of the area (After Rodriguez, 1991)

Jamaica structurally consists of an east-west trending anticline and is super imposed by two dominant sets of block faulting (Fig. 2.2). Two major east-northeast sets of rift faults, a series of east-west trending strike slip faults, the Wagwater and Monpelier- Newmarket belts subdivide the island into three major blocks as Hanover to the west, Clarendon in the center and Blue Mountain block in the east (Pigott, written communication, 2010). The area of investigation is located in the Hanover Block.

## 2.3 General Setting of Hanover Inlier

### 2.3.1 Geology of Hanover Inlier

The areas represented on the Lucea (Hanover) Inlier are explained in this chapter. The Lucea Inlier has been mapped by numerous researchers, including Grippi J. (1978), Baxter C., Crooks R., Donovan S., and Schmidt W. (1987). Some of the

lithological boundaries and faults have been extended or modified from aerial photogeological interpretation by these researchers.

### 2.3.1.1 Cretaceous

The Cretaceous rocks are Santonian to Campanian in age, consist of undifferentiated sandstone and shale and include the Hanover Group (Fig. 2.3).

The Birchs Hill Formation (Kbh) is a nearly 820-meter-thick sequence of medium to thickly bedded, massive volcanic lithic and feldspatic arenites with minor intercalated siltstones (Grippi, 1980).

The Lower Birch Hill Formation is 50 m to 160 m thick, medium to coarse sandstone beds with granite–to-cobble-sized volcanic clasts. On fresh surfaces the units have a light bluish-grey color and weather from dark blue-gray to buff-tan. Intermittent Ta and Tb intervals of the Bouma Sequence are seen (Jamaica Mines and Geology Division, 1984).

The Smithfield Formation (Ks) consists of a series of massive channelized sandstones, pebbly conglomerates and a thinly bedded sandstone/siltstone/shale sequence.

In the White Gut River Section, 200 m of graded sandstones, siltstones and shales are exposed. The underside of the beds exhibit large load casts and fluid escape casts, whereas the tops are plane parallel, show no indications of scouring, have sharp contacts to parted siltstone and shale beds (Jamaica Mines and Geology Division, 1984).

The Tom Spring Formation (Kts) is an unbedded, irregularly-shaped thick body of mafic volcanic conglomerate and shaley beds unconformably incised into the upper

section of the Smithfield Formation. It comprises mass transport deposits, named the Purple Volcanoclastics Member, and deformed sediment layers called The Georgia Shale Member and the Mafic Intrusive Rock Member (Jamaica Mines and Geology Division, 1984).

The Purple Volcanoclastics Member (Kts-v) is a purple-green matrix-supported conglomerate that is comprised of andesitic clasts, mafic chlorotized clasts, and sedimentary rock fragments. The clasts are ordered from cobble to boulder size. In addition to primary outcrops, resedimented boulder-size mafic blocks are observed as the most diagnostic feature of the Purple Volcanoclastic Member (Jamaica Mines and Geology Division, 1984).

The Georgia Shale Member (Kts-g) shows the following features: destabilized bedding, slumped strata, incorporation of large blocks of chaotic mass flow deposits, and complex folding. A number of sills and dykes are found in the Tom Spring Formation. Mafic Intrusive Rock Member outcrops are a variety of mafic intrusive rocks. Most outcrops are strictly related to the Tom Spring Formation. Contact relationships vary from massive bulky intrusions to apparently fault-related, elongated bodies or conformable sill-type deposits (Jamaica Mines and Geology Division, 1984).

The Mt. Peace Formation (Kmp) is a sequence of tubiditic thinly bedded shales and sandstones, lenticular limestones, and volcanic ash layers. The absence of thick conglomerate layers is a diagnostic feature of the Mt. Peace Formation. This formation consists of the Harvey River Member, the Lower Shale Member and the Clifton Limestone Member (Jamaica Mines and Geology Division, 1984).

The Harvey River Member is almost 500 m thick, and is a sequence of interbedded sandstones, siltstones, shales and conglomarates (Donovan and Schmidt 1987).

The Lower Shale Member is an almost 200-meters-thick sequence of red weathered shales, sandstones, calcarenites, sporadic thin conglomerates layers, thin bioclastic limestone lenses, and volcanic ash beds that mark the base of the Mount Peace Formation (Mines and Geology Division, 1984).

The Claremont Formation (Kc) is composed of massive polymictic conglomerates, conglomeratic sandstones, interstratified conglomerate and sandstone beds, massive sandstones and thin sandstone/siltstone/shale repetitions. The argillaceous sediments vary in composition from calcareous shales to pure mudstones and siltstones. The thickness of the formation is estimated to be 1,500 m. The beds dip in a NW direction with an average dip of 15 degrees (Schmidt and Donovan, 1987).

The Dias Formation (Kd) is a thinly bedded sequence of greenish-grey shale and siltstone with inter-bedded, generally sandstone units (Grippi 1980). It consists of two units, the Cocoon Shale Member and the Pell River Member.

The Haughton Court Formation (Khc) is mainly composed of shale, interbedded thin sandstone and locally abundant conglomerate. The stratigraphy thickness and lithostratigraphic position of the Haughton Court Formation is unclear due to extensive faulting, thus no type section is defined (Grippi 1980).

The Claremont Formation is the only formation that is encountered in the investigation.

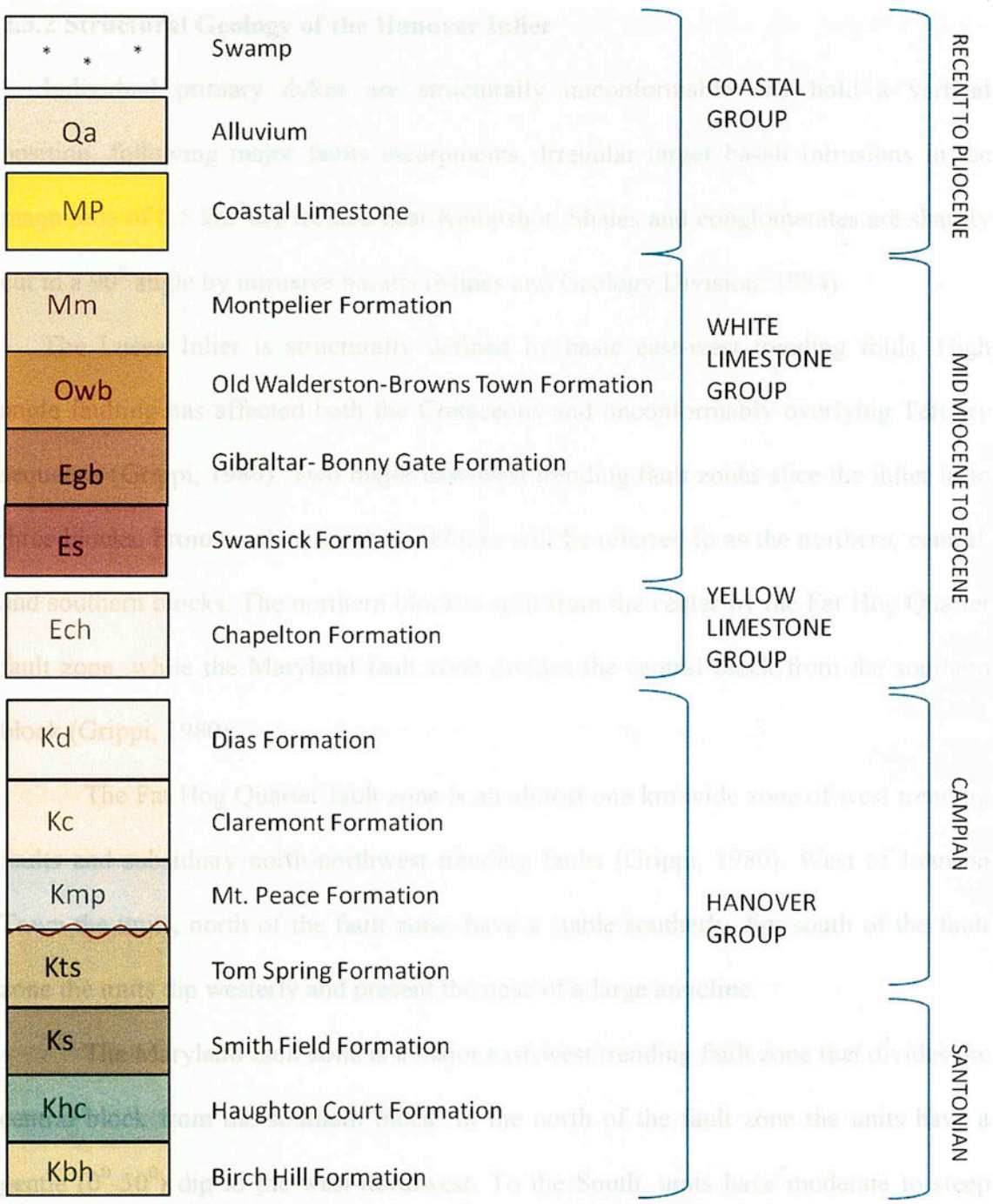


**Figure 2.3** Stratigrapic Legend of Hanover Inlier (Modified from 1:250,000 scaled Geology Map)

### 2.3.2 Structural Geology of the Hanover Inlier

Individual primary dykes are structurally unconformable and hold a vertical position, following major faults escarpments. Irregular larger basalt intrusions in the magnitude of 0.5 $km^2$ are located near Kempshot. Shales and conglomerates are sharply cut in a $90^0$ angle by intrusive basalts (Mines and Geology Division, 1984).

The Lucea Inlier is structurally defined by basic east-west trending folds. High angle faulting has affected both the Cretaceous and unconformably overlying Tertiary sequence (Grippi, 1980). Two major east-west trending fault zones slice the inlier in to three blocks. From north to south the blocks will be referred to as the northern, central, and southern blocks. The northern block is split from the center by the Fat Hog Quarter fault zone, while the Maryland fault zone divides the central block from the southern block (Grippi, 1980).

The Fat Hog Quarter fault zone is an almost one km wide zone of west trending faults and subsidiary north-northwest trending faults (Grippi, 1980). West of Johnson Town the units, north of the fault zone, have a stable southerly dip: south of the fault zone the units dip westerly and present the nose of a large anticline.

The Maryland fault zone is a major east-west trending fault zone that divides the central block from the southern block. In the north of the fault zone the units have a gentle ($0^0$-$30^0$) dip to the west-northwest. To the South, units have moderate to steep dips ($30^0$-$70^0$). This fault elongates from Maryland to Cascade-Pondside Road (Jamaica Mines and Geology Division, 1984).

The age of the east-west faulting is not well defined but the presence of the active easterly trending oriented transform to the north proposes that they are temporarily related (Burke et al, 1984).

The Smidtfield and Tom Spring-Cascade anticlines are NW-trending structures in the oldest exposed Cretaceous units. The structures are cylindrical, tight, and both are faulted (Jamaica Mines and Geology Division, 1984).

The Cash Hill Anticline is a large open, cylindrical fault which has its northern limb truncated by the Dias-Maryland fault zone (Schmidt and Donovan, 1987). The northwest corner of this anticline is complicated by a small double plunging, parasitic anticline and tight easterly closing syncline (Grippi, 1980). The deformational event that formed the east-west trending folds within the Inlier is suggested to be late Cretaceous to Paleocene. A minimum lower Eocene age is probable as the overlying Yellow Limestone, of Mid-Eocene age, is not deformed by this event.

### 2.3.3 Cross-Sections in the Hanover Block

Five geological cross-sections have been generated for the Hanover Block based upon the surface geological maps (Fig. 2.4). Cross-section locations were chosen to approximate the Inliers' regional three dimensional geology, depth section and %Ro sample locations on cross-section lines.

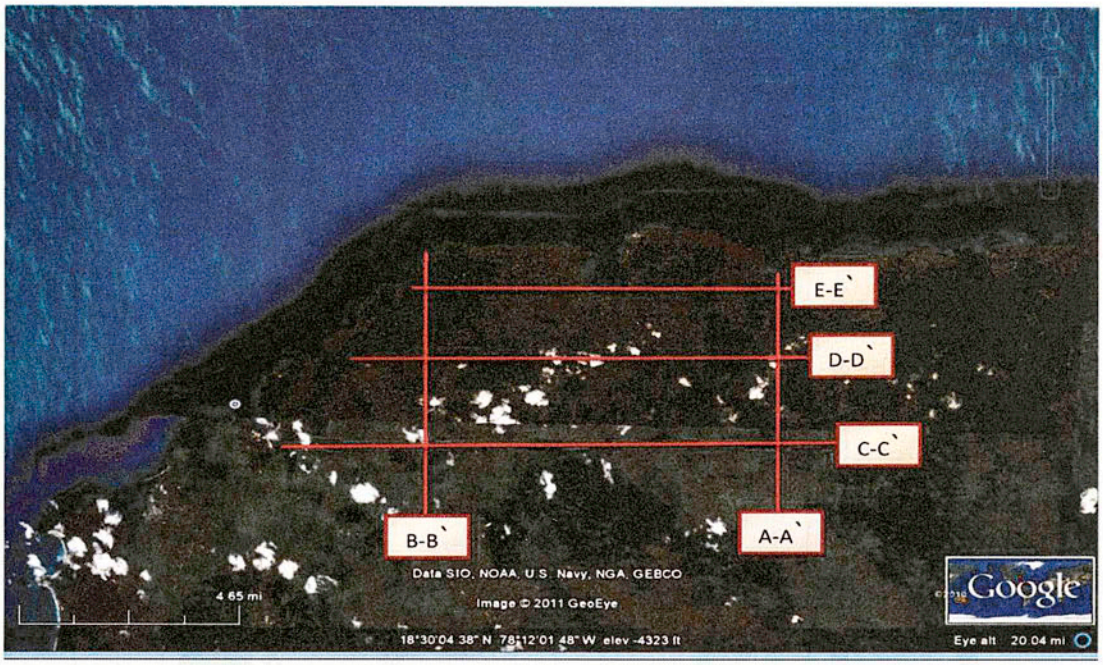


**Figure 2.4** Hanover Inlier with the locations of cross section lines (Satellite image from Google Earth, accessed 2011).

The following figures (Figures 2.5 to 2.9) are geological cross-sections derived from the 1:50,000 scale Geological Sheet #1 of Jamaica.

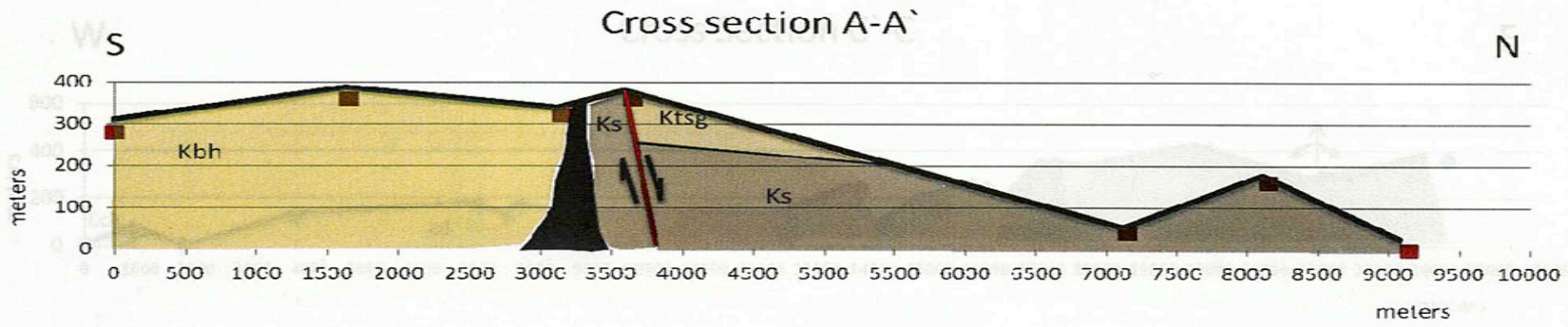


**Figure 2.5** Geological cross-section A-A`. See Figure 2.1 for the associated lithology.

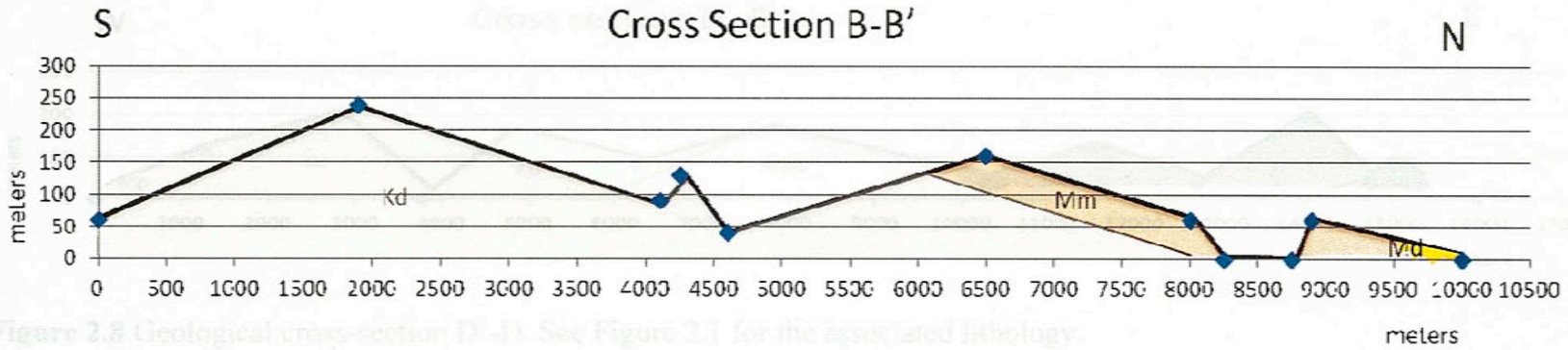


**Figure 2.6** Geological cross-section B-B`. See Figure 2.1 for the associated lithology.

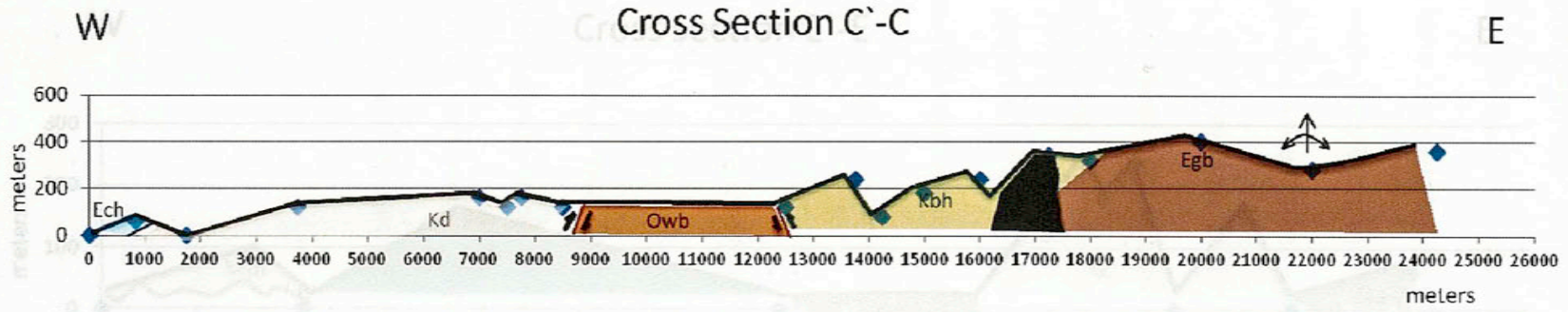


**Figure 2.7** Geological cross-section C`-C. See Figure 2.1 for the associated lithology.

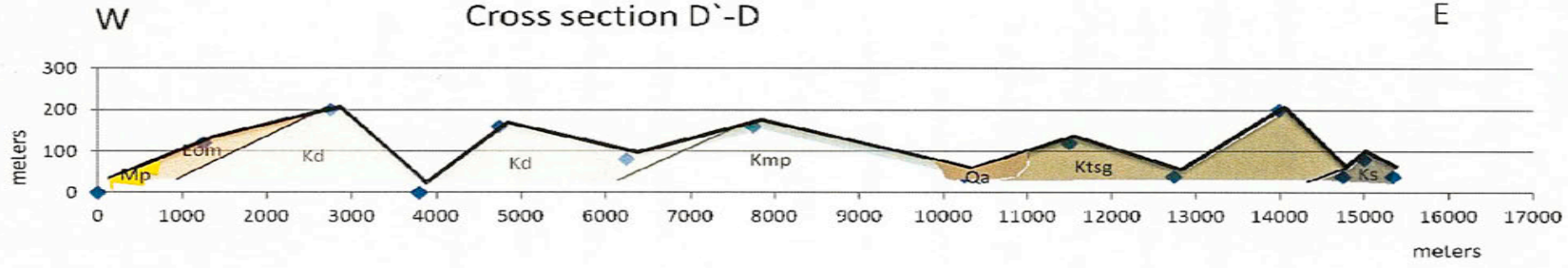


**Figure 2.8** Geological cross-section D`-D. See Figure 2.1 for the associated lithology.

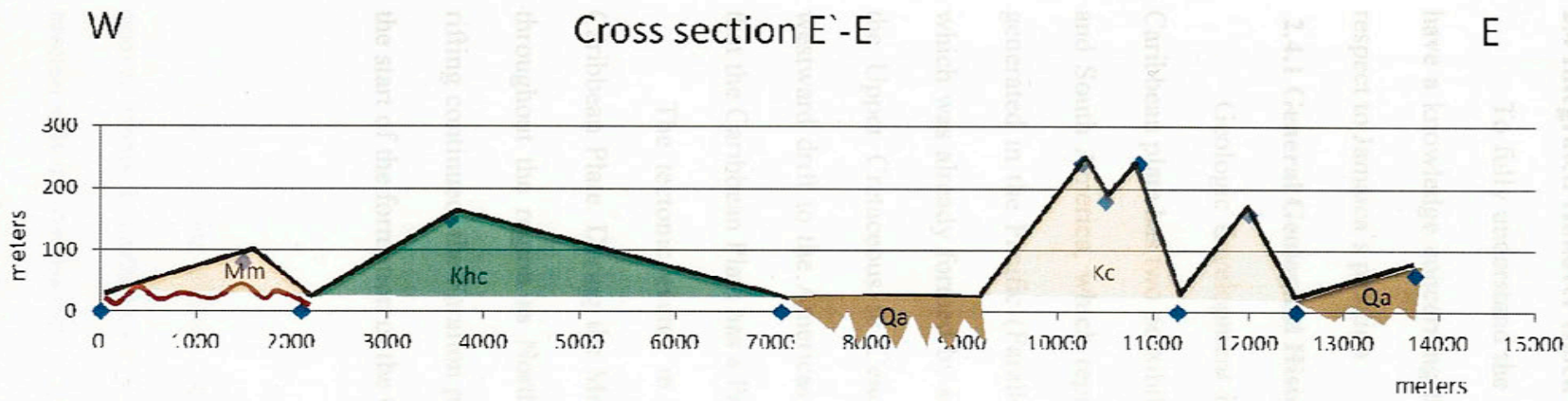


**Figure 2.9** Geological cross-section E`-E. See Figure 2.1 for the associated lithology.

## 2.4 Integrated Hanover Block Geological History

To fully understand the historical Geology of the Hanover Block, it is useful to have a knowledge concerning the general tectonic history of the Caribbean Plate with respect to Jamaica`s position.

### 2.4.1 General Geological History of Caribbean Plate and Jamaica's Position

Geologic development in the Caribbean region is complex. The origin of the Caribbean plate has two possibilities: generated by sea floor spreading between Yucatan and South America, which represents the lithosphere of the arm of the Atlantic. It is generated in the Pacific (Farallon Plate lithosphere) where the Proto-Caribbean crust, which was already formed by separation of the Americas ,was then subducted beneath the Upper Cretaceous to Cenozoic arc systems of the Caribbean Plate during the westward drift to the Americas from Africa ( Pindell, 2001). Pindel (2001) suggested that the Caribbean Plate has a Pacific origin.

The tectonic events in Jamaica are directly related to the movement of the Caribbean Plate. During the Mesozoic, the breakup of Pangea created immense rifting throughout the region as North America separated from South America. While this rifting continued, the Farallon plate continued to subduct beneath the Antilles, which is the start of the formation of the Caribbean Plate.

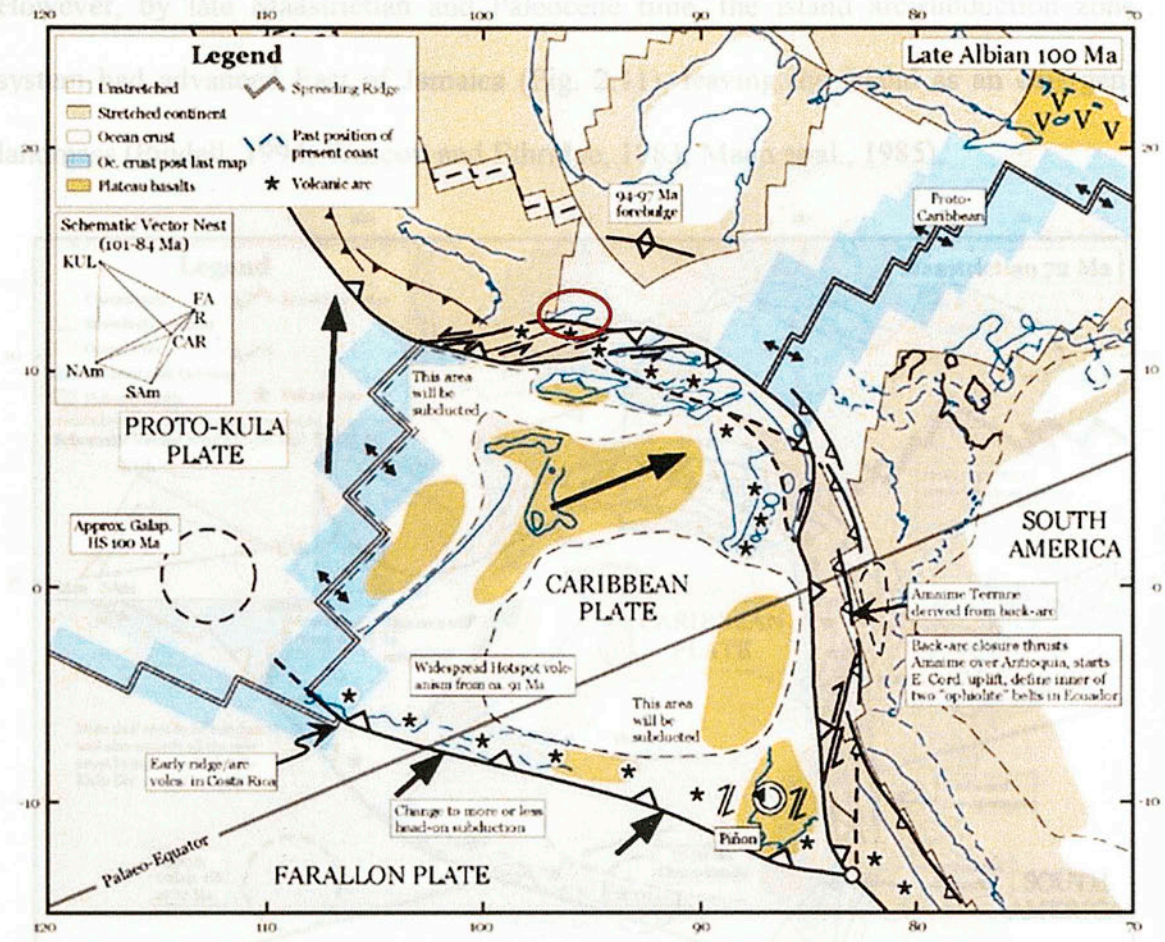


**Figure 2.10** The Caribbean plate reconstruction during the Middle Cretaceous (Late Albian). Subduction began on the eastern side of the Antilles, and the Caribbean Plate began to grow in size and convex eastward. The northwest side of Jamaica was also a part of the island arc above the subduction zone (from Pindell, 2001). Jamaica is located by the red circle.

By the Late Albian, the Caribbean plate began to grow in size and adopt a convex planar boundary eastward into the Atlantic accompanying the subduction of the eastern side of the Antilles (Fig. 2.10). During the time when Jamaica was the part of this island arc, there was little sedimentation in the Hanover Block.

However, by late Maastrictian and Paleocene time, the island arc/subduction zone system had advanced East of Jamaica (Fig. 2.11), leaving the island as an emergent landmass (Pindell, 1994; Wescott and Ethridge, 1983; Mann et al., 1985).

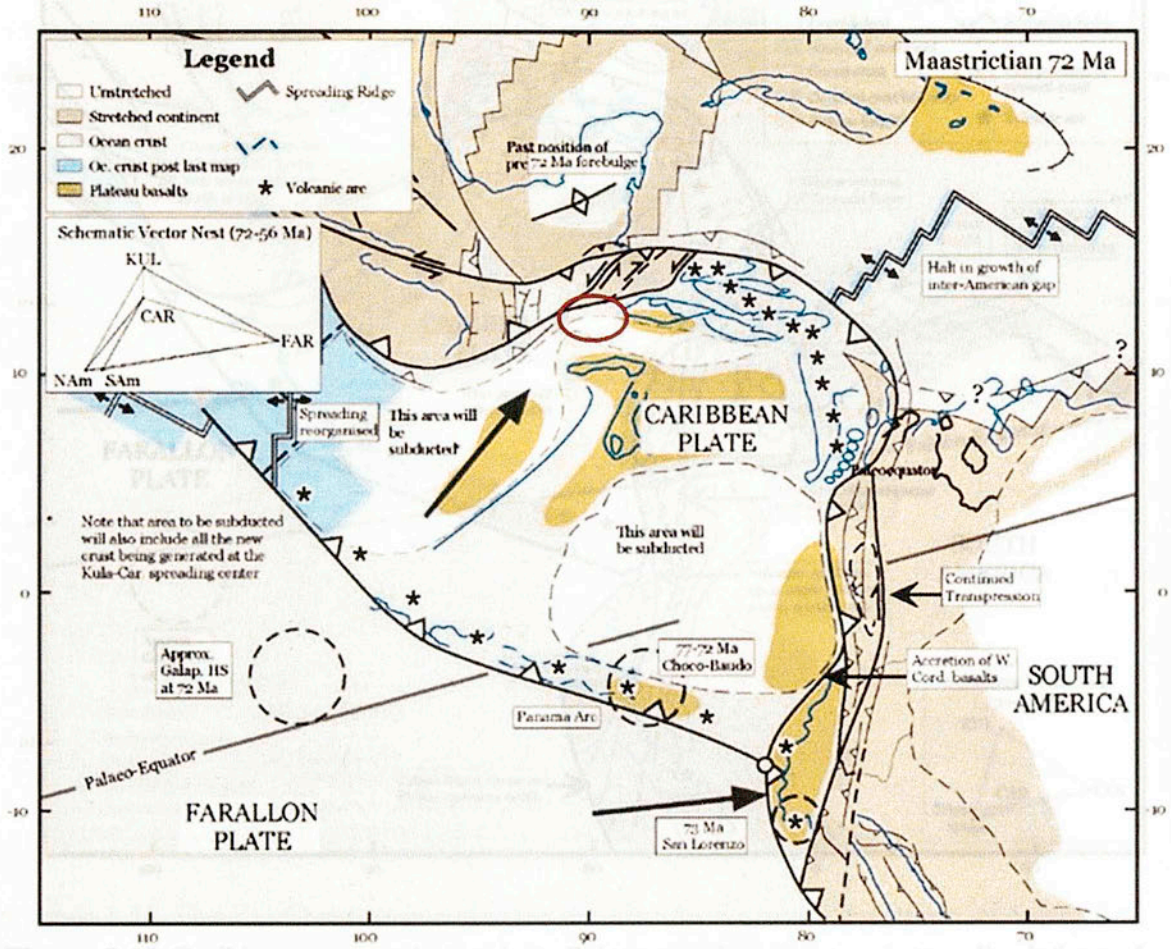


**Figure 2.11** The Caribbean region and Jamaica's position (circled in red) during the end of Maastrichtian and Paleocene. Jamaica was an emergent landmass after advancing from the island arc/subduction zone system to the east of the island.

During the Cenozoic, the Caribbean Plate continued to advance to the east. The Yucatan Block prevented eastward motion of the Jamaica. Thus, Jamaica was internally deformed as the New Market-Montpelier trough and the Hanover Block formed in

Jamaica, (Fig. 2.12), as well as other trough and blocks in Jamaica and rifts in the Nicaraguan rise (Pindell, 2001).

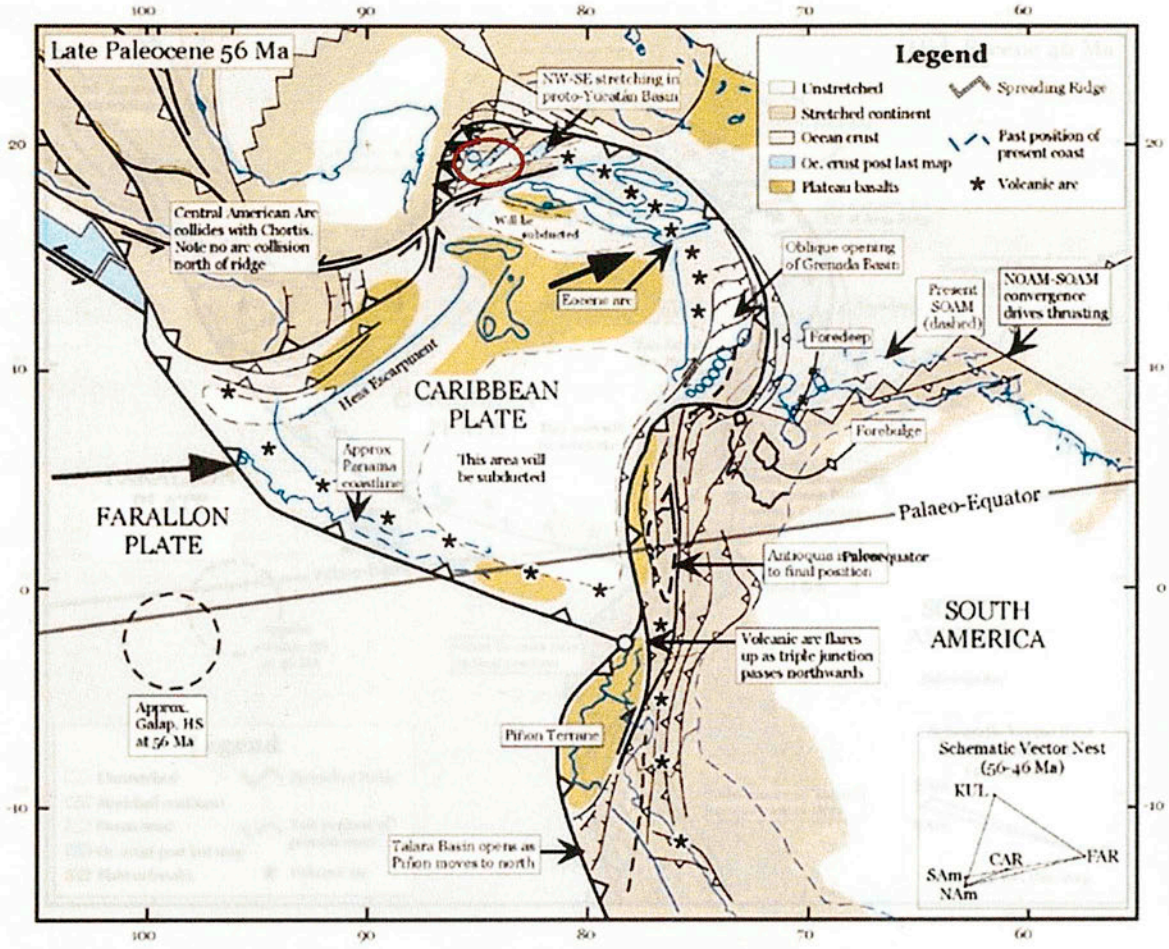


**Figure 2.12** Caribbean region during Late Paleocene, Jamaica was internally deformed yielding New-Market and Wagwater Troughs and Hanover, Clerandon and Blue Mountain blocks (after Pindell, 2001).

The Middle Eocene was marked by the termination of Antillean collision and the onset of platform deposition in Cuba (Fig. 2.13). Cayman Trough nucleated as a pull-apart basin between Yucatan and Jamaica spreading in an east-west direction. At the same time it was slowing down of rifting of New-Market Trough and submergence of the Hanover Block in post-Early Eocene times associated with marine transgression,

which covered the entire Jamaica area by the Early Miocene. The Yellow and White Limestone groups were deposited during this period in the Hanover Block.

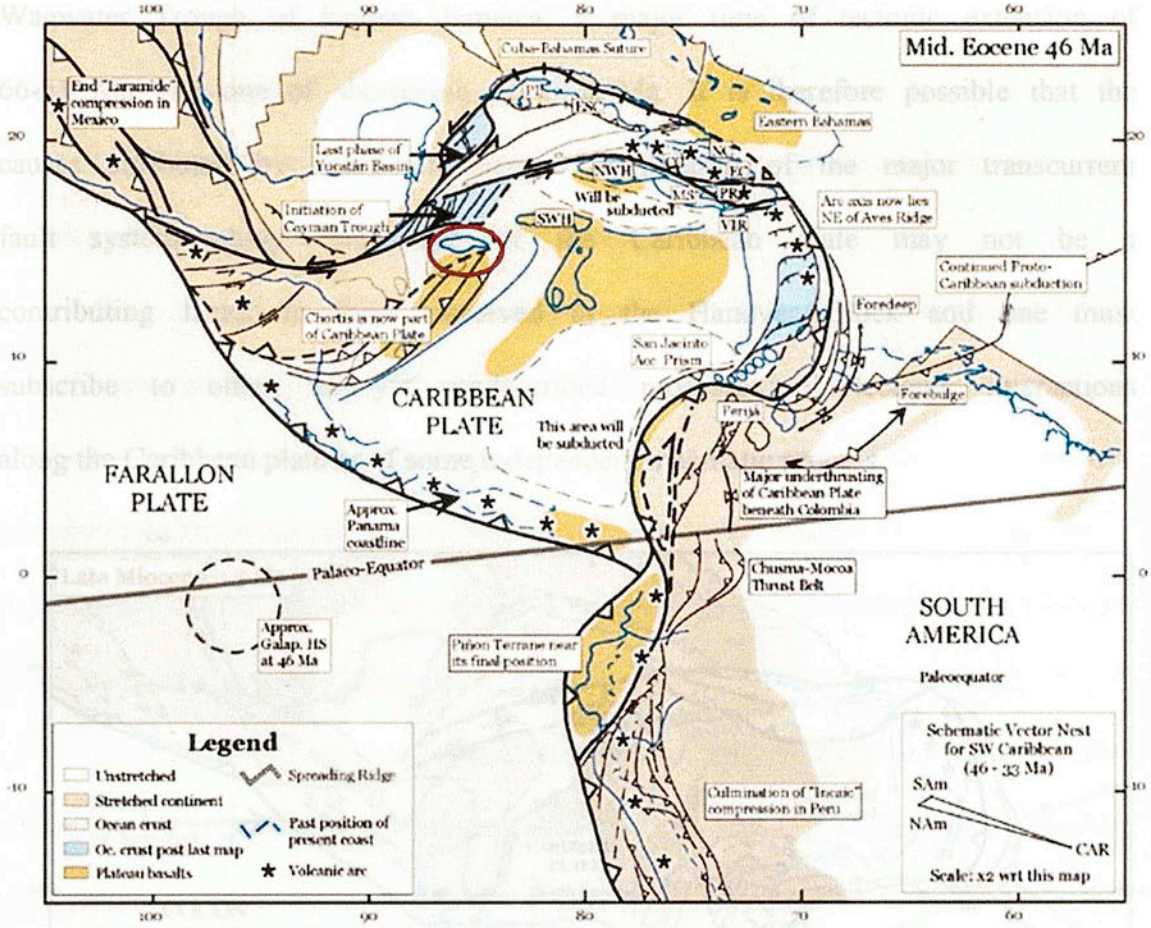


**Figure 2.13** The Caribbean region during the Middle Eocene. Deposition of White and Yellow Limestone covering the entire of the island occurred during this time. Hanover Block was submerged and received that carbonate deposition as well (after Pindel, 2001).

Progressive growth of the Cayman Trough and reciprocal actions of the Caribbean Plate with Cuba and Hispanola caused left-lateral strike-slip faults to form on the northern boundary of the Caribbean Plate between the southern end of the Cayman spreading core and Hispanola (Fig. 2.14).

As the timing of the observed tectonic uplift (85.3-65 Ma) and subsidence (65-48 Ma) is generally inconsistent with those reported by Ward (2009) for the Wagwater Trough of Eastern Jamaica: a major time of tectonic extension of 66-51 Ma and one of shortening of 10-0 Ma. It is therefore possible that the causes attributed by Ward of changes in polarity of the major transcurrent fault system along this edge of the Caribbean plate may not be a contributing factor to these observed in the Hanover Block and one must subscribe to other, as yet, undescribed processes of tectonic interactions along the Caribbean plate or of some independent magmatic process.

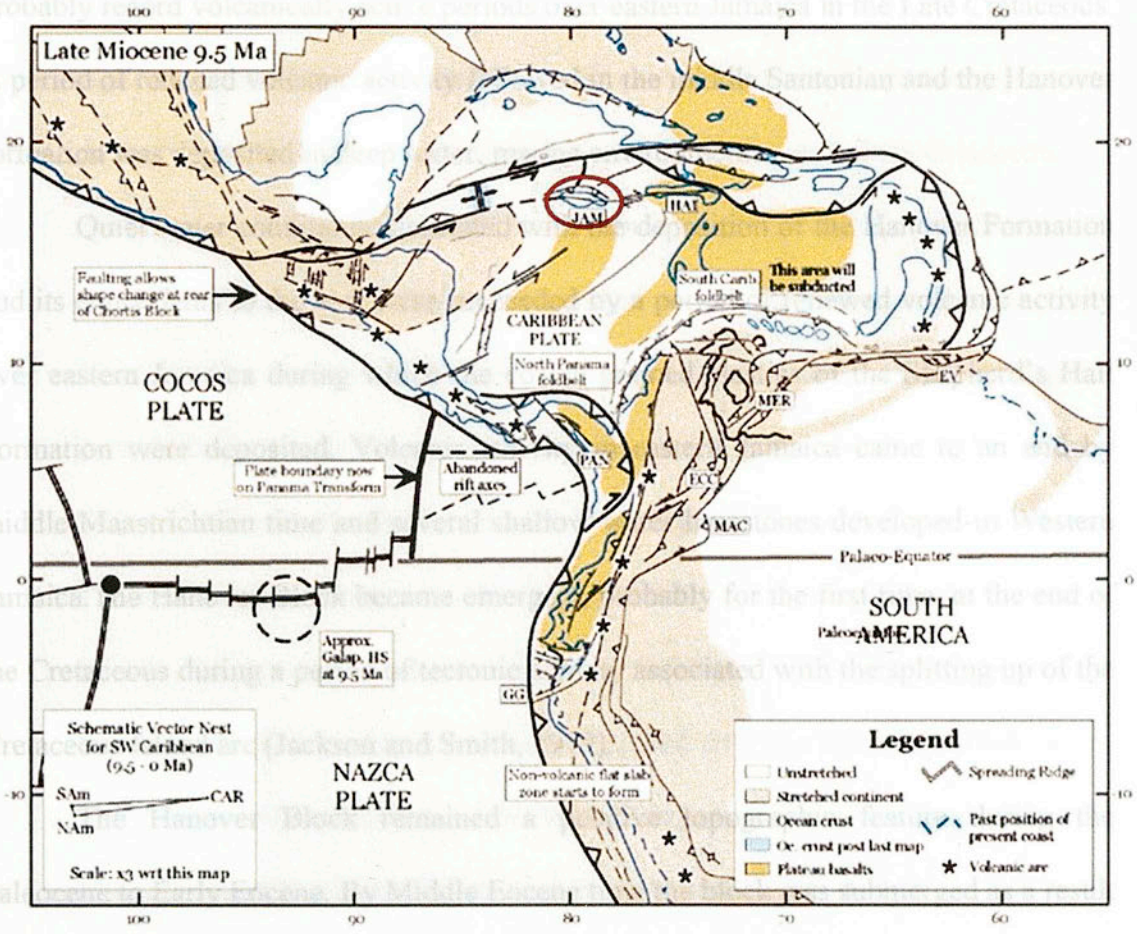

**Figure 2.14** The Caribbean region during the Late Miocene. Strike-slip faults make a constraining bend in the bend on the bounding faults of the Hanover Block causing uplift and erosion of the Block (after Pindell, 2001).

### 2.4.2 Geological History of the Hanover Block

The Hanover block includes the most westerly Cretaceous sediments exposed in Jamaica and comprises the large Hanover (Lucea) Inlier.

Santonian to Middle Campanian sediments in most of the Cretaceous inliers over Jamaica are predominantly shales and siltstones. Conglomeratic horizons above and below these pelitic intervals are present in many of the inliers. These conglomerates probably record volcanically active periods over eastern Jamaica in the Late Cretaceous. A period of reduced volcanic activity followed in the middle Santonian and the Hanover formation was deposited in deep water, marine environment.

Quiet water conditions associated with the deposition of the Hanover Formation and its equivalents to the east were succeeded by a period of renewed volcanic activity over eastern Jamaica during which the coarse grained clastics of the Shepherd`s Hall Formation were deposited. Volcanic activity in eastern Jamaica came to an end by middle Maastrichtian time and several shallow water limestones developed in Western Jamaica.The Hanover Block became emergent, probably for the first time, at the end of the Cretaceous during a period of tectonic activity associated with the splitting up of the Cretaceous Island arc (Jackson and Smith, 1979).

The Hanover Block remained a positive topographic feature during the Paleocene to Early Eocene. By Middle Eocene time the block was submerged as a result of the island-wide marine transgression, and the Yellow and White Limestone Groups

were deposited. Uplift occurred in the Middle Miocene, which puts a broad White limestone deposition to an end. Southward tilting of the island since the Late Miocene has resulted in the Hanover Inlier being the upthrown part of the Hanover Block with the Jerusalem Mountain Inlier to the south as the downthrown part. Erosion associated with the post-Middle Miocene uplift has resulted in the Hanover Block being bared of its Tertiary sedimentary cover and the oldest bed are exposed to the north.

The burial history of Lucea Inlier (Hanover Block) sediments was reconstructed with these major subsidence-uplift events:

i. Deposition of the Hanover Formation in a back arc basin and shelf environments from the Middle Santonian to Middle Campanian

ii. Uplift and erosion of the Hanover Block (at least the Northern part) after deposition of the Jerusalem Mountain Formation at the end of the Cretaceous.

iii. Submergence of the Hanover Block in post-Early Eocene times associated with marine transgression, which covered the entire Jamaica area by the Early Miocene. The Yellow and White Limestone Groups were deposited during this period. Robinson (in Meyerhoff and Krieg, 1977) estimated that 150 m of pre-White Limestone Tertiary sediments were deposited over the Hanover Block. These sediments correspond with the Chapelton formation of late Early to early Middle Eocene age, and on this basis a 150 m thick section of Yellow Limestone is assumed to have been deposited over the Hanover Block in the Early Eocene. The thickness of the White Limestone Group varies spatially and Meyerhoff and Krieg (1977) report thicknesses ranging from 600 to 2400 m. In the absence of a more reliable estimate 750 m of White Limestone are assumed

to have been deposited on the Hanover Block between the Middle Eocene and Middle Miocene.

iv. Uplift of the Hanover Block brought deposition of the White Limestone Group to an end in the Middle Miocene. The Tertiary sedimentary cover has since been removed by erosion.

The depositional history of Hanover Block sediments comprised two distinct periods: the Middle Santonian to Late Campanian (and possibly to Late Maastrichtian) period and the Early Eocene to Middle Miocene period. The available geological data suggest that maximum burial of the Hanover Formation occurred in the Late Cretaceous and that early Tertiary tectonic activity resulted in significant uplift. The Hanover Block area was a significant depo-center in the Late Cretaceous and received four to five km of sediments (Grippi, 1980) derived from erosion of the volcanic centers over eastern Jamaica, which were transported into a backarc basin and shelf environment by turbidity currents and /or prograding deltas.

The Early Tertiary period of uplift and erosion in Jamaica to have been more dramatic since the Middle Miocene:

i. At the beginning of Tertiary the tectonic setting of Jamaica started to altered as a result of splitting of the Cretaceous island arc (Jackson and Smith, 1979). The island was divided into blocks and basins, and the active and inactive marginal basins of the Wagwater and Montpelier-Newmarket belts, respectively, were created. Thus, the early Tertiary was an intense tectonic activity period, which resulted in large scale relative uplift of the blocks on the island.

ii. The onlap of the Middle Eocene Yellow Limestone onto Campanian and Santonian sediments is a strong evidence for significant uplift in the early Tertiary. In the Hanover Inlier the Chapelton formation lies unconformably on the Santonian to Campanian Hanover Formation. That suggests all sediments deposited after the Middle Campanian (probably more than 3000 m) were removed by erosion between 65 and 48 Ma ago, prior to Yellow Limestone group (Rodrigues, 1991).

The Early Tertiary tectonic activity resulted in the large scale uplift of the blocks associated with simultaneous opening up of the intervening troughs. High topographic relief on uplifted blocks resulted in rapid erosion of Late Cretaceous sediments, which were subsequently deposited in adjacent subsiding basins. In western Jamaica the post-Middle Miocene island-wide uplift was much more subdued.

**2.5 Petroleum Potential of Jamaica and Hanover Block**

The exploration for the petroleum in Jamaica has been active since the early 20$^{th}$ century. As early as the 1920s, hydrocarbon was being produced in Trinidad, Barbados, Cuba and the Dominican Republic.

Serious attempts at petroleum exploration in Jamaica began in the mid-1950's. Four wells were drilled between 1955 and 1957, with activity concentrated in western Jamaica. However except for minor hydrocarbon "shows" the results were disappointing. The exploration effort started back again during the 1970s with the first offshore drilling well located on Pedro Bank, 100 km south of the island, and two other wells on shore. All were dry holes to be drilled in Jamaican territory. The third attempt, which was also the most intensive exploration drilling program, was conducted between

November 1981 and October 1982, when an additional three onshore wells and one offshore well was drilled and abandoned as dry. To sum up, a total of eleven dry holes were drilled in Jamaica (Fig. 2.15). Data on these wells are summarized in Table 2.1 (Rodriguez, 1991).

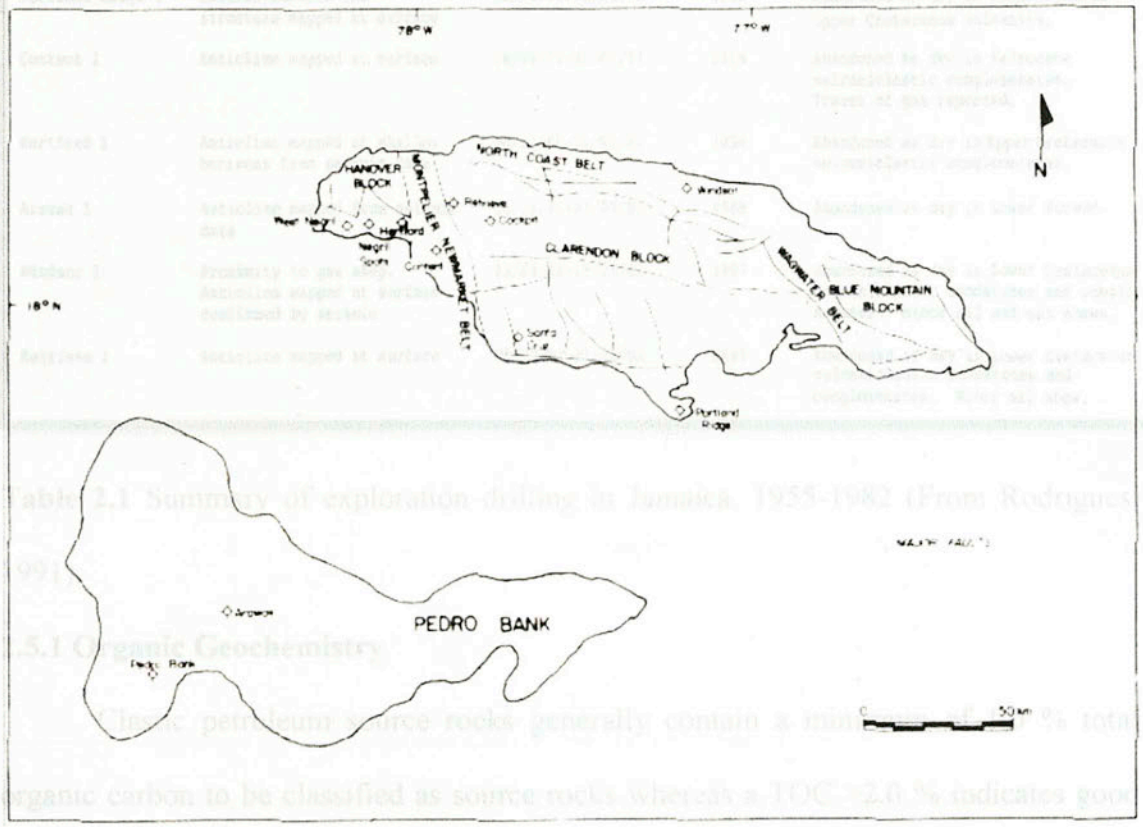


**Figure 2.15** Location of dry holes drilled in Jamaican territory, 1955-1982 (Rodrigues, 1991).

| WELL | GEOLOGICAL BASIS | DATE DRILLED | TOTAL DEPTH (m) | REMARKS |
|---|---|---|---|---|
| Negril Spots 1 | Structure mapped at surface | 05/04/55-10/06/55 | 1924 | Abandoned as dry in dark gray Maastrichtian shales. |
| Santa Cruz 1 | Large faulted anticline mapped at surface | 03/06/56-02/03/57 | 2661 | Abandoned as dry in metamorphosed Upper Cretaceous volcanics. |
| Cockpit 1 | Structural closure mapped at surface | 10/04/57-14/05/57 | 1684 | Abandoned as dry in Upper Cretaceous volcaniclastic conglomerates. |
| West Negril 1 | Structural closure in anticline mapped at surface | 10/06/57-22/08/57 | 2817 | Abandoned as dry in Maastrichtian shales, sandstones and conglomerates |
| Pedro Bank 1 | Seismic control and aero-magnetic survey | 12/01/70-13/04/70 | 1978 | Abandoned as dry in Lower Tertiary granodiorite. |
| Portland Ridge 1 | Seismic control and structure mapped at surface | 22/01/71-02/04/71 | 2262 | Abandoned as dry in metamorphosed Upper Cretaceous volcanics. |
| Content 1 | Anticline mapped at surface | 14/10/72-31/01/73 | 2319 | Abandoned as dry in Paleocene volcaniclastic conglomerates. Traces of gas reported. |
| Hertford 1 | Anticline mapped at shallow horizons from seismic data | 06/11/81-11/02/82 | 3034 | Abandoned as dry in Upper Cretaceous volcaniclastic conglomerates. |
| Arawak 1 | Anticline mapped from seismic data | 16/12/81-27/04/82 | 4588 | Abandoned as dry in Lower Eocene. |
| Windsor 1 | Proximity to gas seep. Anticline mapped at surface confirmed by seismic | 23/03/82-19/07/82 | 3907 | Abandoned as dry in Lower Cretaceous volcaniclastic sandstones and conglomerates. Minor oil and gas shows. |
| Retrieve 1 | Anticline mapped at surface | 28/07/82-21/10/82 | 3447 | Abandoned as dry in Lower Cretaceous volcaniclastic sandstones and conglomerates. Minor oil show. |

**Table 2.1** Summary of exploration drilling in Jamaica, 1955-1982 (From Rodrigues, 1991).

### 2.5.1 Organic Geochemistry

Clastic petroleum source rocks generally contain a minimum of 1.0 % total organic carbon to be classified as source rocks whereas a TOC >2.0 % indicates good source rocks (Tissot and Welte, 1978; Hunt, 1979). Oil-prone organic matter comprises of marine-derived amorphous components, although land-derived exinite-rich kerogens are capable of generating paraffinic crudes (Hedberg, 1968; Connan and Cassou, 1980).

Source rocks with adequate amounts of oil-prone organic matter will generate oil over a maturity range defined by a vitrinite reflectance of 0.6-1.3 Ro, (Dow, 1977). Dry gas can be generated at reflectance values greater than 1.2% Ro.

The major potential source rocks in the Hanover Block are the Hanover/Sunderland shales, and the organic carbon contents of these shales, as reported by Rodriguez (1991), are low in organic matter, with an average TOC of 0.39% (Fig. 2.16). Thus, on the criterion of organic content alone, the Hanover Formation cannot be ranked as a potential petroleum source rock (Rodriguez, K., 1991).

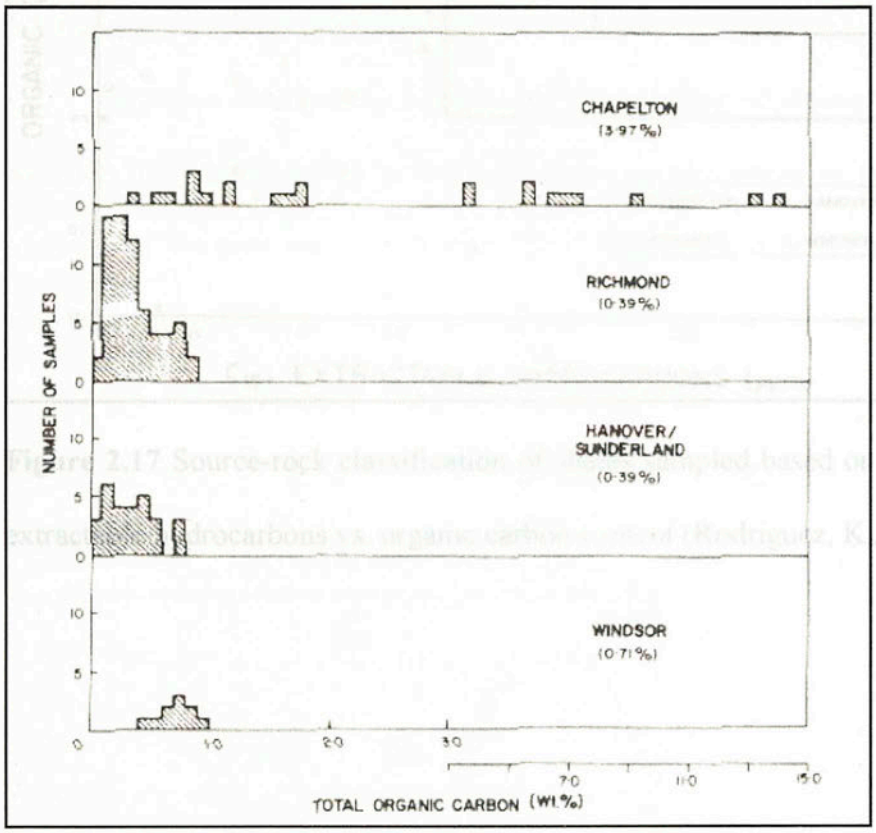


**Figure 2.16** Frequency distribution of Total Organic Content in particular shale layers analyzed (Rodriguez, K., 1991)

With respect to maturity levels of the sediments sampled from Hanover are mature with respect to oil generation. However, as low concentrations of organic matter dominated by non oil-prone components in the Hanover Formation are reflected by very low $C_{15+}$ extractable hydrocarbon contents (generally<150 ppm), this formation should not be considered as a viable source rock for oil generation (Fig. 2.17).

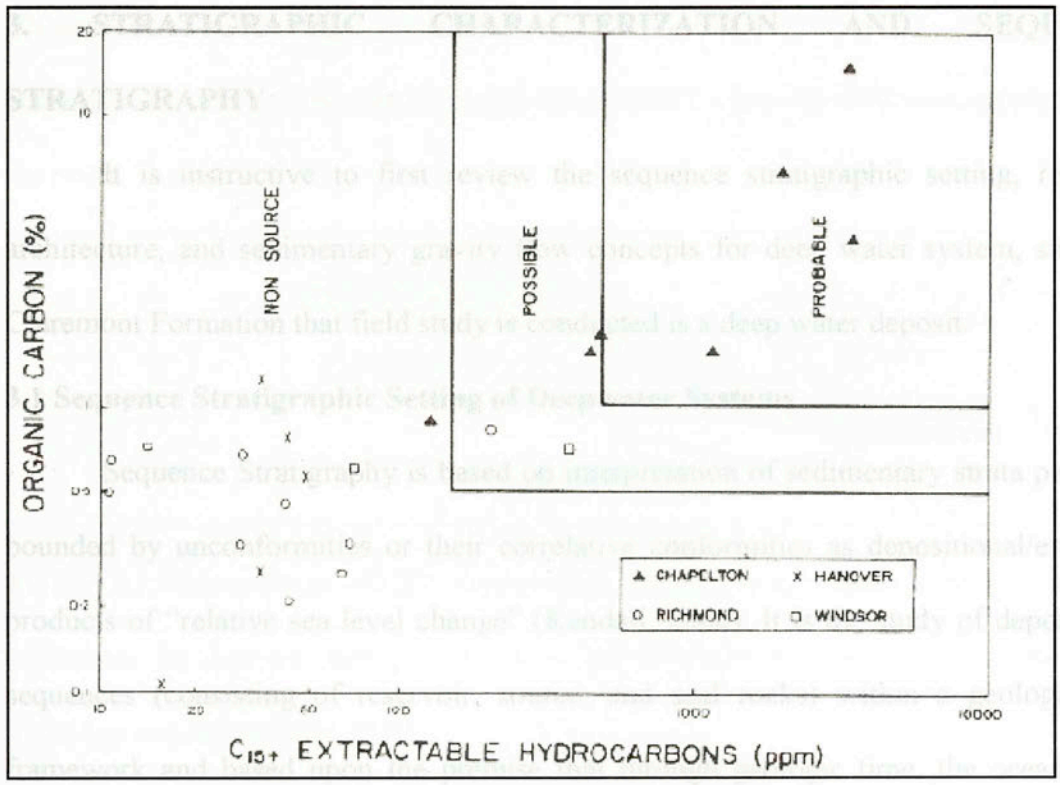


**Figure 2.17** Source-rock classification of shales sampled based on log-log plot of $C_{15+}$ extractable hydrocarbons vs. organic carbon content (Rodriguez, K., 1991).

# 3. STRATIGRAPHIC CHARACTERIZATION AND SEQUENCE STRATIGRAPHY

It is instructive to first review the sequence stratigraphic setting, reservoir architecture, and sedimentary gravity flow concepts for deep water system, since the Claremont Formation that field study is conducted is a deep water deposit.

## 3.1 Sequence Stratigraphic Setting of Deepwater Systems

Sequence Stratigraphy is based on interpretation of sedimentary strata packages bounded by unconformities or their correlative conformities as depositional/erosional products of "relative sea level change" (Kendall, 2006). It is the study of depositional sequences (consisting of reservoir, source, and seal rocks) within a geologic time framework and based upon the premise that through geologic time, the oceans have risen and fallen in a cyclic manner (Fig. 3.1), so that strata are deposited in a predictable, cyclic manner.

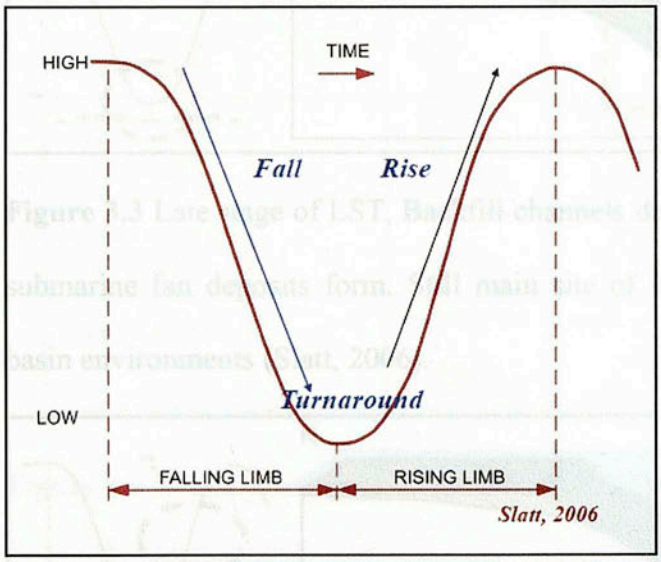


**Figure 3.1** A single relative sea level cycle (From Slatt, 2006)

To understand a full single sea level cycle, the following models (Fig. 3.2 to Fig. 3.5) and illustrations have been developed by Slatt (2006) where the sediment supply is from the north.

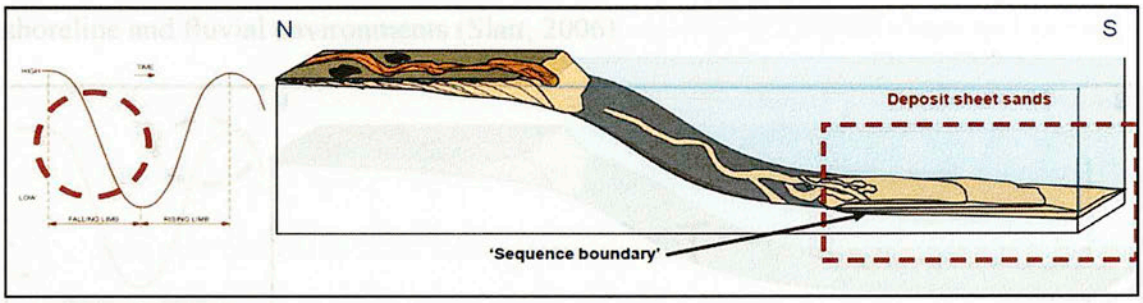


**Figure 3.2** Falling Stage of LST, Distributary channel incises through deltaic deposits, submarine fan deposits form and the main site of sandstone deposition is in slope and basin environments (Slatt, 2006).

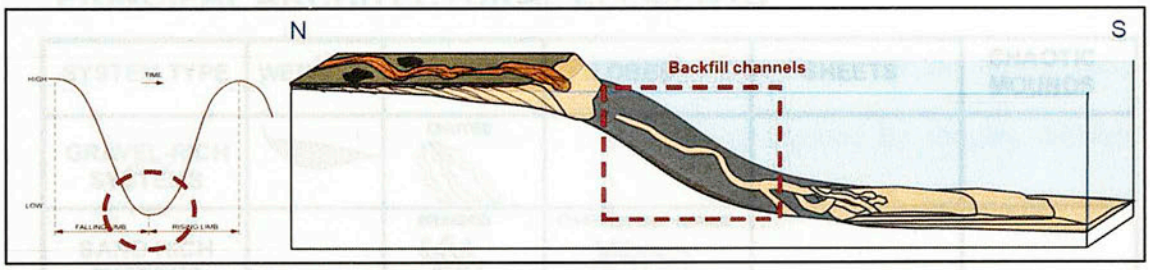


**Figure 3.3** Late stage of LST, Backfill channels deposits (in sea level fall scenario) and submarine fan deposits form. Still main site of sandstone deposition is in slope and basin environments (Slatt, 2006).

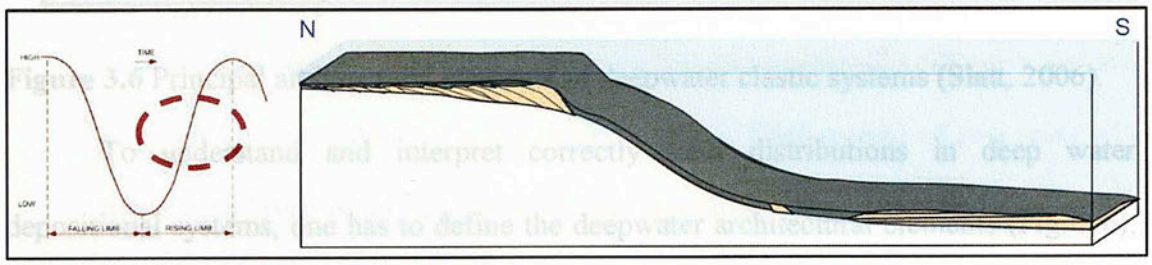

**Figure 3.4** Relative rise in the sea level, representing TST, shoreline is forced in landward direction and a regional extensive, organic-rich condensed section forms in shelf, slope, and basin environments. Only main site of sandstone deposition is in the shoreline and fluvial environments (Slatt, 2006).

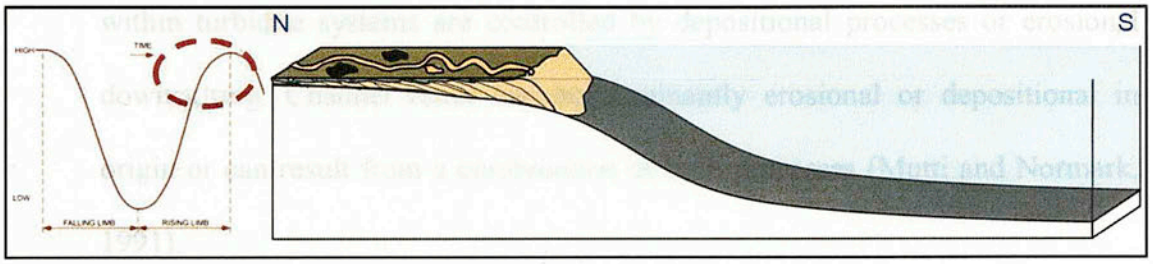


**Figure 3.5** HST, deltas prograde to fill accommodation created by sea level rise. The main site of sandstone deposition is in the delta environment (Slatt, 2006).

### 3.2 Reservoir Architecture

**PRINCIPAL ARCHITECTURAL ELEMENTS**

| SYSTEM TYPE | WEDGES | CHANNELS | LOBES | SHEETS | CHAOTIC MOUNDS |
|---|---|---|---|---|---|
| GRAVEL-RICH SYSTEMS | | CHUTES | | | |
| SAND-RICH SYSTEMS | | BRAIDED | CHANNELIZED-LOBES | | |
| MUD/SAND-RICH SYSTEMS | | CHANNEL-LEVEE | DEPOSITIONAL LOBES | | SLUMPS & SLIDES |
| MUD-RICH SYSTEMS | | CHANNEL-LEVEE | DEPOSITIONAL LOBES | | SLUMPS & SLIDES |

**Figure 3.6** Principal architectural elements of deepwater clastic systems (Slatt, 2006).

To understand and interpret correctly sand distributions in deep water depositional systems, one has to define the deepwater architectural elements (Fig. 3.6). The following definitions do not represent every element one may find in a deep water

system, but these represent ones which occur in the systems observed in the Hanover Block:

Channel: Channels are elongated negative-relief features produced and maintained by slumping and turbidity-current flow. Channel shape and position within turbidite systems are controlled by depositional processes or erosional downcutting. Channel relief can be dominantly erosional or depositional in origin or can result from a combination of both processes (Mutti and Normark, 1991).

Condensed section: These are thin marine stratigraphic units consisting of pelagic to hemipelagic sediments with very low sedimentation rates. They are most extensive at the time of maximum regional transgression of the shoreline (Loutit et al. 1988).

Depositional lobe: These are areas of sand deposition that lie immediately downslope from the main channel. They are represented by roughly tabular, nonchannelized bodies that have individual thicknesses, generally of 3-15 m (10-50 feet). Each lobe is made up of relatively thick and coarse sandstone beds that are generally parallel sided even at the scale of large exposures (Mutti and Normark, 1987, 1991).

Overbank-levee: Overbank-levee deposits are generally (and relatively) fine-grained, thin bedded deep water sediments that can be laterally extensive and are adjacent to main channels in a turbidite system. They consist of two parts: (1) those with levee relief, where overbank deposition along margins of an active

channel has constructed relief and (2) the most distal parts of an overbank environment without major relief (Mutti and Nomark, 1991)

Sheet: Sheet sands resemble fan lobe deposits and are characterized in outcrops by their laterally continuous, tabular external geometries. Internal architecture differences allow them to subdivide into two as amalgamated sheets and layered sheets. Amalgamated sheets are characterized by high net:gross comprising stacked assamblages of top-absent Bouma sequences. Layered sheets are characterized by lower net:gross sand percentages (with) complete or base absent Bouma A sequences (Mahaffie, 1994).

### 3.3 Sediment Gravity Flow Processes

In this thesis, the sediment gravity flow process classification is that of Walker (1978).

#### 3.3.1 Walker Sedimentary Gravity Flow Classification

The Walker (1978) considers two main factors: the sediment concentration and time or space of the sedimentation occurs. As the concentration decreases and time or travel distance increases, the gravity flow process changes from a debris flow to classical turbidites. That process also implements different sediment support mechanisms in different concentration vs time/space (Fig. 3.7).

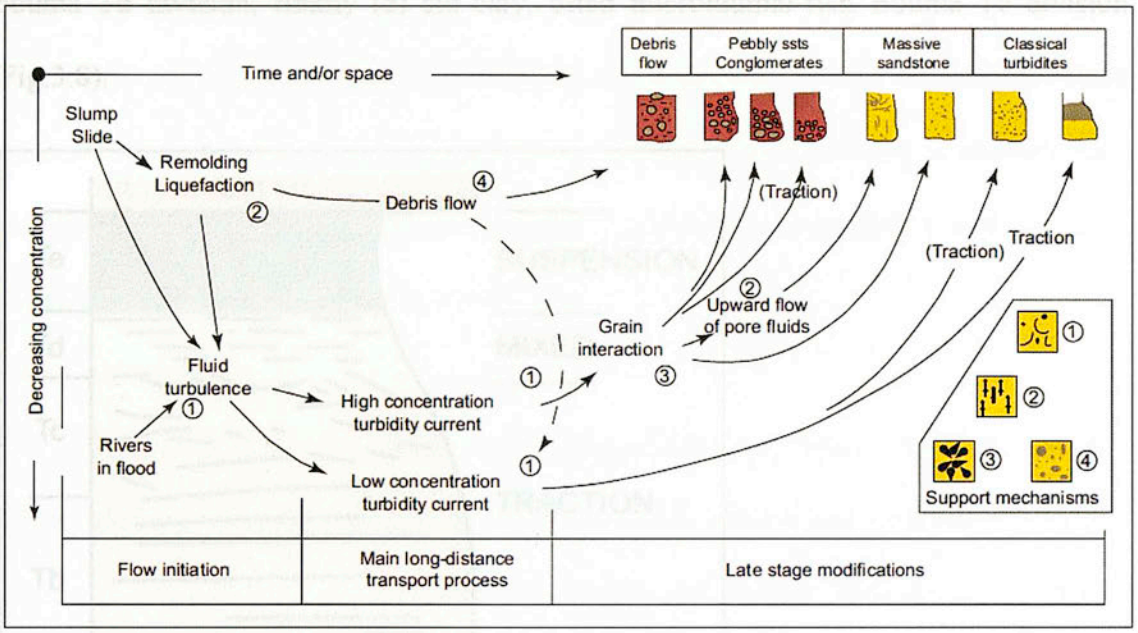


**Figure 3.7** The sediment transport processes of sediment gravity flows and resulting deposits (Walker, 1978). The vertical axis describes sediment concentration, and the horizontal axis represents time and/or space. Sediment support mechanisms are: 1=fluid turbulence, 2=hindered settling, 3=dispersive pressure and 4=matrix strength.

### 3.3.1.1 The Bouma Sequence

One particular stop exhibits excellent examples of Bouma Sequence where we can see numerous Bouma cycles. The samples of Stop 4 are textbook quality examples, so before discussing the Stops let us refer back to Bouma and its definitions.

Bouma (1962) defined this sequence as the product of continuous deposition from turbidity current. A complete Bouma sequence is a grain-size fining-upward succession of (a) massive or normally size-graded, sandy Bouma Ta division; (b) parallel laminated, sandy Bouma Tb division; (c) ripple/climbing-ripple laminated/convoluted, sandy Bouma Tc division; (d) parallel laminated to massive, silty

Bouma Td division, finally (e) silt-clay, often microfaumal-rich Bouma Te division (Fig.3.8).

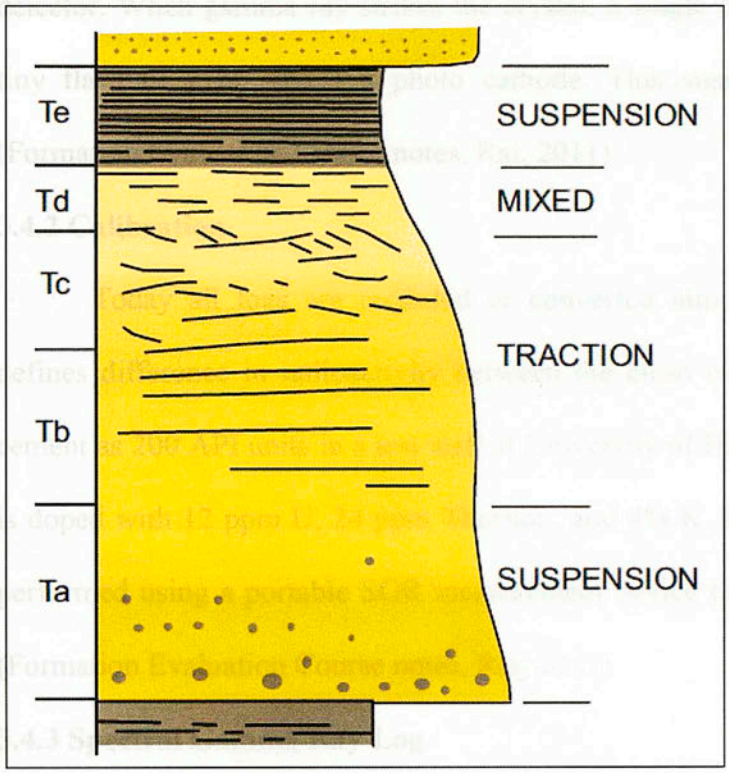


**Figure 3.8** Sediment grain size, structures, divisions, and sediment transport mechanisms of a complete Bouma sequence (Jordan et al. 1993).

### 3.4 Gamma Ray Measurements

Gamma ray tools measure the natural gamma ray emissions from rocks and afford a means for stratigraphic analysis and correlation. During propagation through rock, the gamma ray interacts with rock and loses energy by three processes: photoelectric effect, Compton scattering and pair production. All these processes lead to production of high energy electrons (Formation Evaluation Course notes, Rai, 2011).

### 3.4.1 Operation principle

All gamma ray tools use scintillation detectors that consist of sodium iodide detector. When gamma ray strikes the crystal, a single photon of light is emitted. This tiny flash of light strikes a photo cathode. This signal is amplified and recorded (Formation Evaluation Course notes, Rai, 2011).

### 3.4.2 Calibration

Today all logs are recorded or converted into API units. The API standard defines difference in radioactivity between the clean cement and radioactively doped cement as 200 API units in a test well at University of Houston. The radioactive cement is doped with 12 ppm U, 24 ppm Thorium, and 4% K. In our case, Field calibration is performed using a portable SGR measurement device that contains a radioactive 'pill' (Formation Evaluation Course notes, Rai, 2011).

### 3.4.3 Spectral Gamma Ray Log

The hand-held device RS-230 BGO Spectrometer used in the field is a radiation spectrometer which has a full assay capability with data in %K, ppm U, and ppm Th. The 6.3cu detector provides high sensitivity performance due to the large crystal with an energy response from 30 keV-300keV (User manual RS-230, Radiation Solution Inc.). The SGR- total gamma ray activity was calculated from the raw data with the following equation:

(SGR) $API=4C_{Th}+8\,C_U+C_K$

SGR logs and data have various advantages to describe and interpret petrophysically and geologically (Table 3.1). The following table shows qualitative and quantitative knowledge that one can benefit from SGR data.

In the field, the SGR device was used for the determination of the determination of semi-quantitative and qualitative analyses. The SGR has been used for defining condensed sections, understanding the lateral continuity of units and reservoir elements. Moreover, after studies on the SGR logs, the mineral content of shale units was characterized and in some cases to describe diagenesis.

| | Discipline | Used for | Knowing |
|---|---|---|---|
| Quantitative | Petrophysics | Shale volume ($V_{sh}$) | Th (max), Th (min) for pure shale |
| | | Radioactive mineral volume | $V_{sh}$ (Th), K (max), K (min) for shale |
| Semi-quantitative and qualitative | Geology | Dominant clay material | Th, K, U content of individual clay minerals |
| | | Detrital clay mineral suite | Radioactive content of individual clay minerals |
| | Sedimentology & Sequence Stratigraphy | Condensed section recognition from excess uranium | Normal U and Th content or Th/U ratio of shales |
| | | Climatic changes? | Th/K ratio changes in shale |
| | Reservoir geology | Fracture detection | Uranium contribution to radioactivity |
| | Geochemistry | Marine source rock identification | Uranium content of organic matter |

**Table 3.1** SGR data application examples (Formation Evaluation Course Notes, Rai, 2011). This thesis focused on the lithologic description of formations, the indentification of clay mineral suite, recognition of diagenesis, and determination of condensed section -if any present- .

## 4. FIELD STUDY AND INTERPRETATION

Following field reconnaissance, four workable outcrops were chosen. Field work included outcrop photography and description, measured sections, sample

selection, and analysis. All the stops consist of Kc formation, which is the youngest formation after Kd (Dias Formation) of the Cretaceous volcanoclastics in Hanover Inlier (Fig. 4.1).

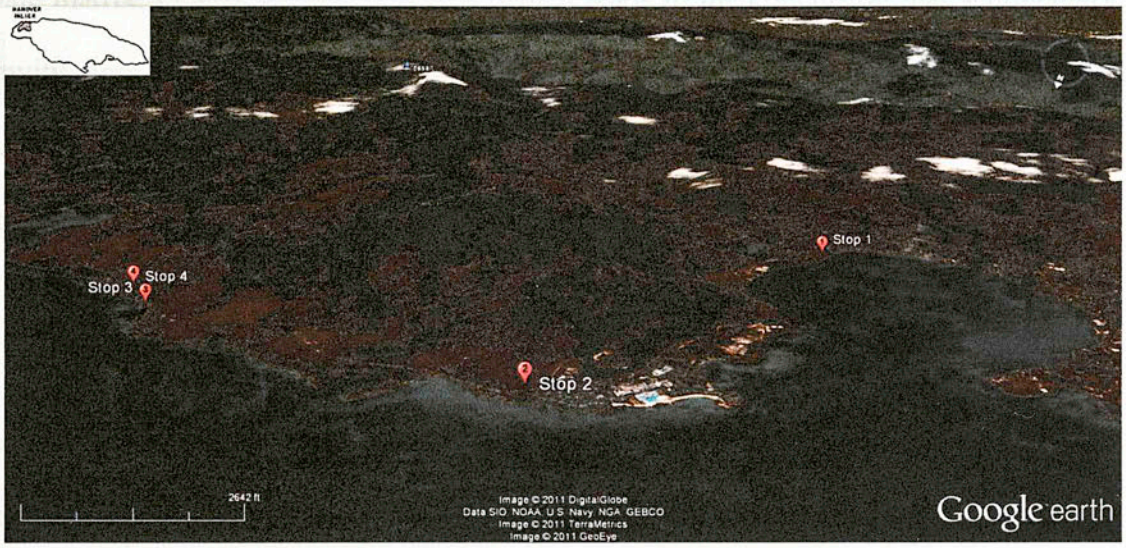


**Figure 4.1** The Locations of Stop 1, 2, 3, 4 and basalt outcrop generated with Google Earth. Stops start from Stop 1 located on Tom Pipers Bay on the right (west side), end with Stop 4 -located close to Sandy bay (east side).

### 4.1 Stop 1

The first outcrop chosen for analysis is located at 18°26'20.03"N latitude and 78° 9'25.29"W longitude. 16.35 meters of the north wall (north side of A1 main road) of the outcrop have been described and interpreted. On the outcrop, six stations (Station A to Station F) have been established for descriptions and SGR measurements. At this location Kc formation outcrop has dominantly lithified conglomerate beds at the lower parts, and the strata package generally consist of layered sand and silt beds. At some parts of the outcrop there are some thin shale units. (See appendix for station locations and descriptions).

At the bottom of the Station E (around 8$^{th}$ m over whole package interpreted), an erosional surface has been interpreted. Below the erosional surface conglomerate units are observed. The conglomerates consist of pebbles and cobbles surrounded by the shale matrix. Grains are poorly sorted, which leads to the conclusion that sedimentary gravity flow (SGF from now on) is debris flow at this lower section. There are also massive sandstone beds at the lower part, with high net:gross sand matrix, clean sand beds with moderately sorted medium size grains, and angular grains showing short distance transportation.

Truncated marker beds are clear evidence of an erosional surface. Adding to that, the erosional surface underlies a sandstone layer on the bottom of which there are remnants of older beds. Overlying beds of the erosional surface are dominantly sandstone and siltstone interbeding, and some thin shale units are also present. These beds consist of relatively lower net:gross sand with a silty matrix in sand layers. Grain size is fine to very fine, sorting is moderate to poor, and the grains have an angular shape.

One can interpret that, with the help of sedimentary descriptions and panoramic outcrop studies, below the erosion surface is an updip channel deposit with rapid flow. The deposition of conglomeratic units and medium to coarse grain massive sand beds are also evidence of updip channel deposit with rapid flow. The updip Channel abandons that location so an erosion surface is present at that location. A fan lobe sheet deposition starts to occur on top of the channel deposits (Fig. 4.2 and Fig. 4.3).

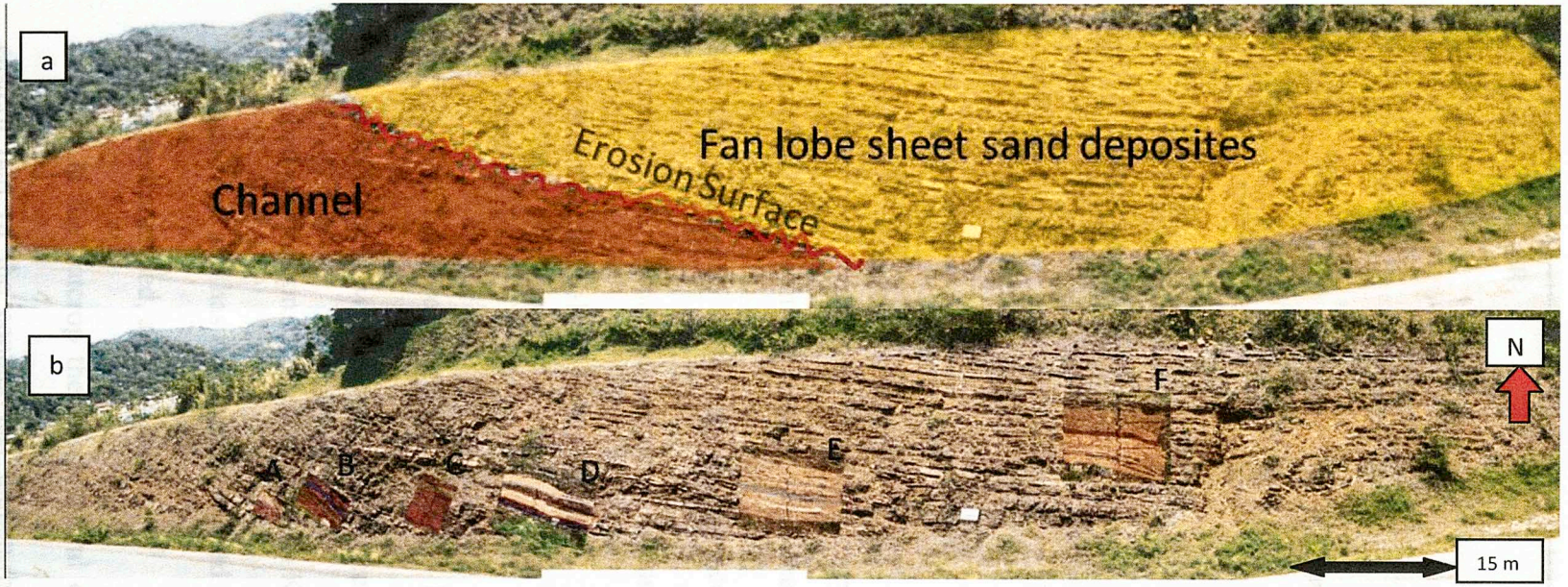


**Figure 4.2** Stop 1 panoramic images. Picture (a) shows interpretations on outcrop and (b) shows station locations. Due to rapid sediment flow, conglomerate units and massive sandstone beds are dominant in channel deposits. Truncated beds below indicate the erosion surface, which can be explained as channel abandoned the location. On top of the erosion surface a stack of layered sand is deposited, which can be elucidated as fan lobe sheet sand deposits. Some time after physical abandonment of the channel, the fan lobe sheet truncated part of the channel and then deposited the layered sand and silt interbeding.

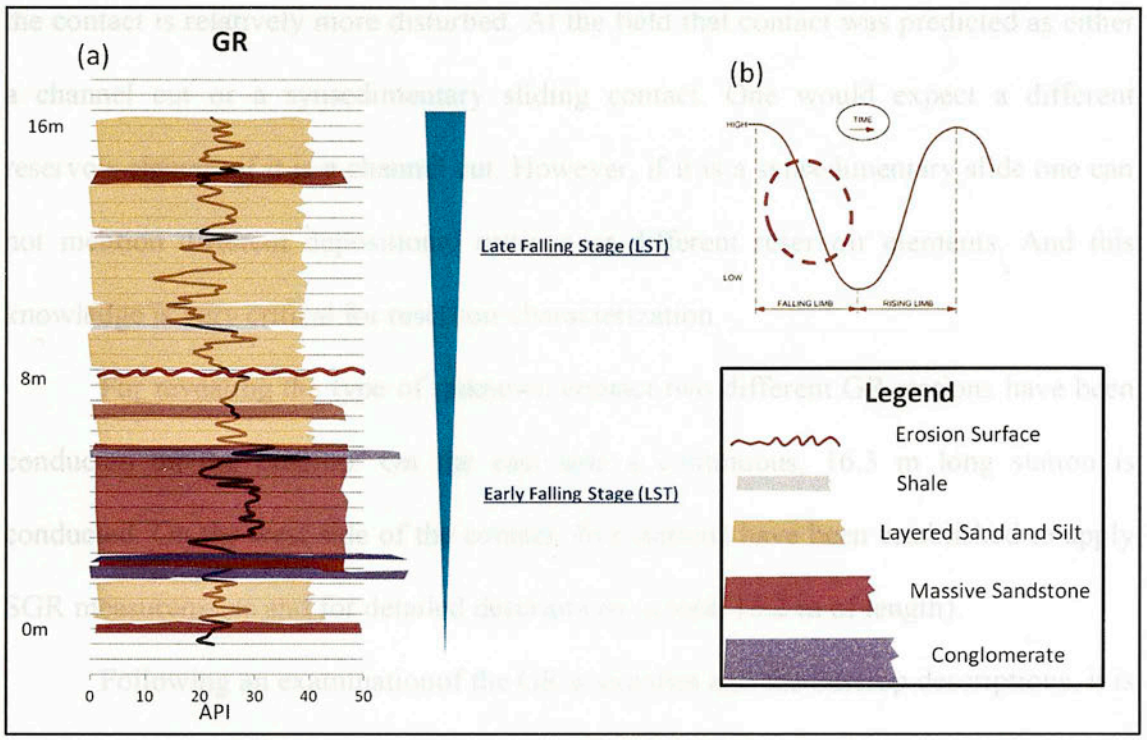


**Figure 4.3** Stop 1 interpretations. High energy Channel cut refers to a sea level fall, so that the lower part of the erosion surface, which is a channel deposit, reveals the information that deposition occurred in Early Falling Stage (LST). Fan lobe deposition indicates the Late Falling State (LST).

### 4.2 Stop 2

Stop 2 is located at 18°27'34.37"N latitude and 78° 8'48.24"W longitude. 16.30 meters of outcrop, which is exposed at the south side of the A1 main road, have been described and interpreted. At this location Kc formation outcrops at the south side of the A1 main road and has dominantly layered sand beds. Sand beds consist of moderately sorted medium sized, angular grains.

On the outcrop there is a lateral discontinuity separated by a listric contact. eastern part of the contact has undisturbed layered sand beds on top of a lateral accretionary unit (Fig. 4.4). However, beds stop on the listric contact, and west side of

the contact is relatively more disturbed. At the field that contact was predicted as either a channel cut or a synsedimentary sliding contact. One would expect a different reservoir element if it is a channel cut. However, if it is a synsedimentary slide one can not mention different depositional settings or different reservoir elements. And this knowledge is very critical for reservoir characterization.

For revealing the type of unknown contact two different GR stations have been conducted on the outcrop. On the east side a continuous, 16.3 m long station is conducted. On the west side of the contact, five stations have been established to apply SGR measurements and for detailed descriptions (a total 13.2 m of length).

Following an examinationof the GR anomalies and the outcrop descriptions, it is concluded that the listric contact is a synsedimentary sliding surface. There is a lateral accretionary unit (LAU) at the lower part of the Stop 2, which is very distinct at the eastern side of the wall, but is also present approximately twenty m away from the listric contact. Comparison of the two GR logs with the marker beds LAU indicates both the marker beds and the above GR log have similar anomalies (Fig. 4.5).

After concluding that the contact is a synsedimentary slide, one should conduct outcrop descriptions and interpretation. In this chapter, the study will be focused on the eastern station (Fig. 4.6). At the bottom part of the outcrop there is 2 m thick lateral accretionary unit. Sigmoidal shaped sand beds are interbedding with shale units. On top of the lateral accretionary unit, there are almost twelve meter thick layered sandstones. Thinningg upward packages (TUP) have been recognized throughout layered sandstones, and seven TUP have been interpreted (Fig. 4.6). Sandstone beds consist of

moderately to poor sorted, angular, medium to fine grains. Moreover, lower net:gross is observed, and the matrix is silt supported.

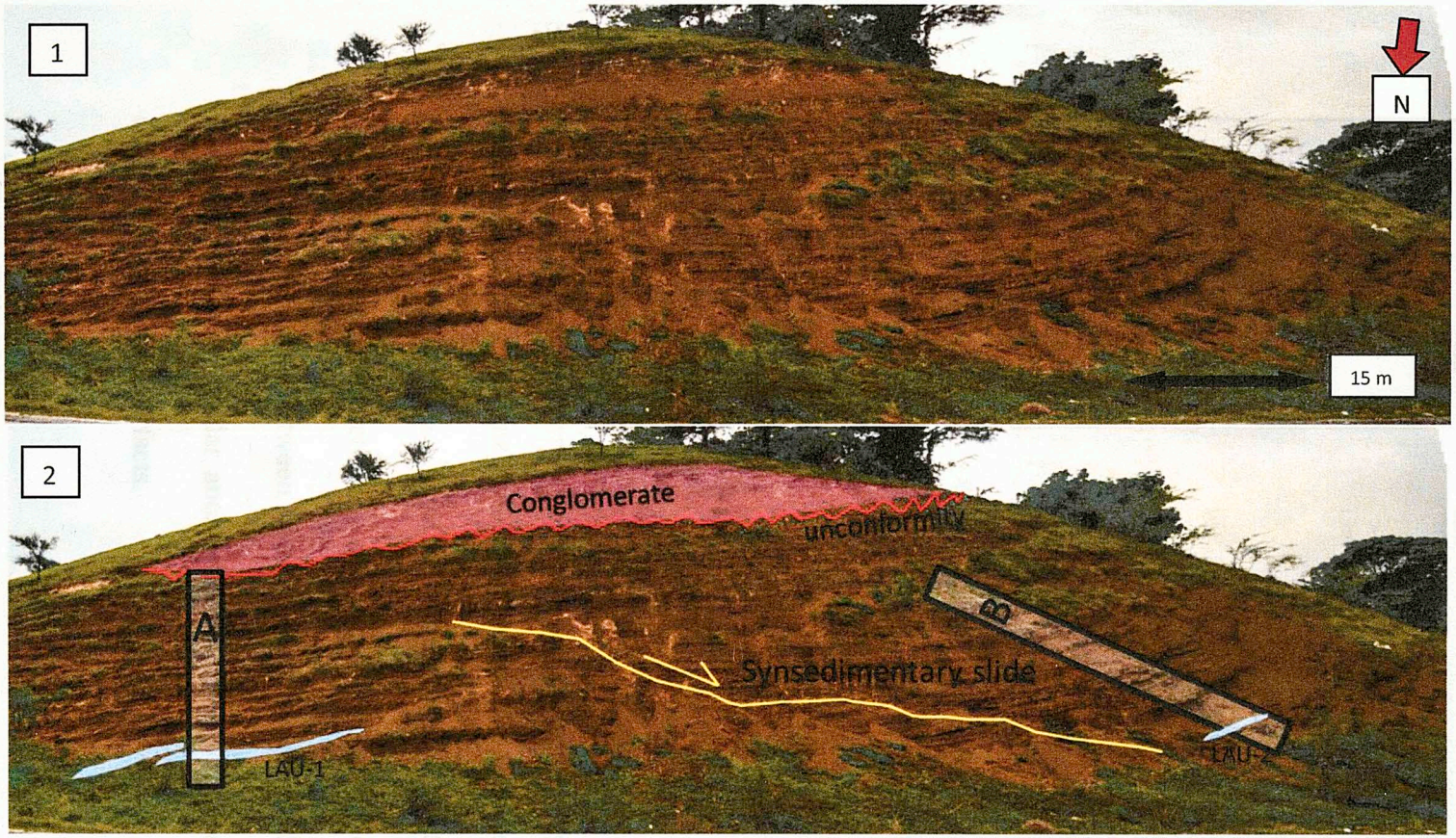


**Figure 4.4** Stop 2 panoramic images. Picture 1 shows an uninterpretted outcrop with the unknown contact in the middle. Picture 2 is mapped discontinuity with two station locations as Station A and Station B. Marker beds are lateral accretionary units (Lateral Accretionary Units-1 and Lateral Accretionary Units-2). Above the contact, layered sand beds are continuous with no distortion, and they underlay uncomfortably a thick conglomerate section.

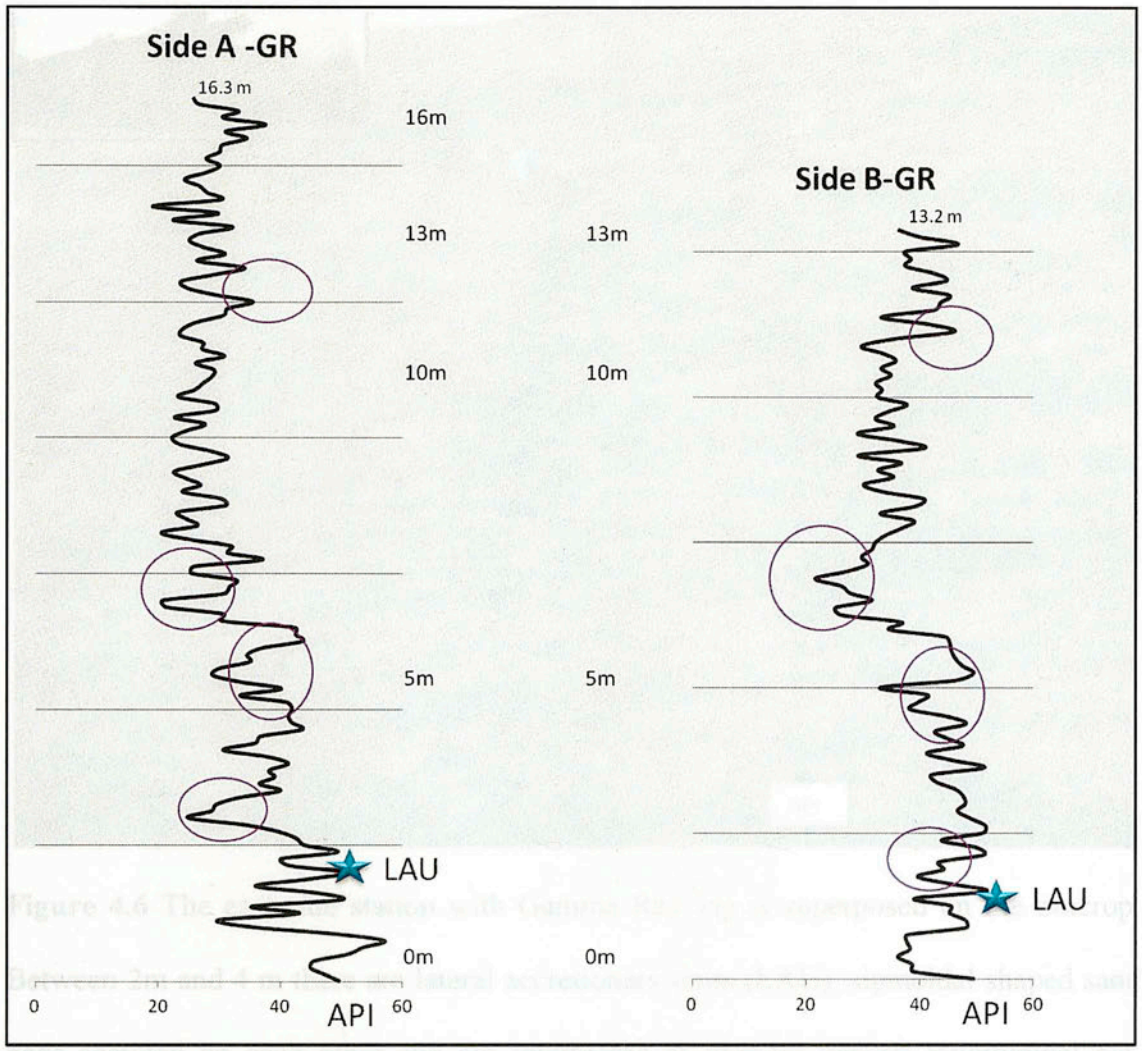


**Figure 4.5** Stop 2 Gamma Ray logs. Station A is the main station on the east side and the Station B is western part of the discontinuity (the Gamma Ray logs are scaled). LAU are the lateral accretionary units described in the field. See the purple circles and the anomaly relations between, above, and below the circles. Two different Gamma Ray Stations have very similar anomalies. The slight differences may be related to field Gamma Ray logging artifacts.

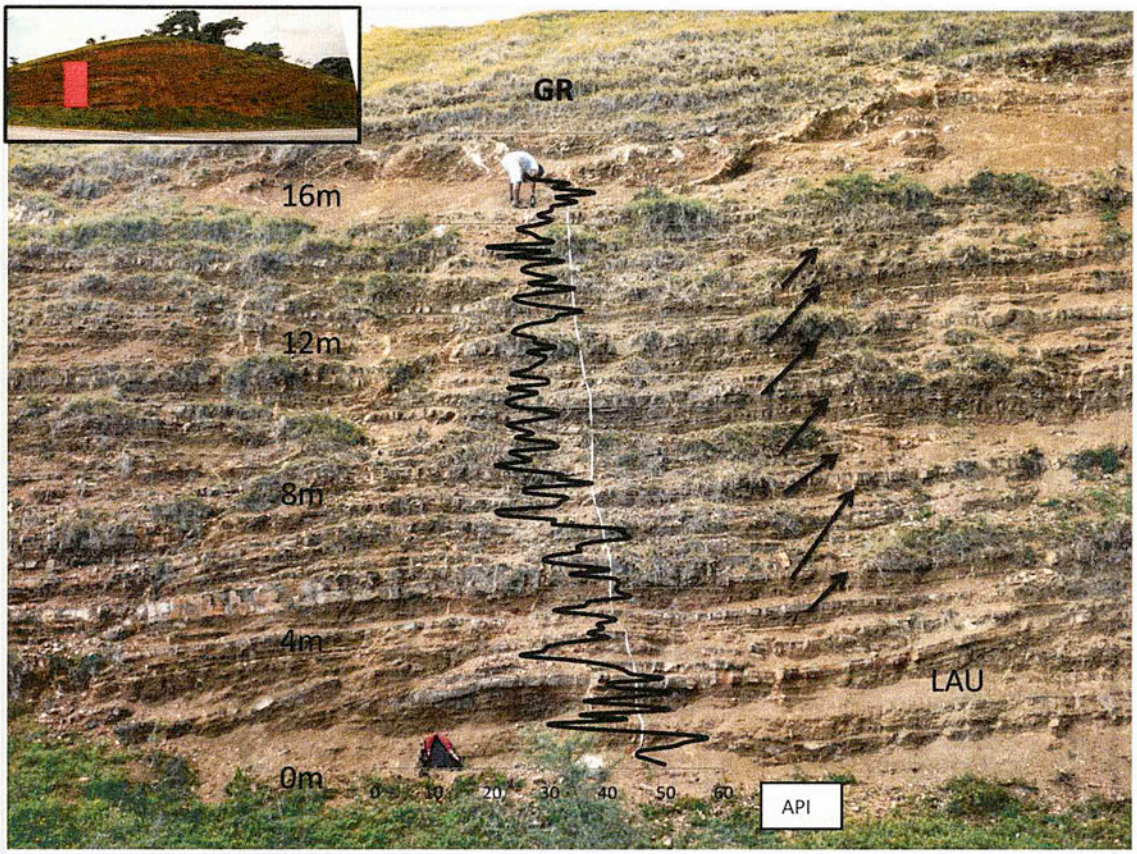


**Figure 4.6** The east side station with Gamma Ray log is superposed on the outcrop. Between 2m and 4 m there are lateral accretionary units (LAU), sigmoidal shaped sand beds accreted on each other and are interpreted as channel deposit longitudinal cut. Arrows are showing the Thinning Upward Packages. Thinning Upward Packages consist of layered sand beds gradually becoming finer from bottom to the top as energy wanes. They may be related to distal fan lobe deposits as a reservoir element (Slatt, 2006).

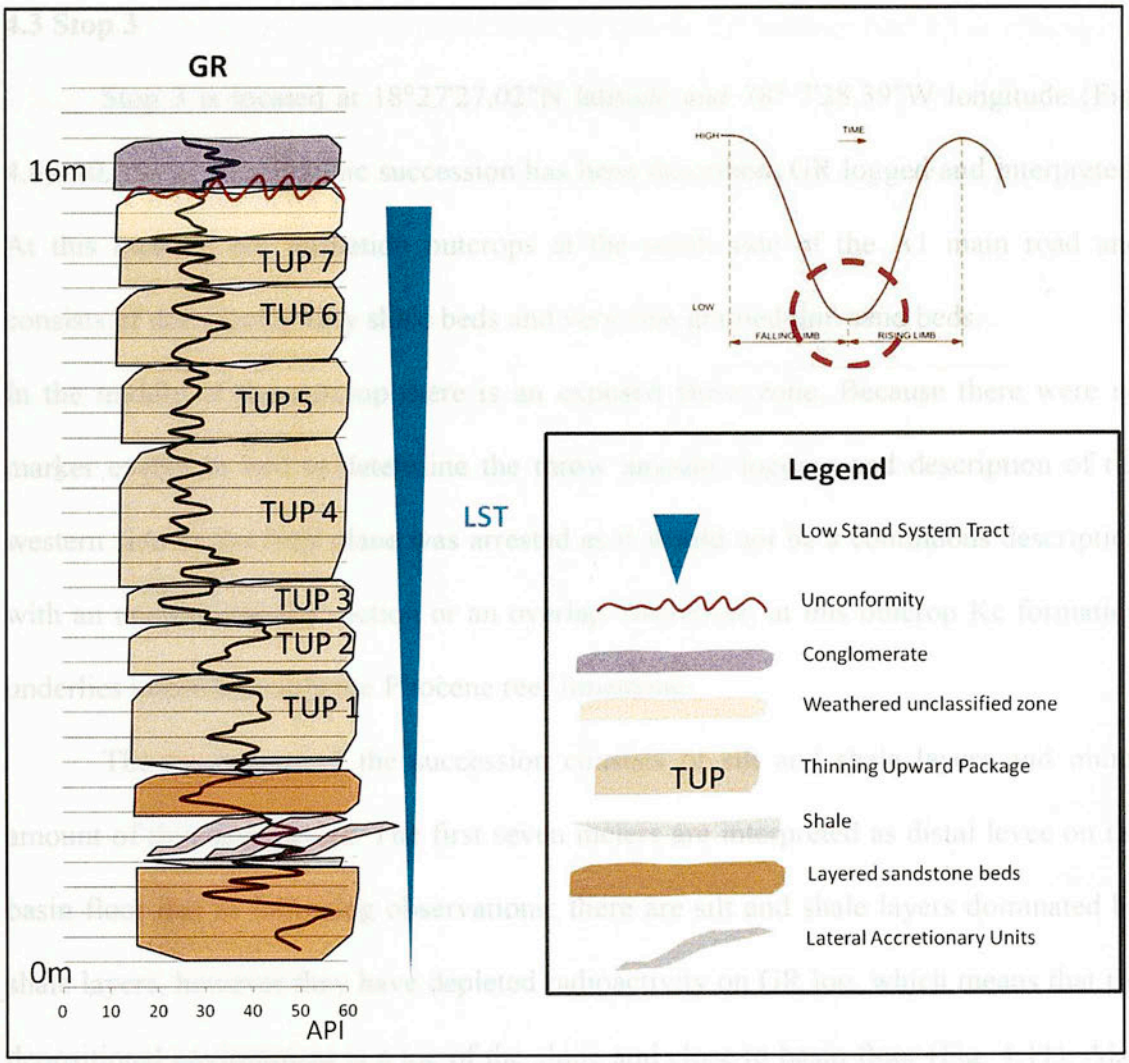


**Figure 4.7** Stop 2 interpretations. On top of a thick layered Sandstone layer, there is a, 2 m thick, lateral (sigmoidal) accretionary unit. On top of lateral accretionary units, seven different thinning upward packages have been interpreted. Conglomerate unit overlays uncomformably on the thinning upward packages. The lateral accretionary units are interpreted as a longitudinal cut of a channel downdip, on top of which there are seven pulses of distal fan lobe deposits as thinning upward packages. The system is interpreted as Turnaround stage of Lowstand Systems Tract.

### 4.3 Stop 3

Stop 3 is located at 18°27'27.02"N latitude and 78° 7'28.39"W longitude (Fig. 4.8). 10.2 m of stratigraphic succession has been described, GR logged and interpreted. At this location Kc formation outcrops at the south side of the A1 main road and consists of dominantly silty shale beds and very fine grained thin sand beds. In the middle of the outcrop there is an exposed shear zone. Because there were no marker events or bed to determine the throw amount, logging and description of the western side of the fault plane was arrested as it would not be a continuous description with an unclear missing section or an overlap. Moreover, at this outcrop Kc formation underlies unconformably the Pliocene reef limestone.

The lower part of the succession consists of silt and shale layers and minor amount of thin sand layers. The first seven meters are interpreted as distal levee on the basin floor due to following observations; there are silt and shale layers dominated by shale layers, however they have depleted radioactivity on GR log, which means that the depositional environment is a toe of the slope and close to basin floor (Fig. 4.11). Also thin sand layer can be interpreted as levee deposits. They may indicate the pulses of relatively rapid sedimentation, which might be related to earthquakes or other sedimentation pulses.

The upper three meters are generally thin layered sand beds that are mostly fine grained sand beds. It is hard to give sorting or grain shape information due to fine to very fine sized grains. Dominantly thin sand layers refer to more proximal levee deposits, relative to lower succession.

According to descriptions and analysis above, the outcrop may be interpreted as a levee deposit where the lower part is the distal levee and upper part represents the proximal levee (Fig. 4.9). The levee deposits are correlated with turnaround stage of Lowstand Systems Tract (Slatt, 2006).

To gain further information, there is another study about describing the mineralogy of the shale layers. Th(ppm) vs K (%) chart gives the mineralogy of the formation. In this case, there are dominantly glauconite minerals in this formation at that location (Fig. 4.10).




**Figure 4.8** Stop 3 panoramic images. P(A) shows an uninterpreted panoramic picture. P(B) shows Pliocene Reef Lst overlaying the Kc formation unconformably. Yellow lines are fault planes and between two fault planes there is a shear zone, in which the units are densely folded and distorted. One can observe the drag fold on the east side of the fault zone and fault bend fold on the west side of the fault zone. 10.2 meters of descriptions, Gamma Ray logs and interpretation have been conducted inside the box shown in picture 2.

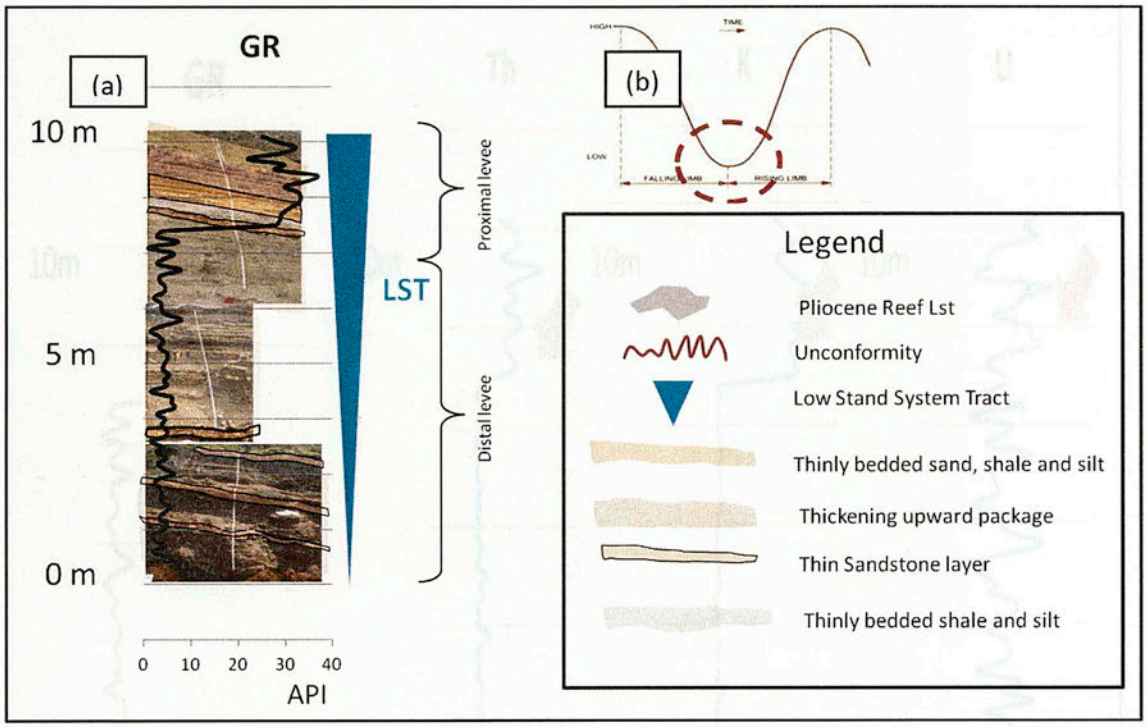


**Figure 4.9** Stop 3 interpretations. Gamma Ray log superposed on outcrop and lithology (shown at side (a)). The lower 4 meters consist of dominantly thinly bedded shale and silt; however there are several intervals of thin sand beds. On top of which there are another three meters of thinly bedded shale and silt deposition. This part is interpreted as distal levee deposits. The upper three meters are dominantly thin bedded sand units. A thinning upward package of sand beds is observed at that interval. The upper part is interpreted as proximal levee deposits. The overall sequence stratigraphic stage has been determined as the Turnaround stage of Lowstand Systems Tract (shown at side (b)).

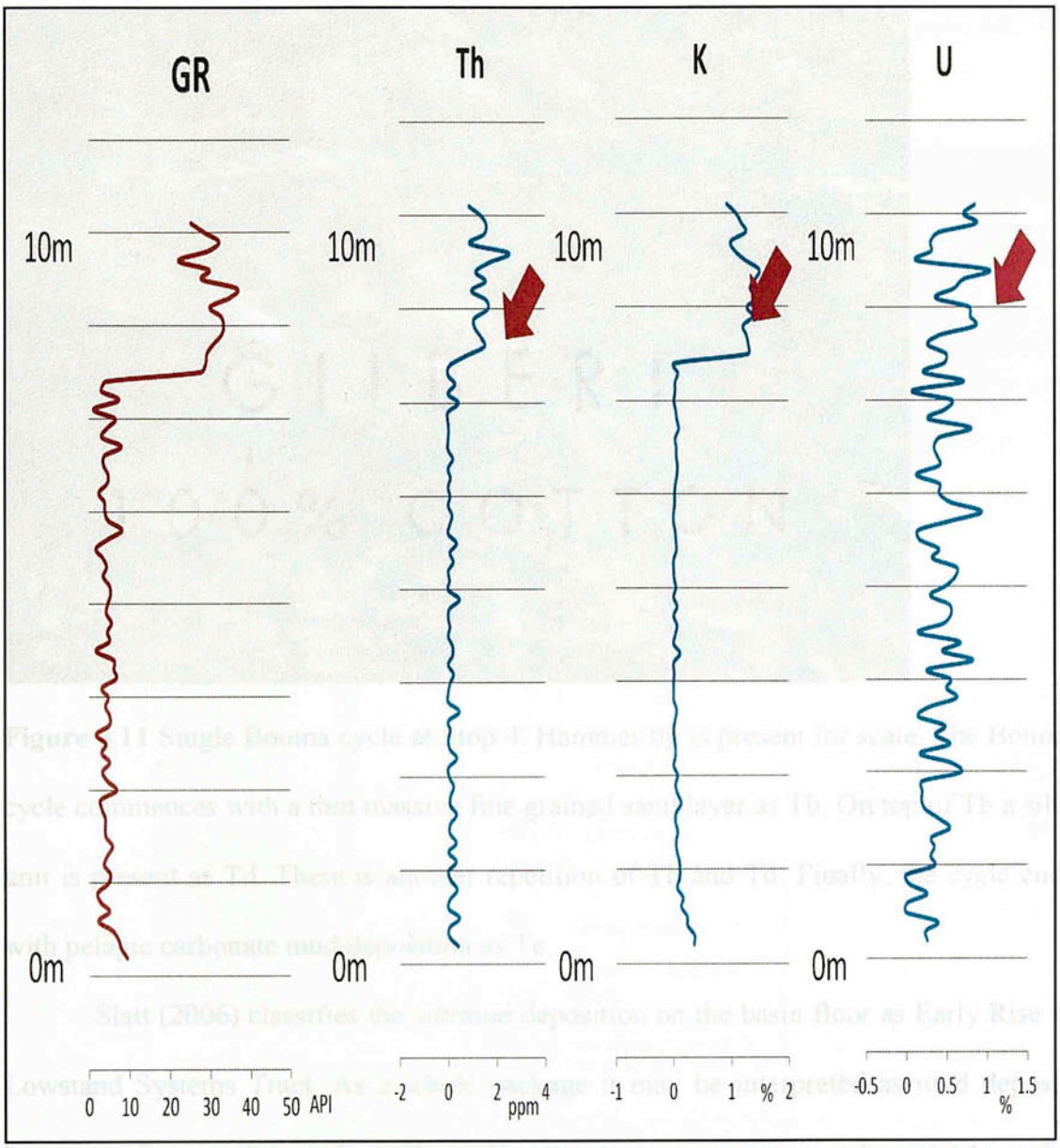


**Figure 4.10** Stop 3 Gamma Ray, Th, K, U logs. Although the formation is continuous without any unconformity or structural discontinuity, there is a high kick starting from 7m to 10 m. That anomaly comes from Th and K contents, which is explained by lithologic change from thin silt and shale layers to sand layers.

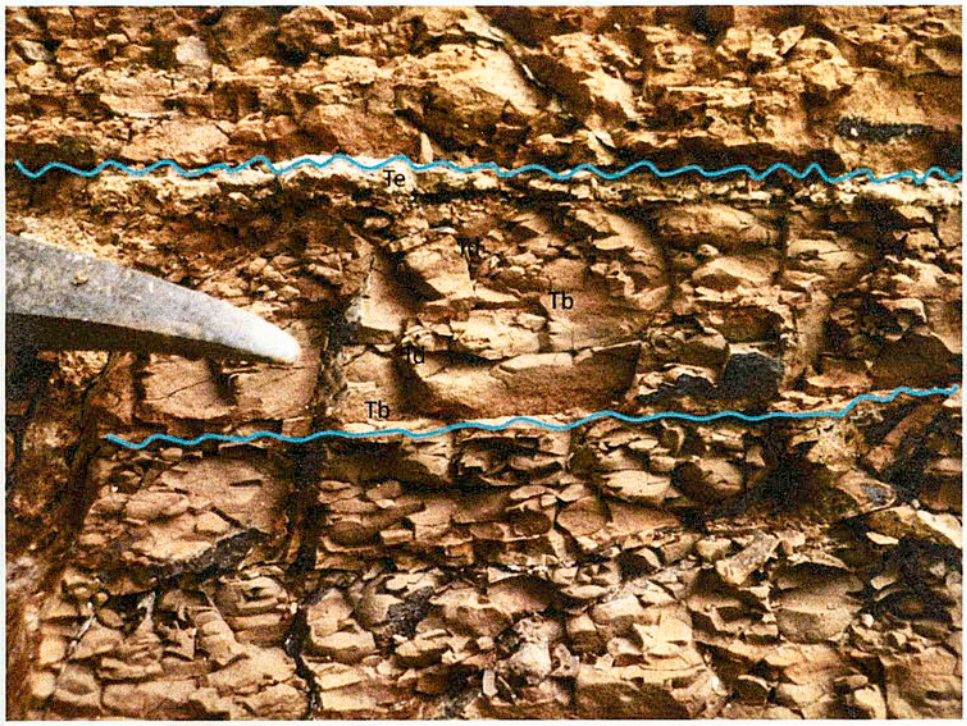


**Figure 4.11** Single Bouma cycle at Stop 4. Hammer tip is present for scale. The Bouma cycle commences with a thin massive fine grained sand layer as Tb. On top of Tb a silty unit is present as Td. There is another repetition of Tb and Td. Finally, the cycle ends with pelagic carbonate mud deposition as Te.

Slatt (2006) classifies the silt/mud deposition on the basin floor as Early Rise of Lowstand Systems Tract. As a whole package it may be interpreted as mud deposit, however after careful study each cycle appears to represent a sedimentation pulse bounded by Te suspended loads. The environment can be interpreted as the toe of depositional lobes on basin floor, because of very thin sand layers and thin Bouma cycles. Moreover the Bouma cycle is also defined with respect to sedimentary gravity flow type as long distance deposition. In addition to that, thin beds refer to the distal part of the deposition lobes and distal levee depositions. In the light of these facts, this

study suggests Stop 4 is a mud deposition on basin floor or the toe of a deposition lobe with 26 Bouma cycles as a part of Early Rise Stage of Low Systems Tract.

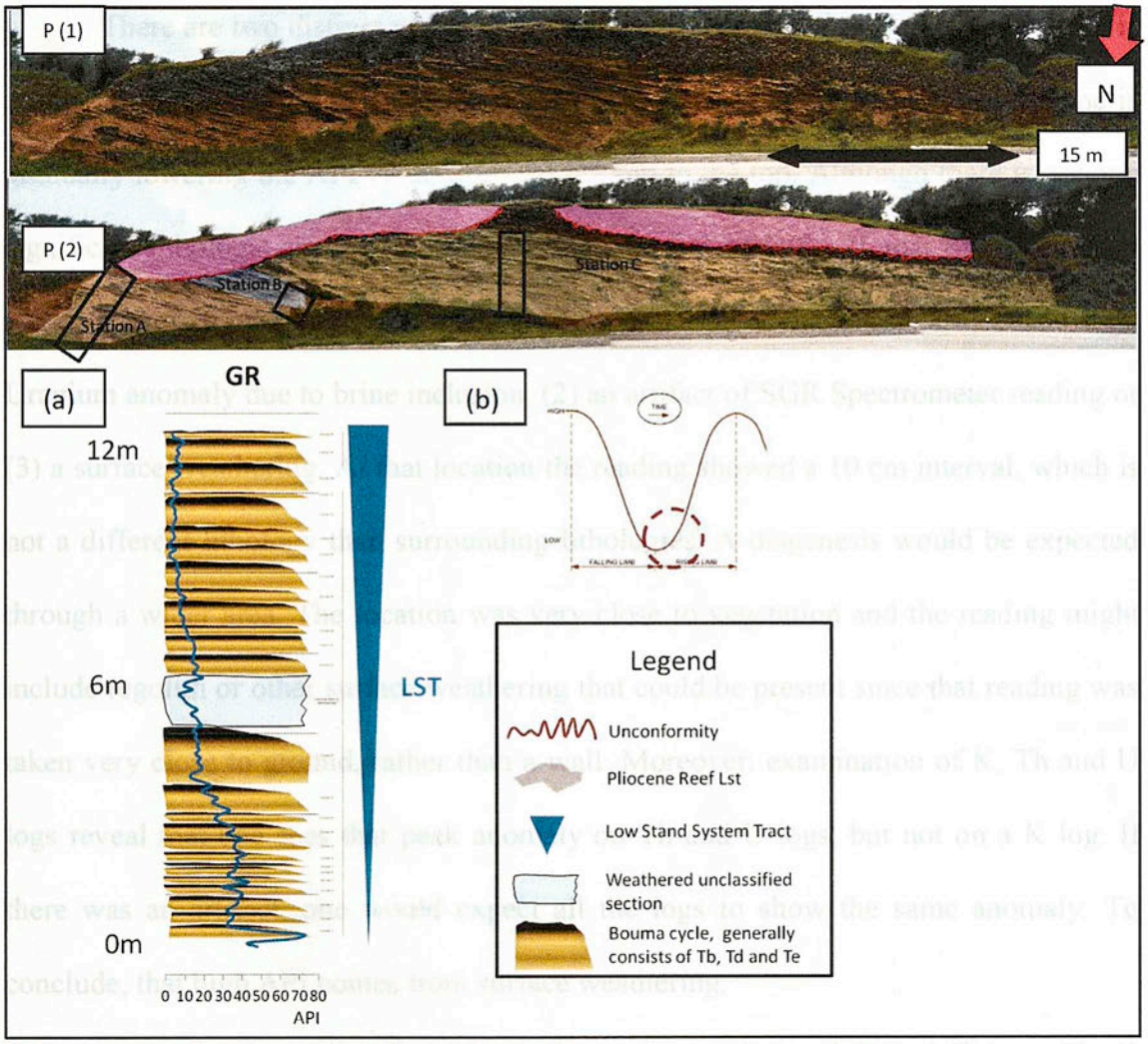


**Figure 4.12** Stop 4 interpretations. P (1) shows uninterpreted panoramic photo of Stop 4. P (2) shows the station locations covering the stratigraphic package and Pliocene Reef Lst overlaying unconformably the Kc formation. Part (a) of the Figure there is GR lof superposed on stratigraphic description. 26 different Bouma cycles have been interpreted on the outcrop. Each Bouma cycle consist of Tb, Td and Te throughout the outcrop. Fine grained Turbidites are associated with distal depositional lobes on the

basin floor. Moreover mud deposition to basin floor is classified as Early Rise Stage of Low Systems Tract.

There are two distinct anomalies on GR to study at this location. The first one is at the bottom of the log as a high kick API in a small interval, and the second one is gradually lowering the API value from the bottom to the top. Although there is not any significant lithologic change surrounding the high peak of GR API, that anomaly is still there. There can be three scenarios for this fact: (1) a diagenesis can cause high Uranium anomaly due to brine inclusion, (2) an artifact of SGR Spectrometer reading or (3) a surface weathering. At that location the reading showed a 10 cm interval, which is not a different lithology than surrounding lithologies. A diagenesis would be expected through a wider area. The location was very close to vegetation and the reading might include regolith or other surface weathering that could be present since that reading was taken very close to ground, rather than a wall. Moreover, examination of K, Th and U logs reveal that one sees that peak anomaly on Th and U logs, but not on a K log. If there was an artifact, one would expect all the logs to show the same anomaly. To conclude, that high API comes from surface weathering.

Secondly, the gradual low GR reading is observed at each K and Th logs. The K and Th content of the formation are responsible for the grain size and that can be associated with primary porosity. The lower API reading on the log means coarse grains and higher porosity values. That knowledge is important with respect to reservoir characterization, as well as high order sequence stratigraphy applications. Although field study did not reveal any information about porosity change along the Stop 4, GR reading implies that Kc formation is cleaning upward on Stop 4.

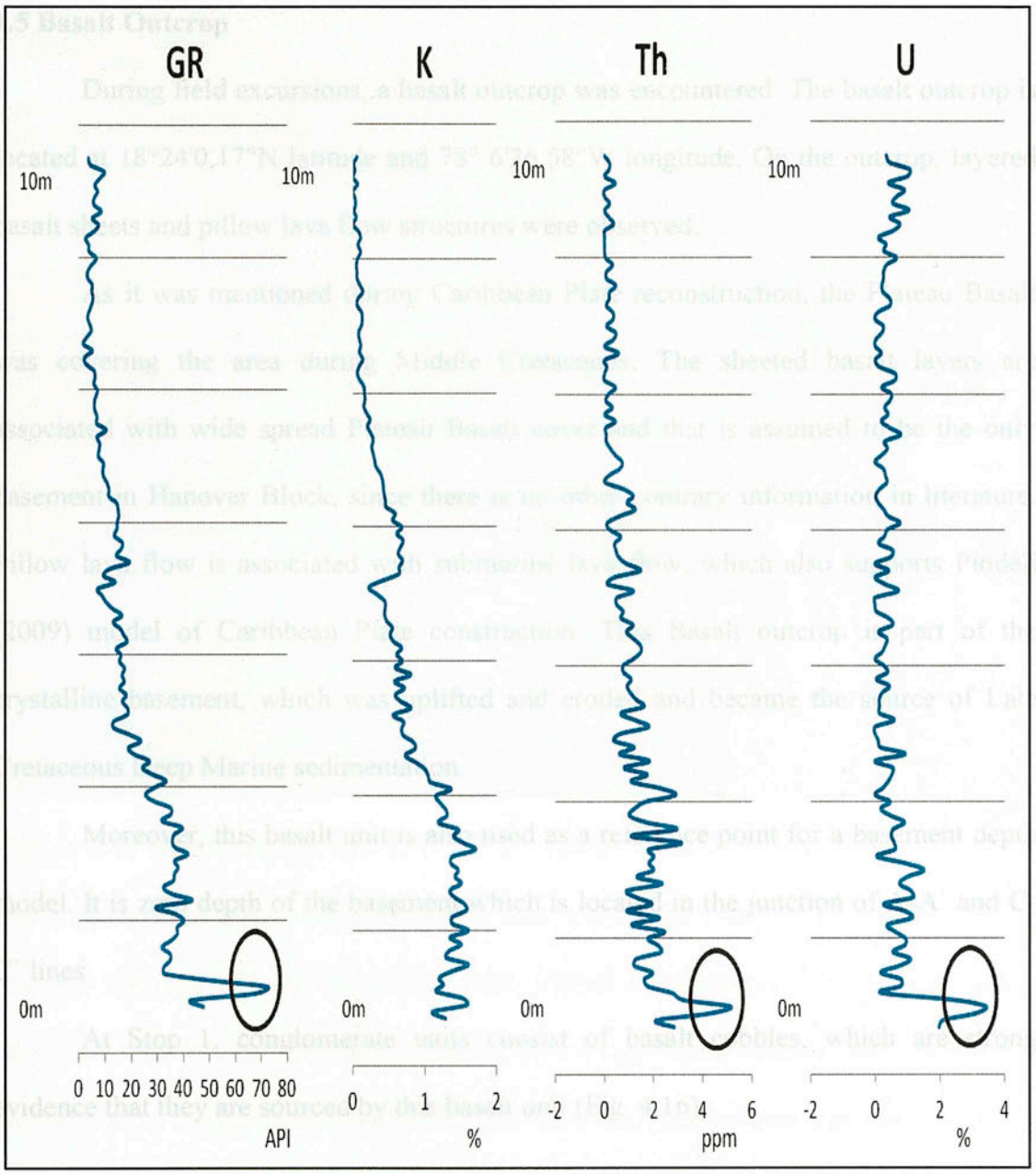


**Figure 4.13** Stop 4 GR, K, Th, U logs. Surface weathering, at the bottom of the outcrop, which is located in the field almost at the base, causes the high anomaly of API on GR log

## 4.5 Basalt Outcrop

During field excursions, a basalt outcrop was encountered. The basalt outcrop is located at 18°24'0.17"N latitude and 78° 6'26.58"W longitude. On the outcrop, layered basalt sheets and pillow lava flow structures were observed.

As it was mentioned during Caribbean Plate reconstruction, the Plateau Basalt was covering the area during Middle Cretaceous. The sheeted basalt layers are associated with wide spread Plateau Basalt cover and that is assumed to be the only basement in Hanover Block, since there is no other contrary information in literature. Pillow lava flow is associated with submarine lava flow, which also supports Pindell (2009) model of Caribbean Plate construction. This Basalt outcrop is part of the crystalline basement, which was uplifted and eroded and became the source of Late Cretaceous Deep Marine sedimentation.

Moreover, this basalt unit is also used as a reference point for a basement depth model. It is zero depth of the basement which is located in the junction of A-A` and C-C` lines.

At Stop 1, conglomerate units consist of basalt cobbles, which are strong evidence that they are sourced by this basalt unit (Fig. 4.16).




**Figure 4.14** Basalt outcrop and Stop 1. P (1) (Bora Yalcin is present as scale) Sheeted basalt outcrop has been discovered in the inner part of the Hanover Block which is the possible sourcing of Late Cretaceous Deep Marine Sedimentation. P (2) is an image map with scale where a star shows the location of the basalt outcrop, and the circle is the location of conglomeratic unit at Stop 1. P (3) is a conglomerate unit that consists of basaltic pebbles and cobbles (hammer is present as scale). Conglomerate with basaltic pebbles and cobbles are the proof that the sedimentation of Kc formation is sourced from basaltic crystalline basement.

### 4.6 Sedimentary Gravity Flow Type Comparison of Outcrops

The sedimentary gravity flow type determination is important for the diagnosis of a depositional system's reservoir architecture and paleoenvironment. The Walker

(1978) classification has been used in this study to differentiate the flow processes throughout the stops that have been studied in the field (Fig. 4.17).

Stop 1 consists of conglomeratic units at the bottom in the channel deposit and massive sandstone beds in the fan lobe sand deposit. The conglomeratic unit includes unsorted cobbles and pebbles inside a clay matrix. According to Walker (1978), it can be interpreted that this deposit is classified as a Debris Flow with the matrix strength support mechanism. Moreover, sandstone beds without any sedimentary structure lead one to classify the sedimentary gravity flow type as Massive Sandstone with intermediate to long distance transportation with fluid turbulence and dispersive pressure support mechanisms, respectively.

At Stop 2 layered sand beds also share the same Sedimentary Gravity Flow process as Stop 1 massive sand layers do.

At Stop 3 and Stop 4 mud deposition can be associated with the Classical Turbidites. Fluid turbulence accompanied by the low concentration turbidity current and finally traction results in the Classical Turbidites deposition. The deposition at Stop 3 and Stop 4 also display late stages of deposition, that is to say, longest distance transportation according to Walker (1978).

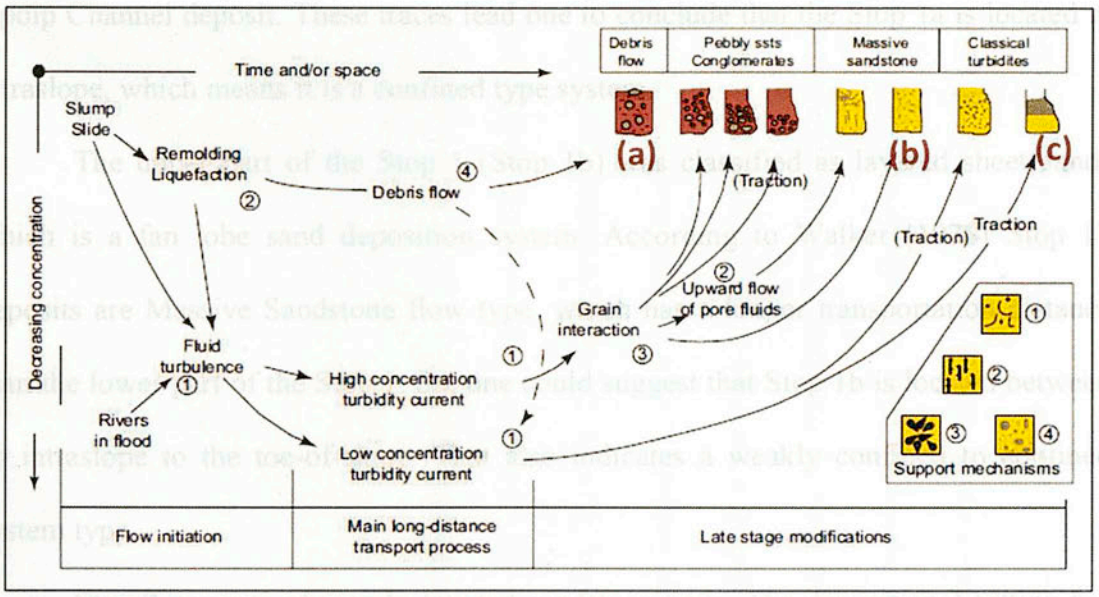


**Figure 4.15** Modified Walker sedimentary gravity flow process classification (1978). Stop 1a consists of poorly sorted conglomeratic units, represented here as Debris Flow (a). Stop 1b and Stop 2 consist of dominantly layered sand sheets, represented here as Massive Sandstone (b). Stop 3 and Stop 4 consist of mainly silt and mud deposits, represented here as Classical Turbidites (c).

### 4.7 General Stratigraphic Architecture and Relative Positions of Studied Outcrops

Beaubouef (2008, unpublished) suggested reservoir architecture related to the position of the deposition along the continental slope and in the basin floor (Fig. 4.18). Former classification already defined the transportation distance and gravity flow type. Moreover, outcrop studies revealed the depositional systems of each stop. One can apply Beabouef's study to understand and discuss the relative positions of each stop beyond the shelf edge all the way to the Basin Floor/Abyssal Plain. It also suggests the system type for each interval of the continental slope.

The lower part of Stop 1 (Stop 1a) was classified as the shortest transportation distance due to its debris flow process type. In addition, the deposit is defined as an

Updip Channel deposit. These traces lead one to conclude that the Stop 1a is located in intraslope, which means it is a confined type system.

The upper part of the Stop 1 (Stop 1b) was classified as layered sheet sands which is a fan lobe sand deposition system. According to Walker (1978) Stop 1b deposits are Massive Sandstone flow type, which has a longer transportation distance than the lower part of the Stop 1. So, one could suggest that Stop 1b is located between an intraslope to the toe-of-slope. That also indicates a weakly confined to confined system type.

Stop 2 consists of mainly layered sandstone beds. The depositional setting has been defined as a downdip channel, because the thinning upward packages are referring to distal fan lobe deposites. They are generally positioned downdip of channels. According to Beaubouef (2008), it is classified as a toe-of-slope with a weakly confined system.

Stop 3 has been interpreted as distal and proximal levee deposits. The silt and mud deposit at that location can also be classified as Classical Turbidites without Bouma cycles according to Walker (1978). That points one to interpret longer distance transportation relative to Stop 2. It indicates that, according to Beaubouef (2008), Stop 3 is located between the toe-of-slope and the basin floor.

Stop 4 is a classical turbidite with textbook examples of Bouma Cycles. That is the longest transportation distance according to Walker (1978). Moreover, it has been interpreted as a distal fan deposit, which could be located in the basin floor.

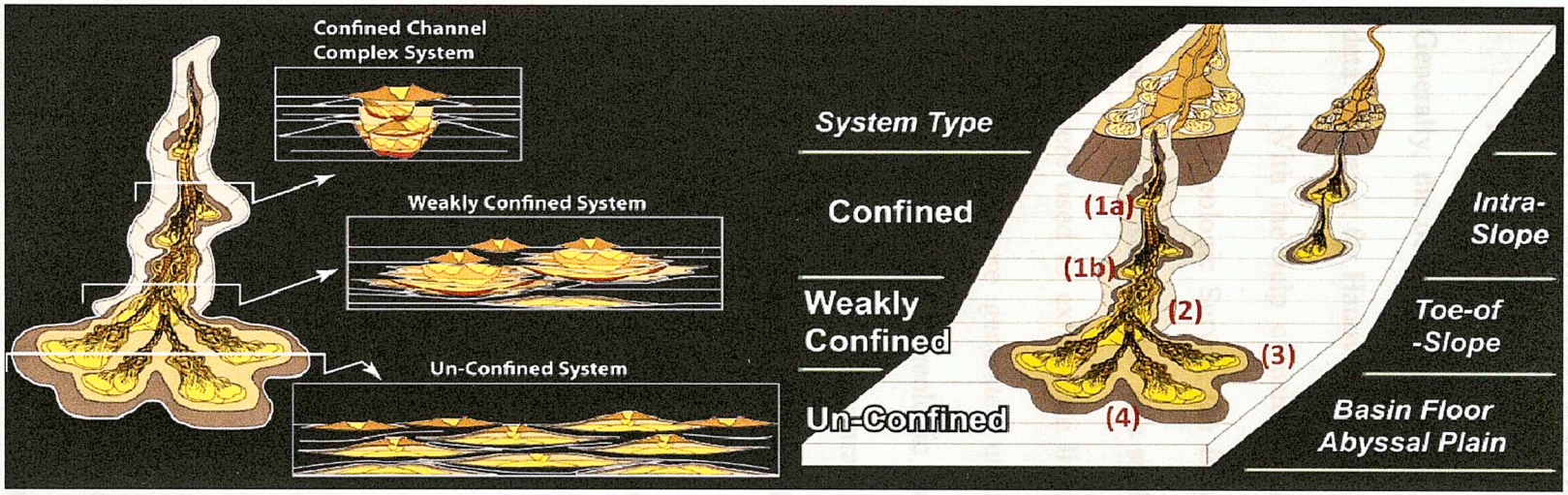


**Figure 4.16** Modified Beabouef`s (2008) illustration is shown to understand and discuss the relative positions of each stop between shelf edge and the Basin Floor/Abyssal Plain. The lower part of Stop 1 (Stop 1a) was classified as the shortest transportation distance and updip channel deposit. So Stop 1a is located in the intraslope with a confined system type. The upper part of the Stop 1 (Stop 1b) was classified as layered sheet sands, which is a fan lobe sand deposition system with massive sandstones. Therefore Stop 1b is a longer transportation distance than Stop 1a. So, Stop 1b is located between the intraslope to toe-of-slope with a confined to weakly confined system. Stop 2 is a crevasse splay downdip channel deposit, and it is located at the toe-of-slope with a weakly confined system. Stop 3 is interpreted as distal and proximal levee mud and silt deposit, and is located between the toe-of-slope and basin floor with a weakly confined system. Stop 4 is a classic turbidite (distal fan) deposit with the longest transportation distance and it is located on the basin floor with an unconfined system.

## 5. GRAVITY MODELING AND BASEMENT DEFINITION

In order to perform a basin analysis, the depth of the basement must be known. Generally, the best methodology is to determine the basement from seismic and well data. However, for Hanover Inlier no such data exists.

With the help of using a regional Bouguer anomaly map published by the Jamaican Geologic Survey, the Bouguer anomaly data can be used to determine the depth of the basement. For this study a combination of published data and published maps were used to extrapolate lithologic formation and facies into subsurface. Five cross-sections were generated using a combination of densities of the published formation, a published geologic map and a published gravity map. The Bouguer anomaly data were used to constrain the cross-sections. The fundamental theory behind the methods used is described in the following section.

### 5.1 Bouguer Anomaly

Free-Air Correction: The free-air correction which is added to the measured gravity value to correct it to sea-level value is calculated in equation 5.1 (Fowler, 1990).

**Equation 5.1** Free air correction formula. Where, is the free air-correction, is the measured gravity, is the gravity at elevation *h*, and R is the radius of the Earth.

As gravity decreases with height above the surface, points above sea level are corrected to sea level by adding . This correction amounts to $3.1\times 10^{-6}$ m $s^{-2}$ per meter of elevation. A detailed equation with a high accuracy of this correction can be made by

using McCullagh`s formula for the gravitational attraction of the rotating spheroid (Eqn. 5.2).

**Equation 5.2** McCullah`s formula for the gravitational attraction of rotating spheroid. is the free-air anomaly, is the observed or measured gravity value, is the latitude variation correction, and is the free-air correction (Fowler, 1990)

Bouguer plate correction compensates for the effect of a layer of rock whose thickness corresponds to the elevation difference between the measurement and the reference levels, and it compensates for the gravitational attraction of the rocks between the measurement point and sea level.

Combining the free air, Bouguer plate, and terrain corrections together allows the Bouguer anomaly to be calculated as (Eqn. 5.3):

**Equation 5.3** The Bouguer anomaly. is the Bouguer anomaly, is the free air anomaly, is the Bouguer correction, is the terrain correction, is the observed or measured gravity value, is the latitude variation correction, and is the free air correction (Fowler,1990).

## 5.2 Basement Depth Modeling Using the Bouguer Anomaly

Since the Bouguer anomaly corrects the elevation change and is, thus, unaffected by surface elevation changes; it can be used to determine the depth to igneous basement. Bouguer gravity maps principally show three things considering the basin: (i) change in depth of the igneous basement rocks, (ii) change in density of either the crusta basement rocks or overlying strata, or (iii) existence of an igneous intrusion.

As we know stratigraphicaly the Hanover inlier consist of the oldest clastics on top of the basement and there is not additional data to know whether the change in the Bouguer anomaly is controlled by a change in the depth of the basement or density of the basement or sedimentary rocks. A simplistic assumption has been used in this model as a change in depth of the basement rocks and with density for all formations staying constant.

In this model Late Cretaceous sediments have an average density value of 2.62 g/cm$^3$ and the Crustal Basement have an average density value of 2.82 g/cm$^3$ (Table 5.1). There is no intrusion documented in literature or explored during the field excursion. Densities for the rock layers are found from published data by Wadge et al. (1983).

**Saturated bulk rock densities of representative samples from the main lithological types in eastern Jamaica.**

| Rock Type | Average Density kg m$^{-3}$ | Number of Samples | Range kg m$^{-3}$ |
|---|---|---|---|
| Blueschists | 2990 | 10 | 3080–2760 |
| Basalts | 2820 | 5 | 2930–2710 |
| Granodiorite | 2720 | 5 | 2750–2689 |
| Cretaceous sandstones, shales, tuffs | 2620 | 5 | 2690–2550 |
| Cretaceous conglomerates | 2710 | 4 | 2850–2540 |
| Tertiary sandstones shales | 2590 | 4 | 2680–2500 |
| Tertiary limestones | 2610 | 15 | 2670–2510 |

**Table 5.1** Jamaican rock density values (Wadge, 1983). The values were incorporated into the GM-SYS (PRO) software. Since Hanover inlier only consists of Cretaceous volcanoclastic sediments and the basement is Basalt; Cretaceous sandstones, shales, tuffs average density value and Basalts average density values were used.

Each cross-section (Fig. 5.1) is generated separately in GM-SYS (PRO), developed by Northwest Geophysics Association. To obtain a high resolution, extracted gravity anomalies interpolated between each adjacent value along the cross section lines. In this case, published well control, seismic data and published cross-section

interpretations are lacking. Moreover, as the structural geology of the area has been only coarsely studied and almost all fault plane interpretations are based on Geomorphology, these facts limiting the resolution of the generated cross-sections which show only the basement depth relations. When the observed gravity transect fits that calculated with < 1% error, the geologic model is considered to be adequate. Thus only simple models are exhibited which can be improved if subsequent information (lithology, density, etc.) is provided (Fig. 5.2 to Fig. 5.6).

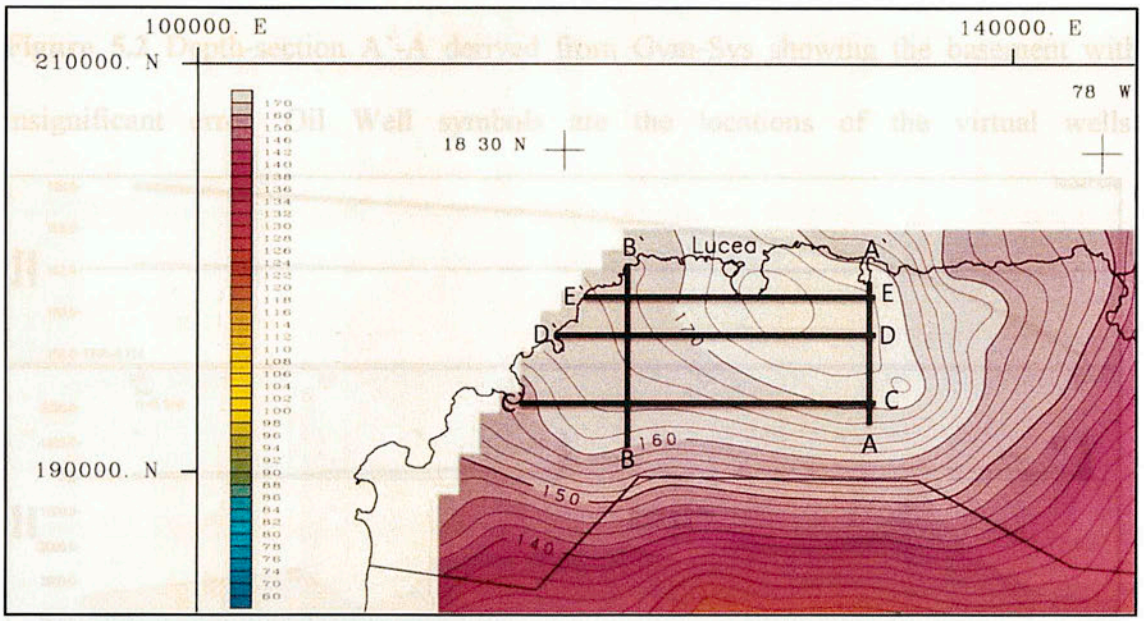


**Figure 5.1** Bouguer Gravity Map (after Ministry of Production, Mining and Commerce, 1992) showing the Cross-section locations. The junction of A-A` and C-C` is a basalt outcrop. Our reference point is that outcrop, where in our Gym-Sys model we can see as basement of zero elevation. The gravity values were extracted along the cross-section lines and inputted in the model after interpolation between each adjacent gravity value. See Figure 2.2 for Satellite image.

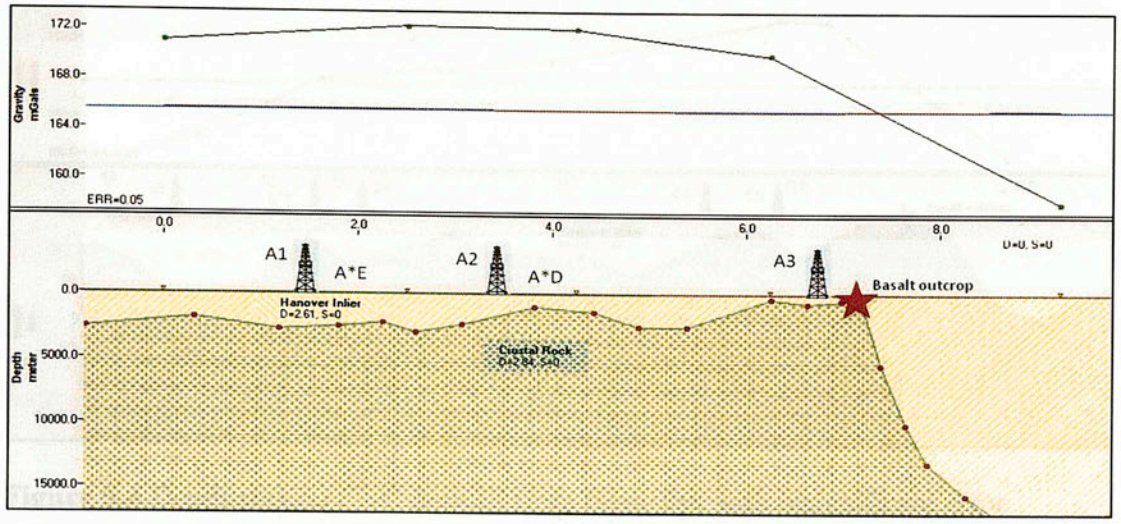


**Figure 5.2** Depth-section A`-A derived from Gym-Sys showing the basement with insignificant error. Oil Well symbols are the locations of the virtual wells.

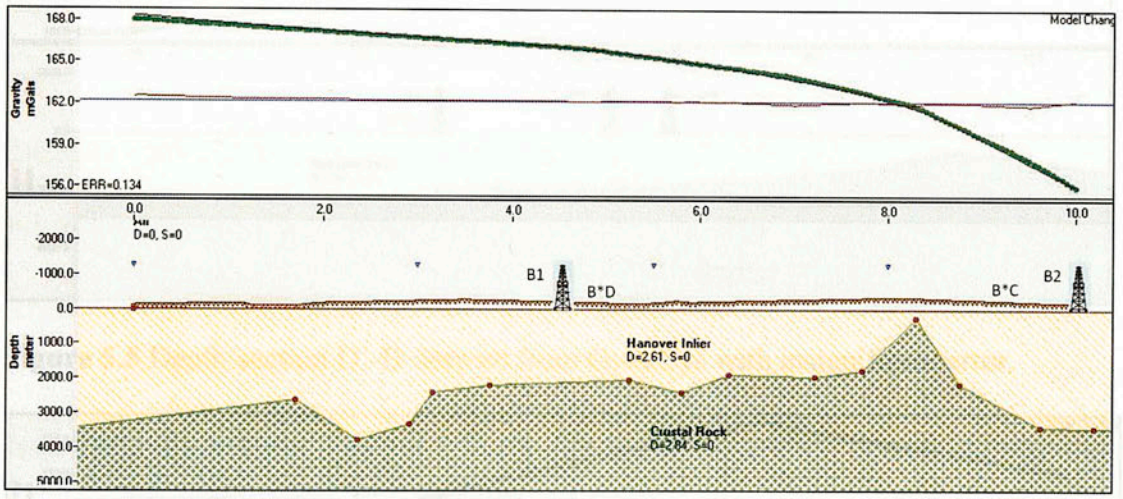


**Figure 5.3** Depth-section B`-B derived from Gym-Sys with insignificant error.

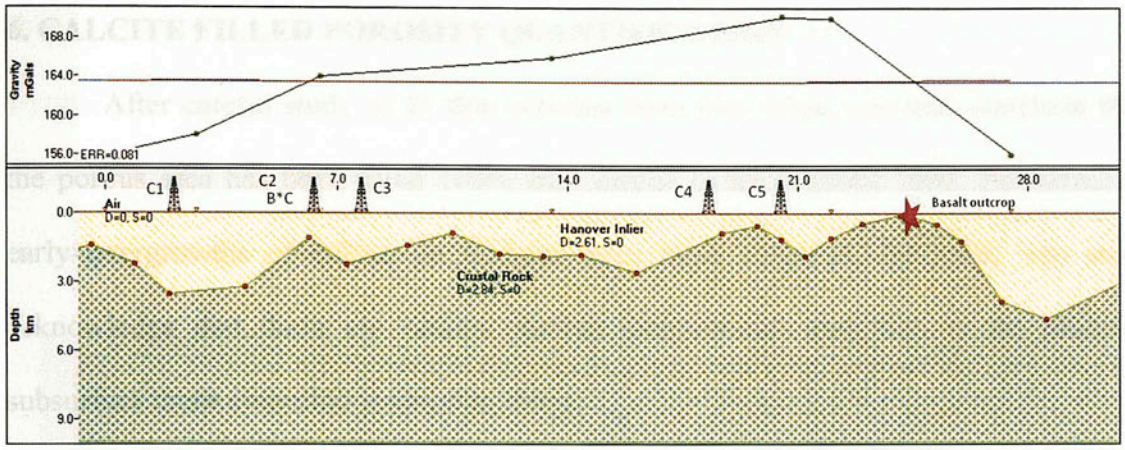


**Figure 5.4** Depth-section C`-C derived from Gym-Sys with insignificant error.

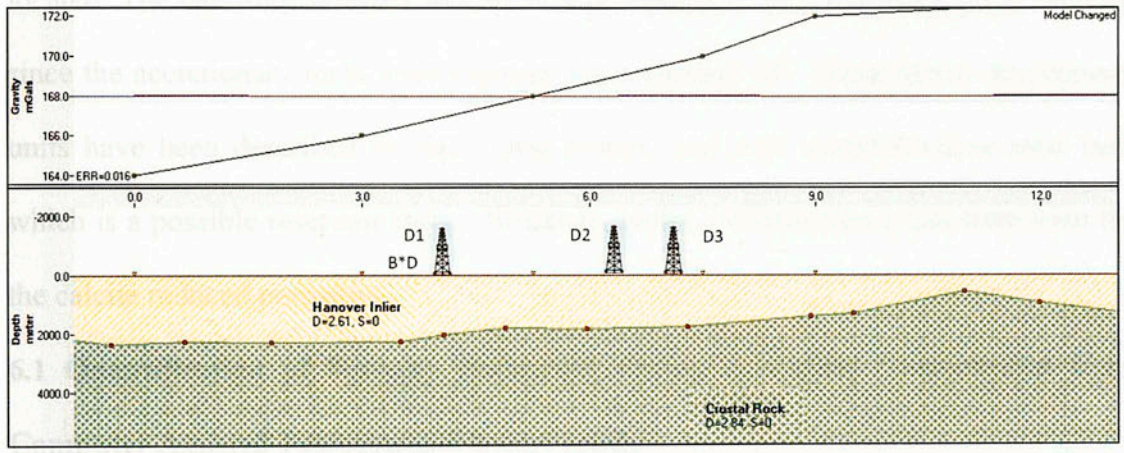


**Figure 5.5** Depth-section D`-D derived from Gym-Sys with insignificant error.

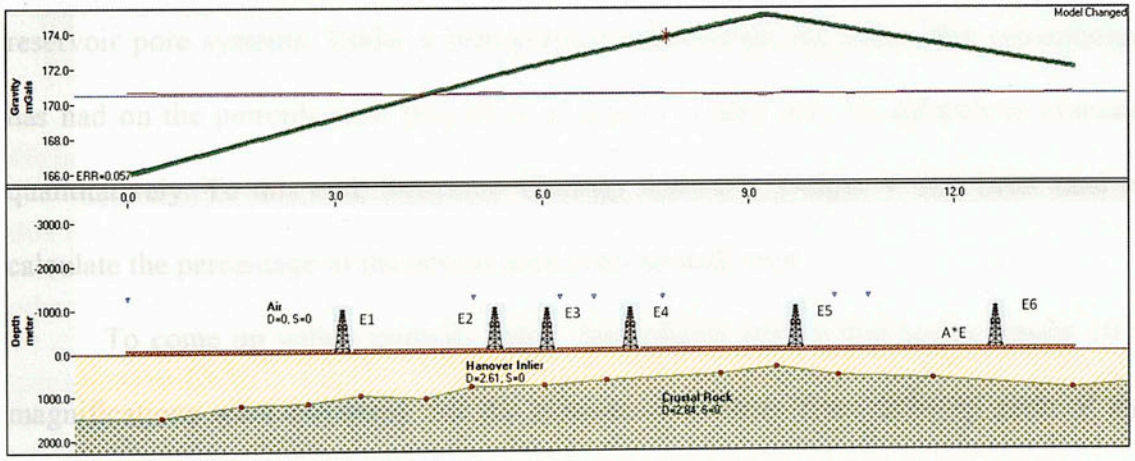


**Figure 5.6** Depth-section D`-D derived from Gym-Sys with insignificant error.

## 6. CALCITE FILLED POROSITY QUANTIFICATION

After careful study of 21 thin sections from four stops, one may conclude that the porous area has been filled 100% with calcite in the phreatic zone. Furthermore, early overgrowths of calcite on feldspar have been observed. However, one must acknowledge that these are vadose outcrop observations, and thus in the phreatic subsurface these cemented zones may differ.

The sample was taken from Stop 2 where the lateral accretionary unit was located. The carefully selected sample was presumed to be a relatively good reservoir since the accretionary units were representing a channel fill. Those lateral accretionary units have been described as clean sand bodies, and well sorted massive sand beds, which is a possible reservoir target. However, under a microscope it has been seen that the calcite reduced porosities.

### 6.1 Quantification of Porosity Reduction Owing to Calcite Cementation Using Computer Assisted Petrographic Image Study

Calcite cementation is an important factor in the destructive evolution of reservoir pore systems. Under a petrographic microscope, the effect that cementation has had on the petrophysical properties of a pore system may be difficult to evaluate quantitatively. To this end, Structural Geology software "Didger 4" has been used to calculate the percentage of the porous area over the total area.

To come up with a porosity value, four photos from a thin section under 10 x magnifications were exhibited. All the pictures were taken from different parts of the same thin section. Those pictures have been imported to the software "Didger 4 Demo." The calcite mineral color under the microscope shows vague pastel hues in views (in

this case images). After careful mapping of the porous medium on thin sections and summation of the calcite filling areas over total area, a porosity value for each image was defined (Fig. 6.1). Simply, arithmetic averaging each porosity value resulted in a minimum estimated porosity value for the Sandstone in Kc formation as 10%.

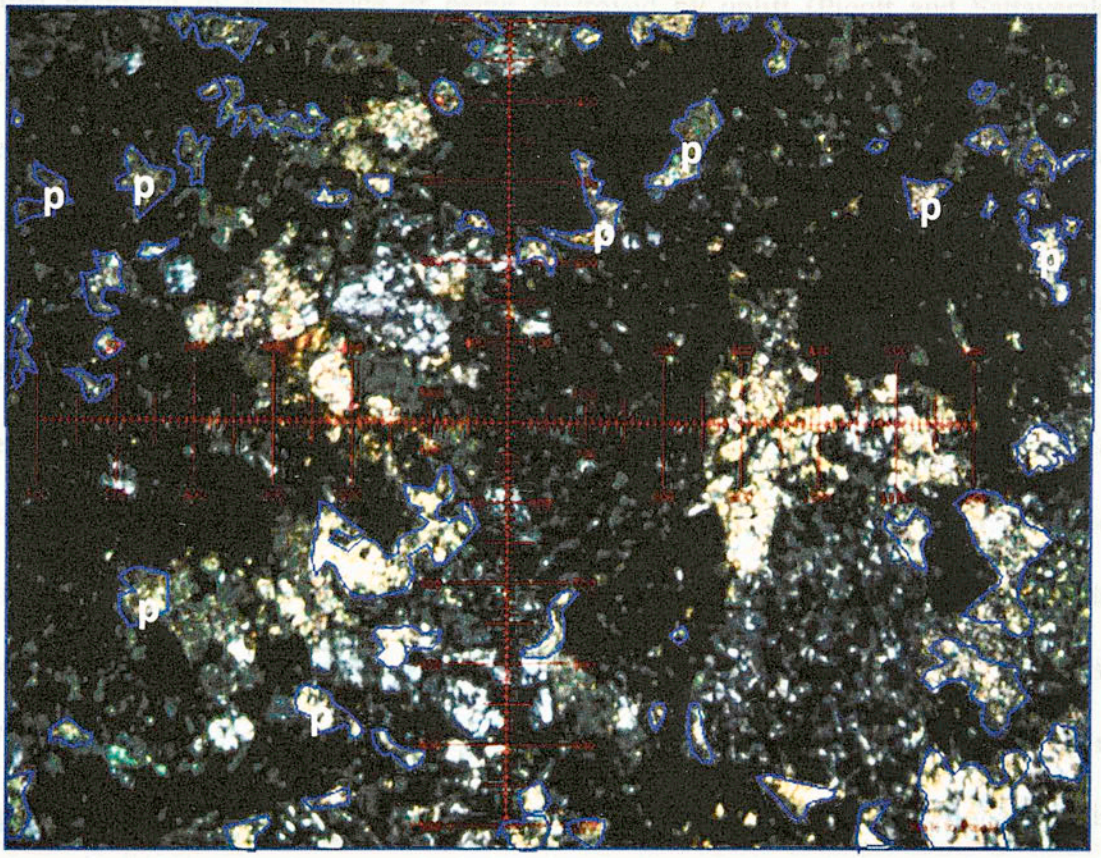


**Figure 6.1** Thin section image-3. The blue circled areas are calcite filling porosities. In this image the calculated calcite filling porosity is 8.58%. With the same method the 3 other images have been analyzed and the average porosity for Kc Sandstone is calculated as 10 %.

# 7. BASIN MODELING PRINCIPLES

## 7.1 Introduction

The evolution of a sedimentary basin and its petroleum systems are a complicated result of a combination of tectonic, geological, and geochemical factors, either evolving by subsidence or being destroyed by uplift (Pigott and Sattayarak, 1993). Metwalli and Pigott (2005) expand the Magoon and Dow (1994) definition of a petroleum system in a sedimentary basin as "a dynamic, inter-dependent assemblage of materials and processes linked together within non-discrete spatial temporal boundaries in a sedimentary basin, which provides the accumulation of hydrocarbons". A complete petroleum system requires the presence of various factors essential to the formation of petroleum deposits, including thermal elements. These critical elements are source rocks, reservoir rocks, and seals, and the essential processes which include the formation of traps, migration pathways, accumulation of hydrocarbons, and its preservation through increments of time. Specifically, source generation criticals consist of source generation volume (total organic carbon), quantity (richness), quality (kerogen type), and maturity (designated source rocks). Reservoir-trap accumulation criticals address quality (permeability and porosity), hydrocarbon type (richness of liquid and/or gas hydrocarbons), seal, and closure of reservoir rocks. Migration criticals defines the migration pathway and the principal transport mechanisms. The timing criticals address when the timing of all the three previous criticals are associated appropriately (or disconnected improperly), and when the variables changed through time (Metwalli and Pigott, 2005).

This thesis includes eighteen virtual wells on Hanover Inlier, Jamaica. Platte River BasinMod software is used in one and two dimensions in order to calculate the geoconstrained kinetic maturity of hydrocarbons in source rocks. This chapter will describe the basic theories, methods, and procedures undertaken.

## 7.2 1-D (One-Dimensional) Basin Modeling Principles

The BasinMod 1-D software is used to generate the tectonic subsidence, thermal maturation, and burial history for each well in the basin. For the modeling, the input data derived from the virtual wells and the parameters are: formation top depths, ages, thicknesses, lithologies, and initial TOC values.

## 7.3 Subsidence Principles

There are four fundamental factors that are parts of the subsidence in a basin: (1) isostatic water loading, (2) isostatic sediment loading (deposition or erosion), (3) flexure (sagging versus arching), and (4) tectonics. Tectonics affects the thermal crustal state and is most crucial to determining any dynamic changes in organic maturities, so it is the parameter of focus. In order to determine tectonic parameters, first determine and subtract the nontectonic factors.

Mathematical expression of the subsidence from water loading is, (Eqn. 7.1), (Pigott and Sattayarak, 1993)

$$S_{wl} = \Delta SL * \frac{\rho_w}{\rho_m - \rho_w}$$

**Equation 7.1:** Subsidence due to water-loading. $S_{wl}$ is isostatic subsidence caused by water loading, $\Delta SL$ is sea level change, $\rho_w$ is the density of sea water (usually= 1.028 kg $m^{-3}$), $\rho_m$ is the density of upper mantle (3.3 kg $m^{-3}$).

The relationship between sea level change and subsidence owing to water loading, (Eqn. 7.2), (Pigott, 2009, unpublished lecture notes):

$$S_{wl} = 0.452 * \Delta SL$$

**Equation 7.2:** Relation between sea level changes and subsidence due to water loading.

which claims that in general

for every one kilometer of sea level rise, the basin subsides ~450 meters, and

for every one kilometer of sea level fall, the basin uplifts ~450 meters.

The isostatic subsidence owing to sediment loading ($S_{sedl}$) is related to the amount of sedimentation in a basin by the equation 7.3 (Pigott and Sattayarak, 1993):

$$S_{sedl} = S * \frac{\rho_s - \rho_w}{\rho_m - \rho_w}$$

**Equation 7.3:** Subsidence is related to sediment loading. $S_{sedl}$ is isostatic subsidence related to sediment loading, $S$ is observed sedimentation, and $\rho_s$ is sediment density in clastic systems (2.65 kg $m^{-3}$).

Ideally, this formula, (Eqn. 7.4), expresses the relationship that one kilometer of sediment has upon sediment loading subsidence (Pigott, 2009, unpublished lecture notes):

$$S_{sedl} = 0.71 km$$

**Equation 7.4:** In general, this relationship shows that for every 1 km of sediment loaded onto a basin, 0.71 km of basin subsidence occurs.

Flexure subsidence ($S_{flex}$) generally has an effect of less than one percent upon basin subsidence, and is not significant and is of no concern in this study.

The following equation, (Eqn. 7.5), defines the initial rift subsidence as a function of crustal stretching (from Metwalli and Pigott, 2005).

$$S_{tec} = \frac{t_l\left(1-\frac{1}{\beta}\right)*\left[(\rho_m-\rho_c)*\left(\frac{t_c}{t_l}\right)*\left(1-\frac{\alpha*T_m*t_c}{2*t_l}\right)-\left(\frac{\alpha*T_m*\rho_m}{2}\right)\right]}{\rho_m*(1-\alpha*T_m)-\rho_w}$$

**Equation 7.5:** $S_{tec}$ is amount of initial rift subsidence, $t_c$ is thickness of the crust, $t_l$ is thickness of lithosphere, $\rho_m$ is density of the mantle (3.3 kg $m^{-3}$), $\rho_c$ is density of the crust (2.88 kg $m^{-3}$), $\rho_w$ is density of the seawater (usually= 1.028 kg $m^{-3}$), $\alpha$ is thermal expansion coefficient ($3.3*10^{-5}$ $C^{-1}$), $\beta$ is the stretching factor, and $T_m$ is temperature of the mantle (1350 °C).

Where the stretching factor (McKenzie 1978) beta is defined as (Eqn. 7.6):

β=

**Equation 7.6:** Stretching Factor (β). $T_{lith}$ is the lithosphere thickness immediately after stretching and $T_{lith0}$ is the thickness of the lithosphere before stretching.

The tectonic associations of beta are:

- If β is greater than one, it indicates crustal stretching or extension and heating,
- If β is less than one, it specifies shortening or uplift and cooling,
- If β is equal to one, it signifies that no observed change has occurred in crustal thickness (Pigott, 2009, unpublished lecture notes).

The whole subsidence in a basin is then a sum of the subsidence due to tectonics, sediment loading, and water loading. The process used to determine the amount of load-induced subsidence is computationally termed isostatic back stripping. This method removes sediment layers, correcting for decompaction, fluctuation of sea

level, and sea depth (Metwalli and Pigott, 2005 after Pigott and Sattayarak, 1993). The tectonic subsidence can be described by the following equation, (Eqn. 7.7):

$$S_{tec} = S_{total} - S_{sedl} - S_{wl} \pm \Delta SL$$

**Equation 7.7:** $S_{tec}$ is corrected subsidence, $S_{total}$ is total subsidence, $S_{sedl}$ is sediment loading, $S_{wl}$ is water loading, and $\Delta SL$ is sea level change.

### 7.4. Heat Flow Principles

Temperature is a crucial factor in modeling maturity and kinetics. Detecting the temperature parameters thorough time lets one interpret the thermal conditions to which the potential source rocks of the basin were subjected.

Thermal boundary value solution or temporal heat storage (from Pigott et al., 1996) refers to the transfer of energy or heat in the crustal system (Eqn. 7.8).

$$\frac{\rho c \partial T}{\partial t} = \frac{\partial}{\partial x, y, z}[Kx, y, z]\frac{\partial T}{\partial x, y, z} - F + G$$

Temporal Heat Storage = Heat Flux in - Heat Flux Out + Internal Heat Generation

**Equation 7.8:** The thermal value boundary solution. $\rho c$ represents composit heat flux, $T$ is temperature, $t$ is time, $K$ is thermal conductivity, $F$ is heat flux out, and $G$ is internal heat generation.

The equation can be interpreted in crustal terms as the lithospheric thermal state is;

*Lithospheric Thermal State* = *Spatial Rate of Heat Flow Change* - *Heat Loss by refraction and Fluid Flow* + *Radioactive Heat Generation*

The heat flow data was calculated from observed geothermal gradients using Equation

If cooling plutons, mountain front hydrological flow, and radioactivity are negligible, then a time invariant steady-state condition is present, and the sum of the equation is zero (from Pigott et al., 1996), (Eqn. 7.9):

$$\frac{\rho c \partial T}{\partial t} = \frac{\partial}{\partial x, y, z}\left[Kx, y, z\right]\frac{\partial T}{\partial x, y, z} - F + G = 0$$

**Equation 7.9:** The thermal value boundary solution equation is zero.

If constant temperature endpoints (the Dirichlet Condition) are defined, the integration of the equation gives the classic Fourier Heat Flow Equation:

$$\mathrm{Q}\,x, y, z = -Kx, y, z\frac{\partial T}{\partial x, y, z}$$

**Equation 7.11:** Fourier Heat Flow Equation after integration of the Equation 7.9.

And in one dimension (Eqn. 7.11):

$$\mathrm{Q} = \frac{-k}{10}\left(\frac{\Delta T}{\Delta z}\right)$$

**Equation 7.11:** Q is heat flow in HFU (μcal/cm$^2$sec), $k$ is thermal conductivity in mcal/cm sec °C, and $\frac{\Delta T}{\Delta z}$ is the geothermal gradient in °C/100m (Pigott et al., 1996).

Therefore, if the thermal conductivity is steady in a system, the only factor that controls the heat flow in a system is the geothermal gradient. Modifications in maturation and kinetics change exponentially with respect to temperature, and linearly with respect to time. In this manner, in order to construct paleo heat flow throughout the basin, present-day heat flow can be used. However, rifting causes vivid variations in heat that alters the temperature for millions of years after the rifting event (BasinMod 1-D Manual, 2005).

## 7.5 Rifting Heat Flow

Rifting is a dynamic stage, and it causes disturbances in thermal history which can have evasive results, and it is difficult to model a basin's rifting heat flow precisely. BasinMod offers a rifting heat flow option that is a simplification of the Jarvis and McKenzie finite rifting model (1980) which is the most widely accepted theory (Allen and Allen, 2005). All pervasive rifting heat flow models agree that rifting involves two phases, a rifting phase and a subsidence phase (Fig. 7.1) (Pigott and Ru, 1994):

- The rifting phase: stretching, thinning, and faulting of the crust accompanied by increased heat flow owing to crustal thinning and upwelling of the asthenosphere
- The subsidence phase: post-rift period with logarithmically declining thermal decay owing to re-establishment of thermal equilibrium in the mantle lithosphere and asthenosphere.

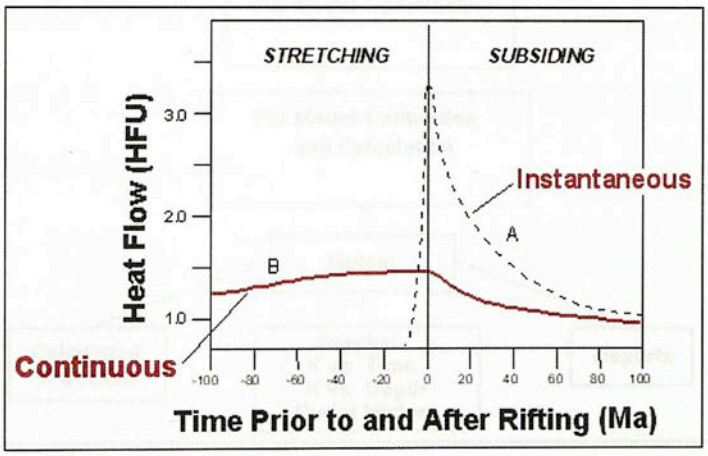


**Figure 7.1** Heat flow changes accompanying rifting events (after BasinMod 1-D Manual, 2005).

Beta is necessary to calculate the rifting heat flow in BasinMod, and was computed from an iterative solution of Equation 7.5 after determining tectonic subsidence.

## 7.6 2-D (Two-Dimensional) Basin Modeling Principles

While one dimensional basin modeling of the Hanover Block displays the significant impact of pulsed tectonics upon the maturation of hydrocarbons in the basin, BasinMod 2-D allows one to reconstruct the basin evolution palinspastically along specified cross sections. These cross sections can display porosity, permeability, temperature, maturity, and expelled hydrocarbons for various formations for time increments. The data are taken from virtual wells in BasinMod 1-D. The workflow is shown in Figure 7.2.

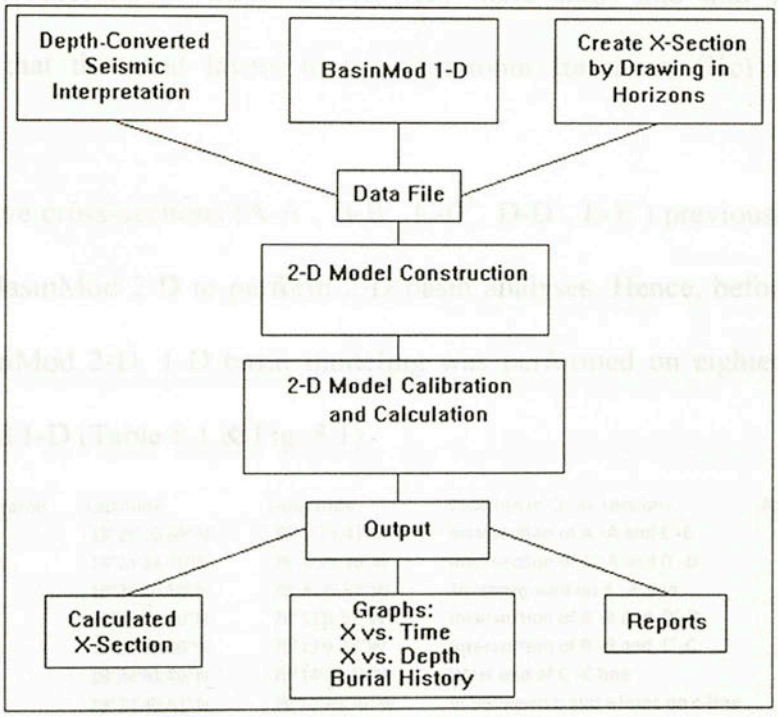


**Figure 7.2** Overview of BasinMod 2-D workflow (from BasinMod 2-D Manual, 2005). In this case, this study has virtual wells created from cross sections.

## 8. BASIN ANALYSIS AND MODEL

### 8.1 Introduction

For petroleum system analysis, source rocks, carrier beds, reservoir rocks, and seals are critical elements, while trap formation, migration pathways, hydrocarbon accumulation, and hyrdrocarbon preservation are essential processes.

The Hanover Group with both Campanian and Santonian Hanover Formations are chosen as the main potential for both source rock and reservoir. The shale layers have poor source rock potential with type II kerogen, but a TOC average of 0.39%. While the reservoir potential is also poor, field study and thin section studies are showing that the sand layers in the Claremont formation (Kc) have calcite filled porosity.

Five cross-sections (A-A`, B-B`, C-C`, D-D`, E-E`) previously mentioned were used in BasinMod 2-D to perform 2-D basin analyses. Hence, before data was loaded into BasinMod 2-D, 1-D basin modeling was performed on eighteen virtual wells in BasinMod 1-D (Table 8.1 & Fig. 8.1).

| Virtual Well Name | Lattitude | Longitude | Location in Cross-sections | Approx. Elevation in meters |
|---|---|---|---|---|
| A1 & E6(A*E) | 18°26'10.65"N | 78° 6'23.41"W | Intersection of A`-A and E`-E | 150 |
| A2 & D5( A*D) | 18°25'34.70"N | 78° 6'24.36"W | Intersection of A`-A and D`-D | 100 |
| A3 | 18°24'39.53"N | 78° 6'25.57"W | Southern well on A`-A line | 400 |
| B1 & D1(B*D) | 18°25'36.00"N | 78°13'9.53"W | Intersection of B`-B and D`-D | 125 |
| B2 & C2 (B*C) | 18°24'40.96"N | 78°13'9.23"W | Intersection of B`-B and C`-C | 200 |
| C1 | 18°24'41.46"N | 78°14'32.18"W | West end of C`-C line | 80 |
| C3 | 18°24'40.51"N | 78°12'40.70"W | in between b and a lines on c-line | 200 |
| C4 | 18°24'37.32"N | 78° 8'11.60"W | in between b and a lines on c-line | 200 |
| C5 | 18°24'36.97"N | 78° 7'5.74"W | in between b and a lines on c-line | 200 |
| D2 | 18°25'35.02"N | 78°11'27.99"W | in between b and a lines on d-line | 120 |
| D3 | 18°25'35.01"N | 78° 9'12.95"W | in between b and a lines on d-line | 100 |
| D4 | 18°25'34.80"N | 78° 8'22.81"W | in between b and a lines on d-line | 90 |
| E1 | 18°26'16.15"N | 78°12'13.50"W | in between b and a lines on e-line | 150 |
| E2 | 18°26'15.04"N | 78°10'28.44"W | in between b and a lines on e-line | 50 |
| E3 | 18°26'14.70"N | 78° 9'53.25"W | in between b and a lines on e-line | 20 |
| E4 | 18°26'13.39"N | 78° 8'46.32"W | in between b and a lines on e-line | 100 |
| E5 | 18°26'12.30"N | 78° 7'6.76"W | in between b and a lines on e-line | 70 |

**Table 8.1** The names and locations of 18 virtual wells in the Hanover Block refer to Figure 8.1.

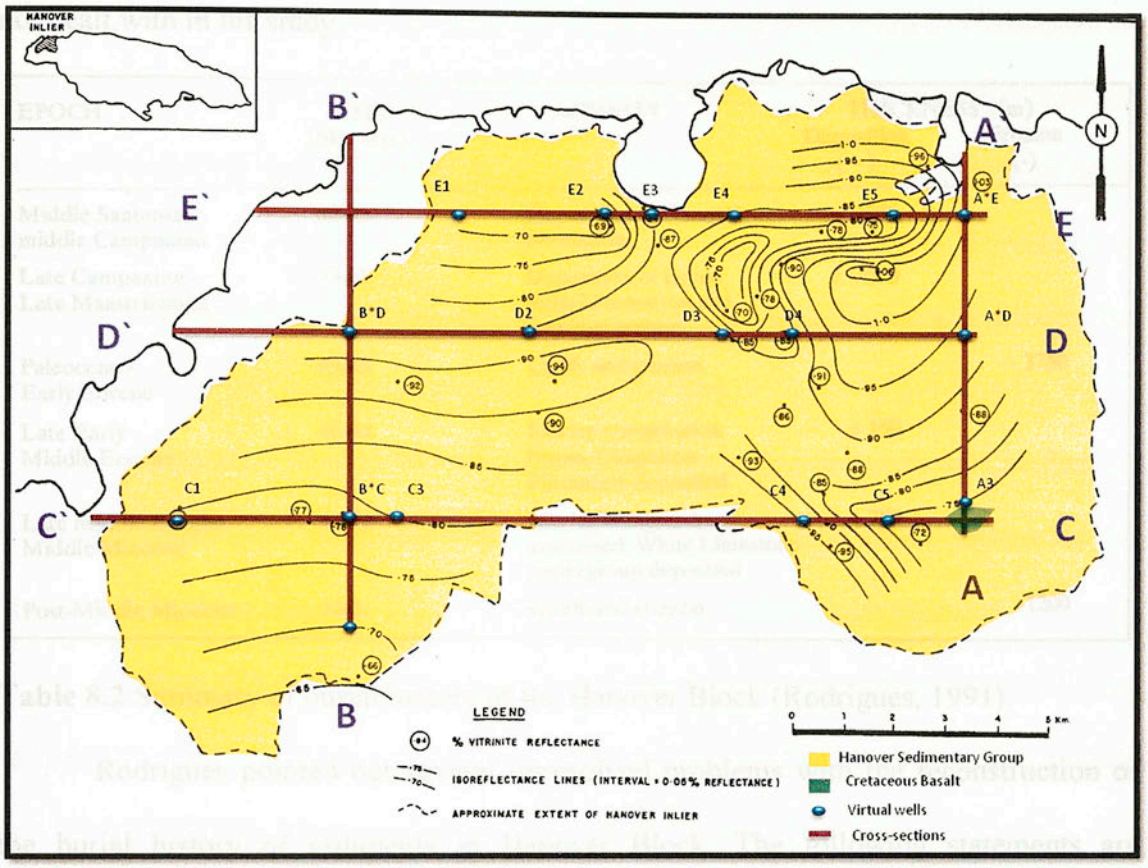


**Figure 8.1** The base map is showing the location of the eighteen virtual wells, five cross-sections. The boundary of Hanover Inlier and isoreflectance lines are shown on the map.

## 8.2 Basin Burial History Analysis

Rodrigues (1991) suggested a burial history of the Hanover Inlier. Although the model is useful in many ways, there are a lot of short comings that are dealt with in this thesis to generate an improved model. Basically this study will suggest one alternative model to the Rodrigues model through reasoning and discussing the shortcomings and suggesting other paths than he had used before.

Rodrigues' study was excellent with respect to determining the time of activities (Table 8.2). However, as he stated in his paper, there are some shortcomings that were not dealt with in his study.

| EPOCH | TIME (Myr b.p.) | ACTIVITY | THICKNESS (m) Deposition (+) | Erosion (-) |
|---|---|---|---|---|
| Middle Santonian - middle Campanian | 80-73 | Deposition of Hanover Formation | + 1950 | |
| Late Campanian - Late Maastrichtian | 73-65 | Deposition of Green Island Formation and 'missing' section | + 3600 | |
| Paleocene - Early Eocene | 65-48 | Uplift and erosion | | - 3750 |
| Late Early - Middle Eocene | 48-44 | Marine trangression began, Chapelton Formation deposited | + 150 | |
| Late Middle Eocene - Middle Miocene | 44-12 | Marine trangression continued, White Limestone Supergroup deposited | + 750 | |
| Post-Middle Miocene | 12-0 | Uplift and erosion | | -1200 |

**Table 8.2** Summary of burial history of the Hanover Block (Rodrigues, 1991).

Rodrigues pointed out several unresolved problems with the reconstruction of the burial history of sediments in Hanover Block. The following statements are problems in Rodrigues' study and corresponding proposed solutions:

Problem (A): No sediments of Early to Late Maastrichtian age have been recorded on the Hanover Block, although a 3000-meter-thick section of equivalent age is present in Cretaceous inliers to the east (Meyerhoff and Krieg, 1977). The Hanover Block may have been a site of deposition, receiving sediments which were subsequently removed by erosion after the uplift at the end of the Cretaceous.

Solution (A): Overburden of a sediment thickness on the Hanover Formation can be calculated by estimating the compaction amount using the (final) reduced

porosity and initial porosity values (Hegarty, Weissel, and Mutter, 1988). (See porosity calculation section.)

Problem (B): A depth section of the Hanover Formation is not available and all the samples were collected at the outcrop. The thickness of the Hanover Formation has been estimated by Sohl (1976) to be as little as 500 m and by Scott (1967) to be as much as 3600 m. A complete stratigraphic section of the Hanover Formation is impossible to measure in the field due to poor exposures, lack of outcrop continuity and the possibility of repeated sections as a result of faulting.

Solution (B): Gravity modeling was conducted in previous chapters to find the basement depth with five cross-sections. The model suggests depth section of the Hanover Formation throughout the Hanover Inlier with insignificant error.

Problem (C): Sediment thicknesses that have been removed by erosion during the periods when the Hanover Block was emergent (end of Cretaceous to Early Eocene and from the Middle Miocene to the present) are unknown.

Solution (C): There are five geologic cross-sections throughout the Hanover Inlier. The Hanover Group is subdivided into seven formations. Assuming constant sedimentation rate during Santonian and Campanian with a known depth section, one can estimate removed sediment thicknesses of the Hanover Group. Moreover, the porosity model reveals the Early Eocene Uplift amount. Finally, calibration of our basin model, with the help of vitrinite reflectance values and thermal conditions, restricts the burial history model.

In addition to suggesting solutions to unsolved problems in Rodrigues (1991), this thesis suggests an alternative heat flow model to the Rodrigues model. Rodrigues

suggested a steady state heat flow between Middle Santonian (80 ma) and the present (0 ma). However, subsidence and/or uplift amounts during a specific interval of time are related to different stretching factors as it is mentioned in Tectonic subsidence and stretching methods earlier. Every stretching factor (beta) refers to a different heat flow value as we have suggested in this study.

**8.3 Calculation of Subsidence and overburden of Sediment**

Assuming rapid deposition of the missing section of the Green Island Formation on top of Hanover Group, we can calculate the thickness of the Green Island Formation by using the compaction equation. In Chapter 6, the porosity quantification using Petrographic Image Analysis suggested a porosity value to use in this study.

Hegarty, Weissel, and Mutter (1988), have found a method to understand the rapid burial depth of a formation by an equation using present porosity values. They have estimated initial porosity values and compaction constants for different lithologies. The equation basically models, in rapid deposition, that the present porosity value is a function of initial porosity and thickness of the deposition on top of the formation (Eqn. 8.1).

—

**Equation 8.1:** Relation between subsidence (z), initial porosity ( ), and final porosity . CK is the compaction constant and there is a rapid flow assumption.

For Kc Sandstone

, , CK(m)=2500

So, the calculated z is

Z=3300 m

The initial porosity and the compaction constant CK has been taken from (Hegarty, Weissel, and Mutter, AAPG, 1988). Under 3300 m of overburden the initial porosity of 34% (which is an estimated standard porosity for Sandstone initial porosity) has been reduced to 9.96 % porosity.

To sum up, the Green Island missing section was calculated as 3300 m thick which was eroded away with adjacent Paleocene uplift, so the 1-D basin model`s stratigraphy was constructed in that manner (Fig. 8.2).

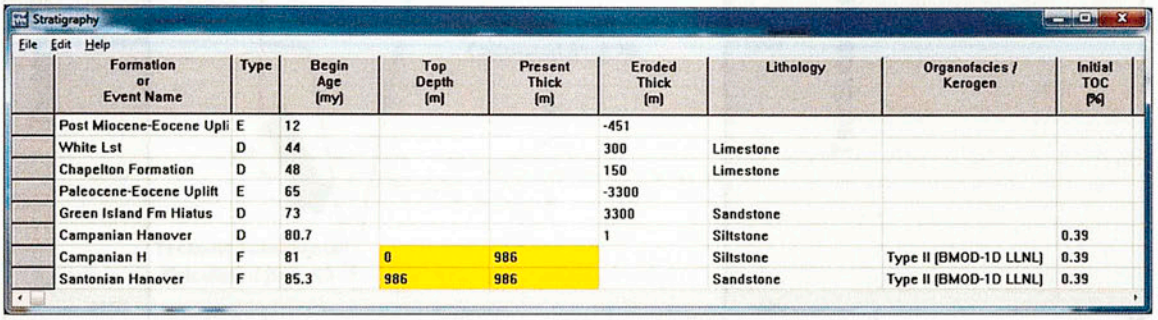
Stratigraphy

File Edit Help

| Formation or Event Name | Type | Begin Age (my) | Top Depth (m) | Present Thick (m) | Eroded Thick (m) | Lithology | Organofacies / Kerogen | Initial TOC (%) |
|---|---|---|---|---|---|---|---|---|
| Post Miocene-Eocene Upli | E | 12 | | | -451 | | | |
| White Lst | D | 44 | | | 300 | Limestone | | |
| Chapelton Formation | D | 48 | | | 150 | Limestone | | |
| Paleocene-Eocene Uplift | E | 65 | | | -3300 | | | |
| Green Island Fm Hiatus | D | 73 | | | 3300 | Sandstone | | |
| Campanian Hanover | D | 80.7 | | | 1 | Siltstone | | 0.39 |
| Campanian H | F | 81 | 0 | 986 | | Siltstone | Type II (BMOD-1D LLNL) | 0.39 |
| Santonian Hanover | F | 85.3 | 986 | 986 | | Sandstone | Type II (BMOD-1D LLNL) | 0.39 |

**Figure 8.2** Data input to BasinMod 1-D for virtual well C3. Formations are entered with top depth, present thickness; eroded deposits are entered with eroded thickness; and erosion events are entered with thickness of erosion. The eroded thickness of the Green Island Formation is inputted as 3300 m as it was previously calculated.

## 8.4 Determining the Stretching Factor from Tectonic Subsidence 1-D, Thermal State, and Heat Flow

Using the amount of tectonic subsidence determined from the BasinMod 1-D models, β can be calculated using Metwalli, Pigott (2005) equation assuming the lithosphere thickness before subsidence is 120 km (Fig. 8.3). Secondly, uplift can be calculated with the same approach using a negative value for tectonic subsidence.

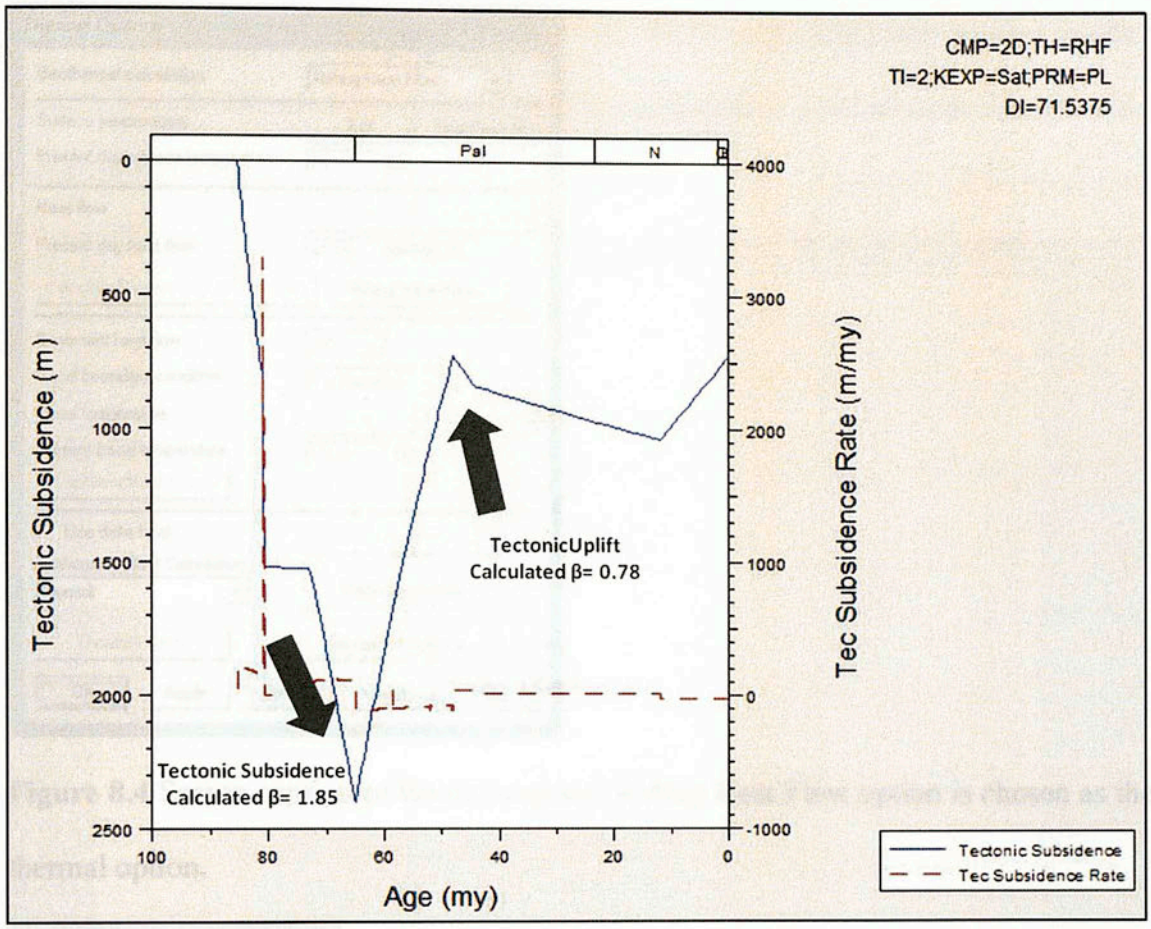


**Figure 8.3** Tectonic Subsidence vs. Time graph with calculated beta values.

After calculating beta values from tectonic subsidence amounts, BasinMod has an option to plot the stretching values and their time intervals into a rifting heat flow thermal option (Fig. 8.4). Since each β refers to a different stretching value, this study suggests using rifting heat flow state rather than steady state heat flow (Fig. 8.5).

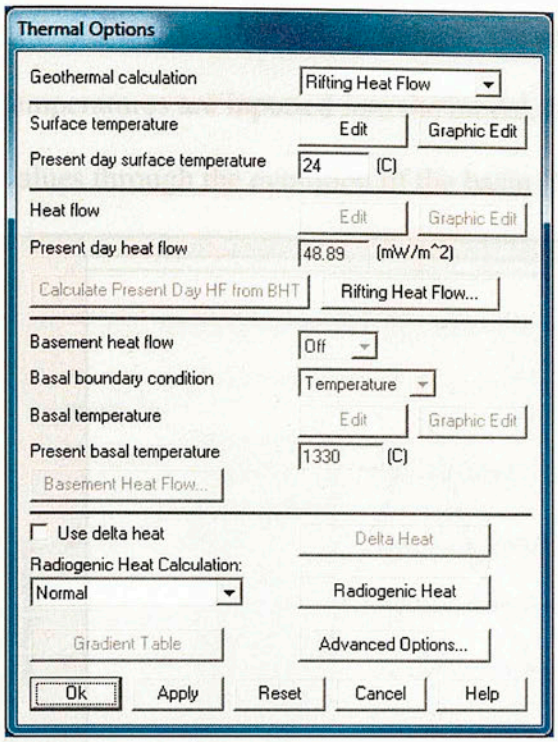


**Figure 8.4** Screen capture of Bmod program. Rifting Heat Flow option is chosen as the thermal option.

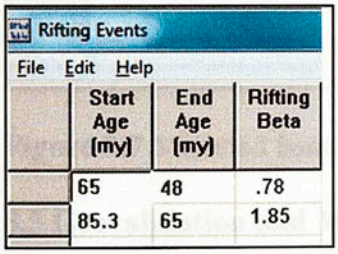


**Figure 8.5** Bmod screen capture illustrating the Beta factors which have been calculated and plotted on rifting events on BasinMod 1-D.

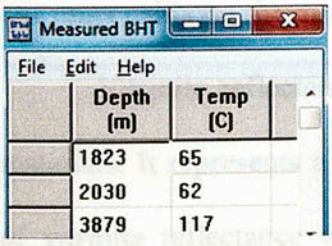


**Figure 8.6** Measured Bore Hole Temperatures have been inputted. The BHT temperatures have taken from Rodrigues (1991).

Finally, after all β values, measured BHT, (Fig. 8.6), and present surface temperatures are inputted into the model. It interpolates and generates the 1-D heat flow values through the evolution of the basin (Fig. 8.7).

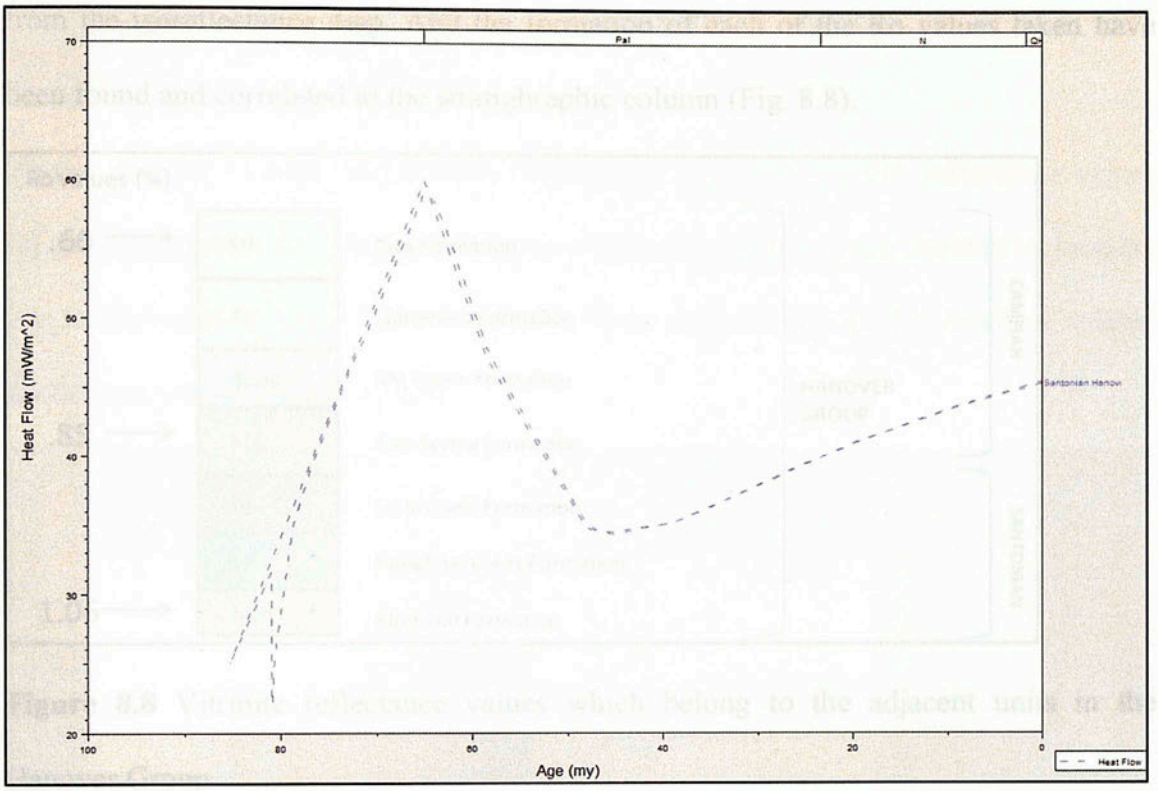


**Figure 8.7** Modeled heat flow for calculated rifting events for virtual well C3.

## 8.5 Geovalidation and Maturity

The thermal model and burial history analyses generated in this thesis, suggest maturity of hydrocarbon generated in the basin. However, to geovalidate the maturity one must calibrate the maturity levels with organic thermal indicators.

Vitrinite reflectance is the most widely used indicator of maturity of organic materials. It represents a nonreversible thermal indicator and knowing the distribution of vitrinite reflectance with depth in a sedimentary basin allows calibration of the thermal model input (Allen & Allen, 2005).

Combining the isoreflectance map from Rodrigues (1991) and five geologic cross-sections, a geochemical calibration has been conducted in the model. Only the vitrinite reflectance values that are measured from surface examples have been used from the isoreflectance map. And the formation of each of the Ro values taken have been found and correlated to the stratighraphic column (Fig. 8.8).

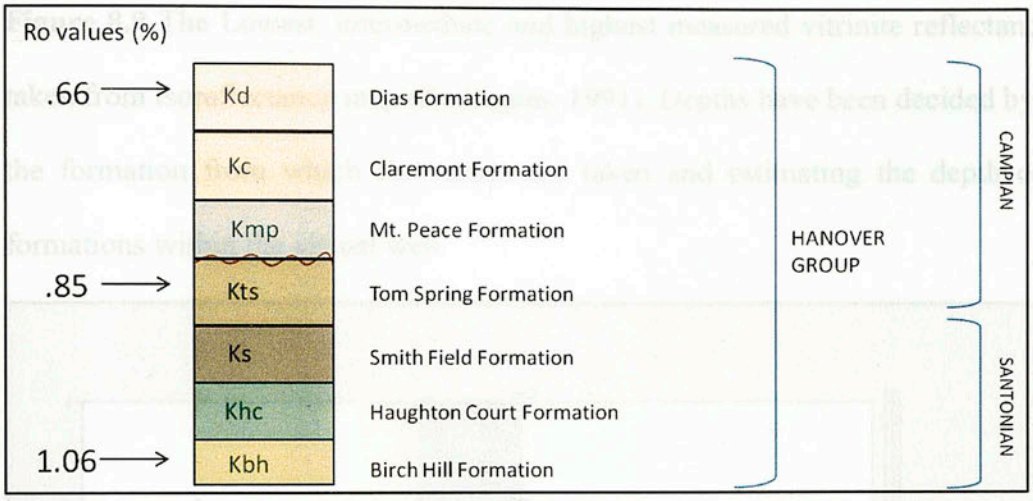


**Figure 8.8** Vitrinite reflectance values which belong to the adjacent units in the Hanover Group.

The C3 virtual well is used to calibrate the model. It is a representative virtual well of Hanover Inlier and located at the mid-south part of the inlier with an average stratigraphic thickness of 1900 meters. The maturity is a function of thermal state and burial history. Since the thermal state does not change laterally, the C3 well, with Santonian and Campanian formations records, is used to calibrate the maturity model (Fig. 8.9 and Fig. 8.10).

Measured %Ro

File Edit Help

| | Depth (m) | %Ro |
|---|---|---|
| | 50 | .66 |
| | 940 | .85 |
| | 1800 | 1.06 |

**Figure 8.9** The Lowest, intermediate and highest measured vitrinite reflectance values taken from isoreflectance map (Rodrigues, 1991). Depths have been decided by locating the formation from which Ro values are taken and estimating the depth of related formations within the virtual well.

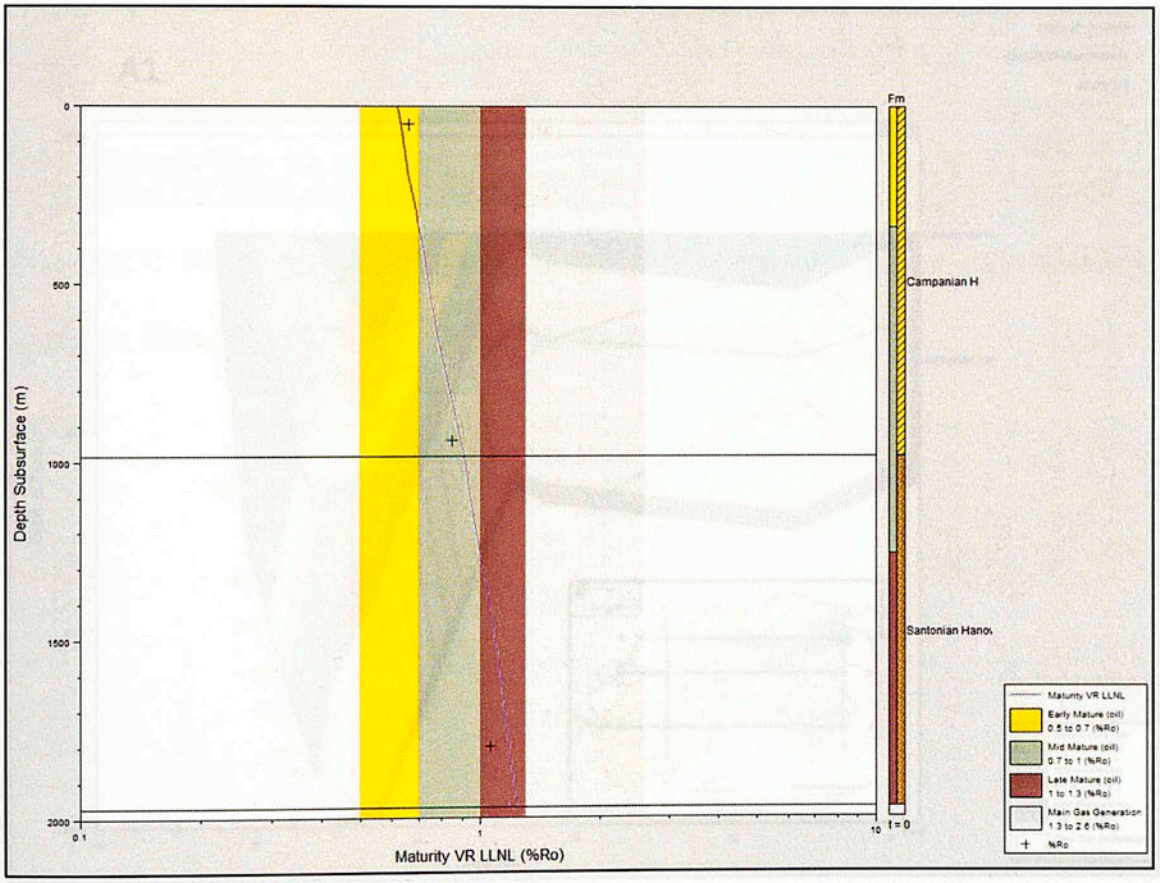

**Figure 8.10** Maturity vs. Depth graphic with % Ro values for geovalidation. The thermal models maturity anomaly shown by the pink line fits with the vitrinite reflectance values.

### 8.5.1 1-D Maturity

After calibrating the basin model for calculated thermal conditions, the following maturity models have been generated for each virtual well (Fig. 8.11 to Fig. 8.27). Note that, each virtual well obeys the calibration. The Surface %Ro value for each well represents the corresponding maturity window. The location of the virtual wells is indicated in each figure.

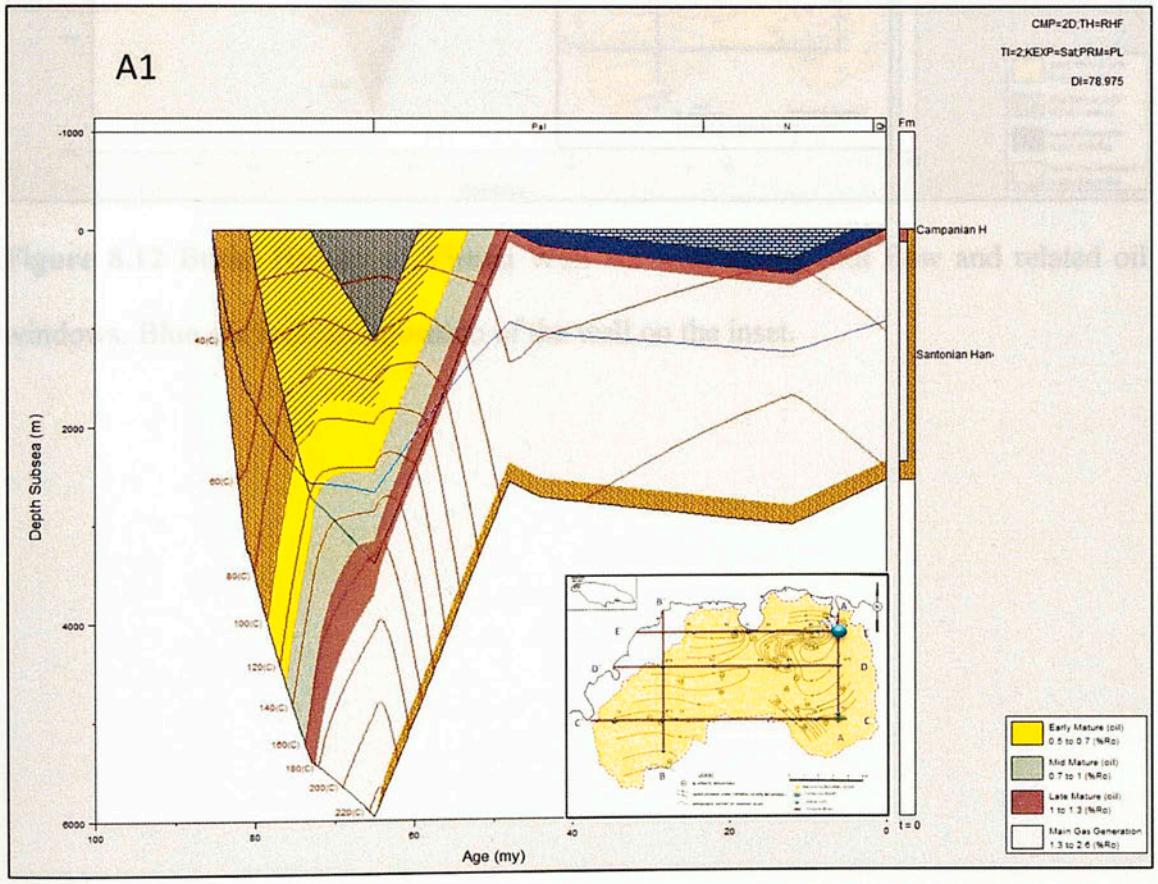


**Figure 8.11** Burial History of Virtual Well A1 with rifting heat flow and related oil windows. Blue dot indicates position of the well on the inset.

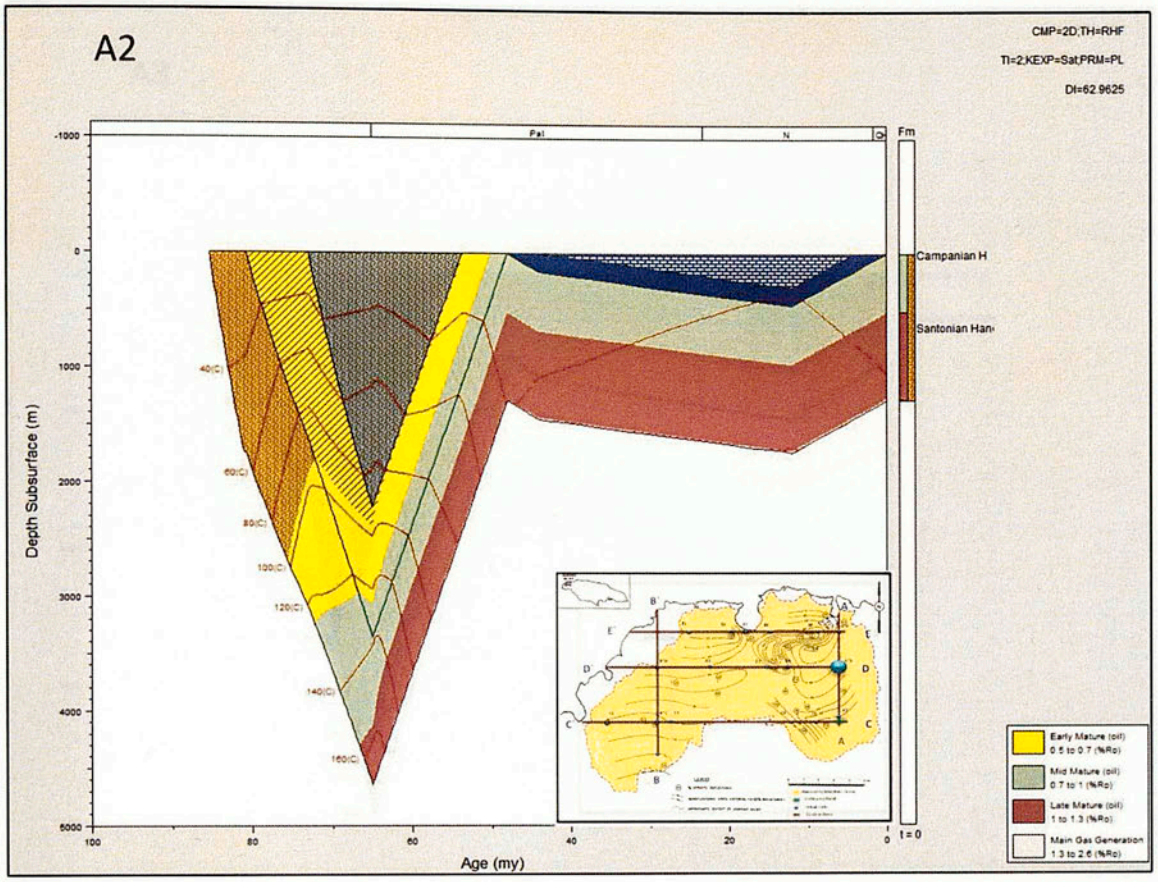


**Figure 8.12** Burial History of Virtual Well A2 with rifting heat flow and related oil windows. Blue dot indicates position of the well on the inset.

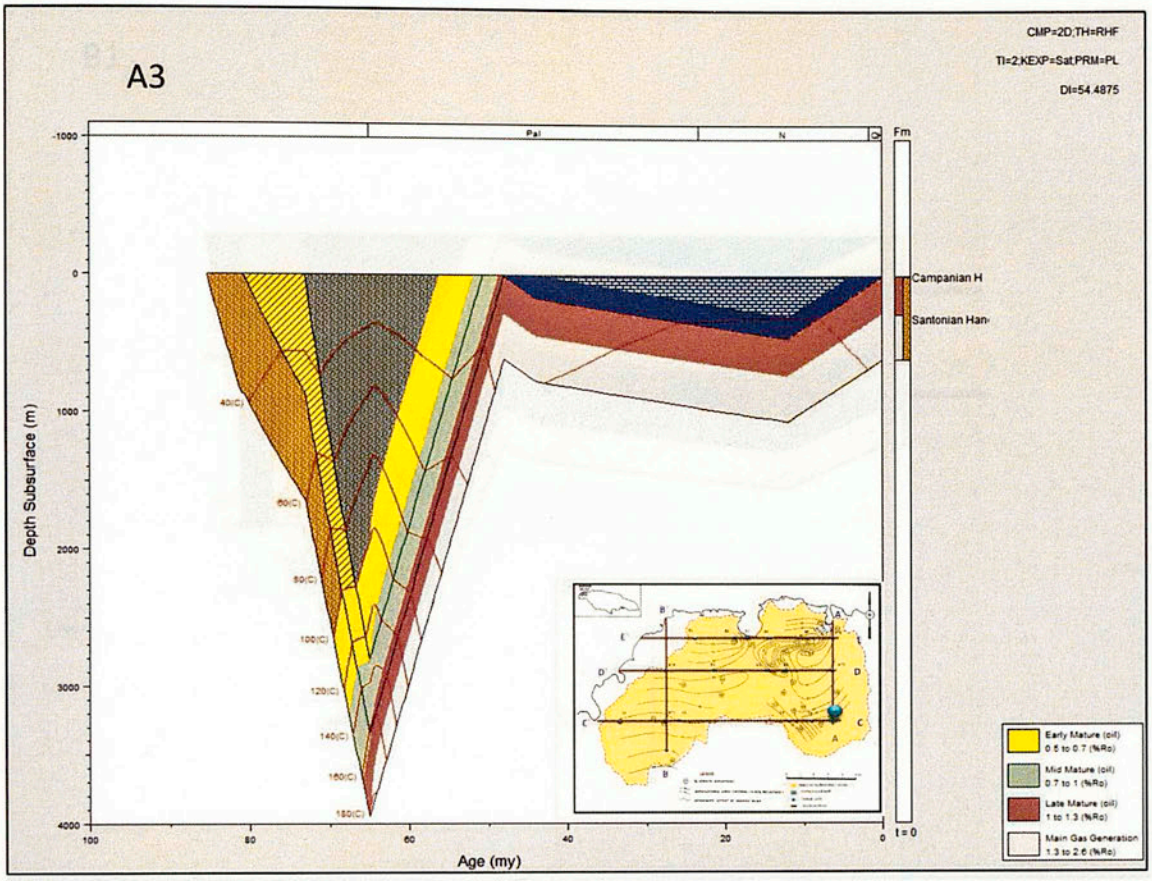


**Figure 8.13** Burial History of Virtual Well A3 with rifting heat flow and related oil windows. Blue dot indicates position of the well on the inset.

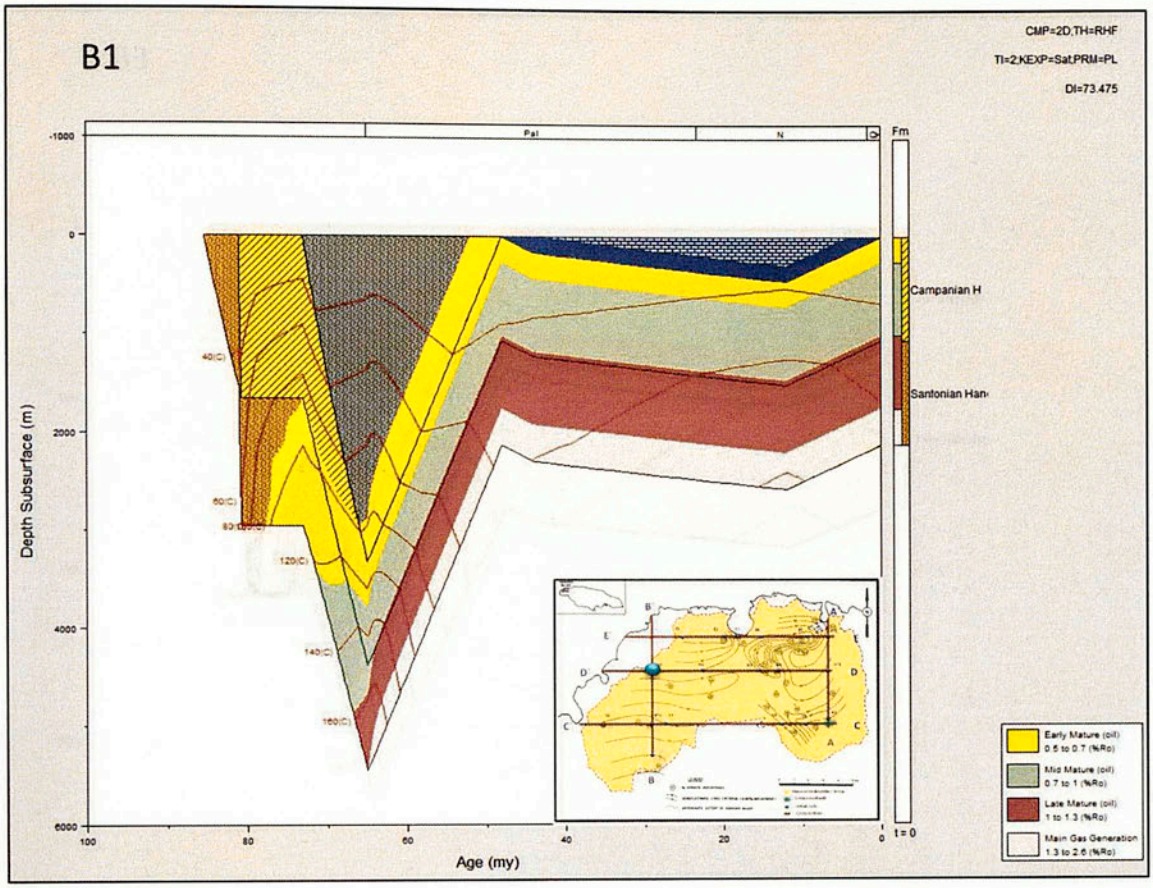


**Figure 8.14** Burial History of Virtual Well B1 with rifting heat flow and related oil windows. Blue dot indicates position of the well on the inset.

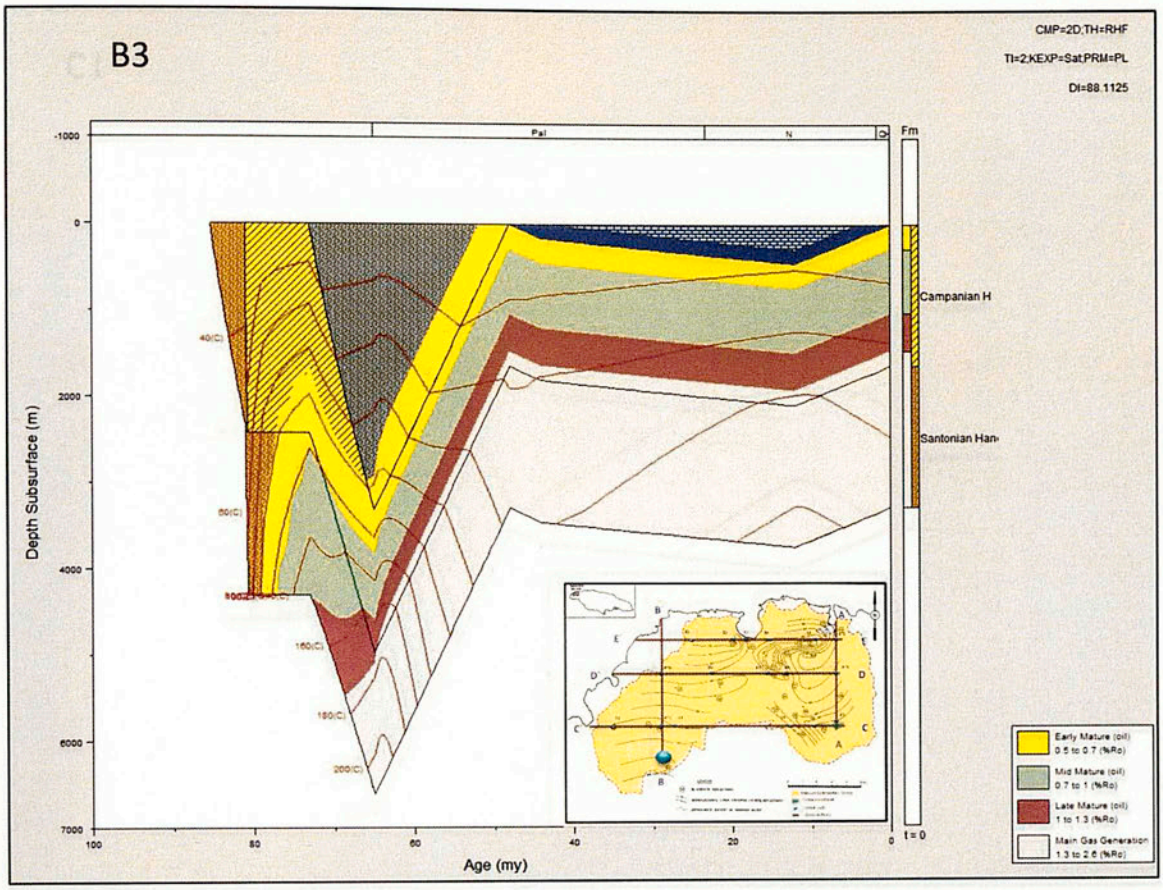


**Figure 8.15** Burial History of Virtual Well B3 with rifting heat flow and related oil windows. Blue dot indicates position of the well on the inset.

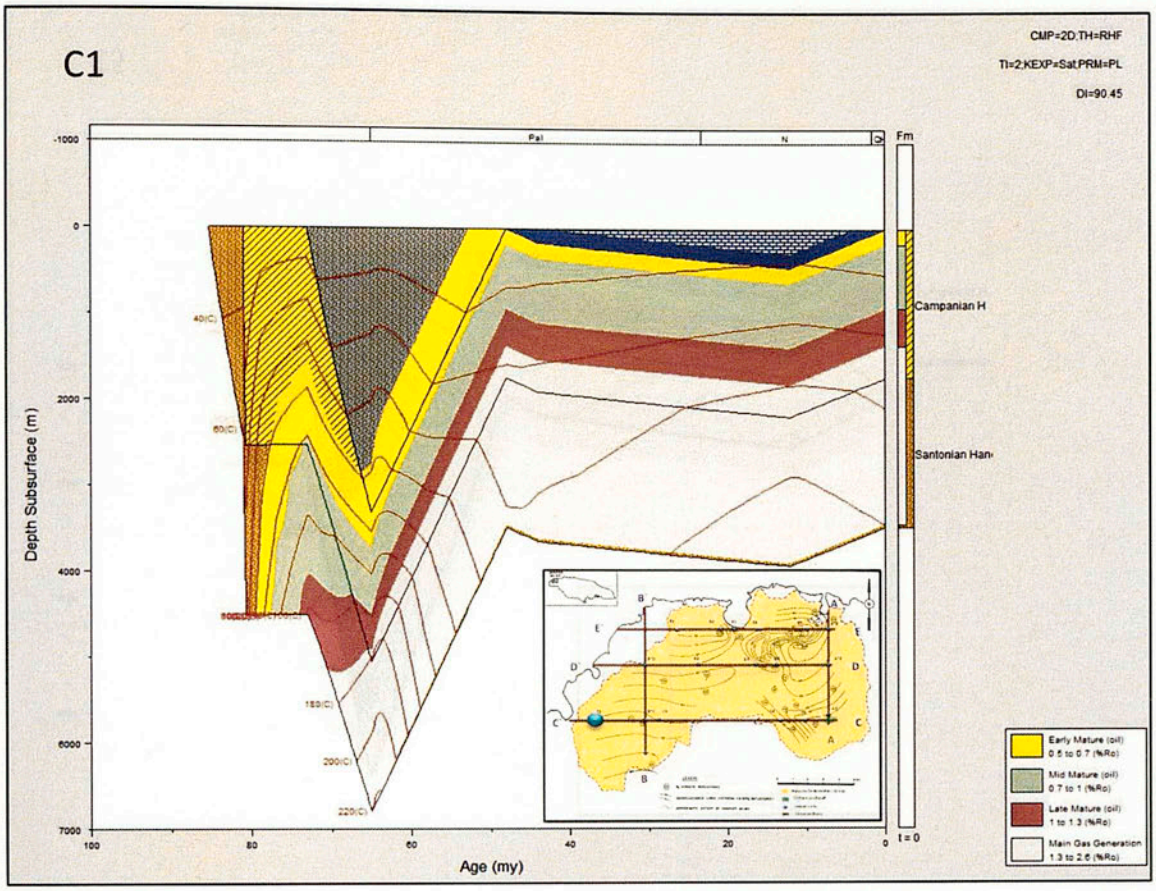


**Figure 8.16** Burial History of Virtual Well C1 with rifting heat flow and related oil windows. Blue dot indicates position of the well on the inset.

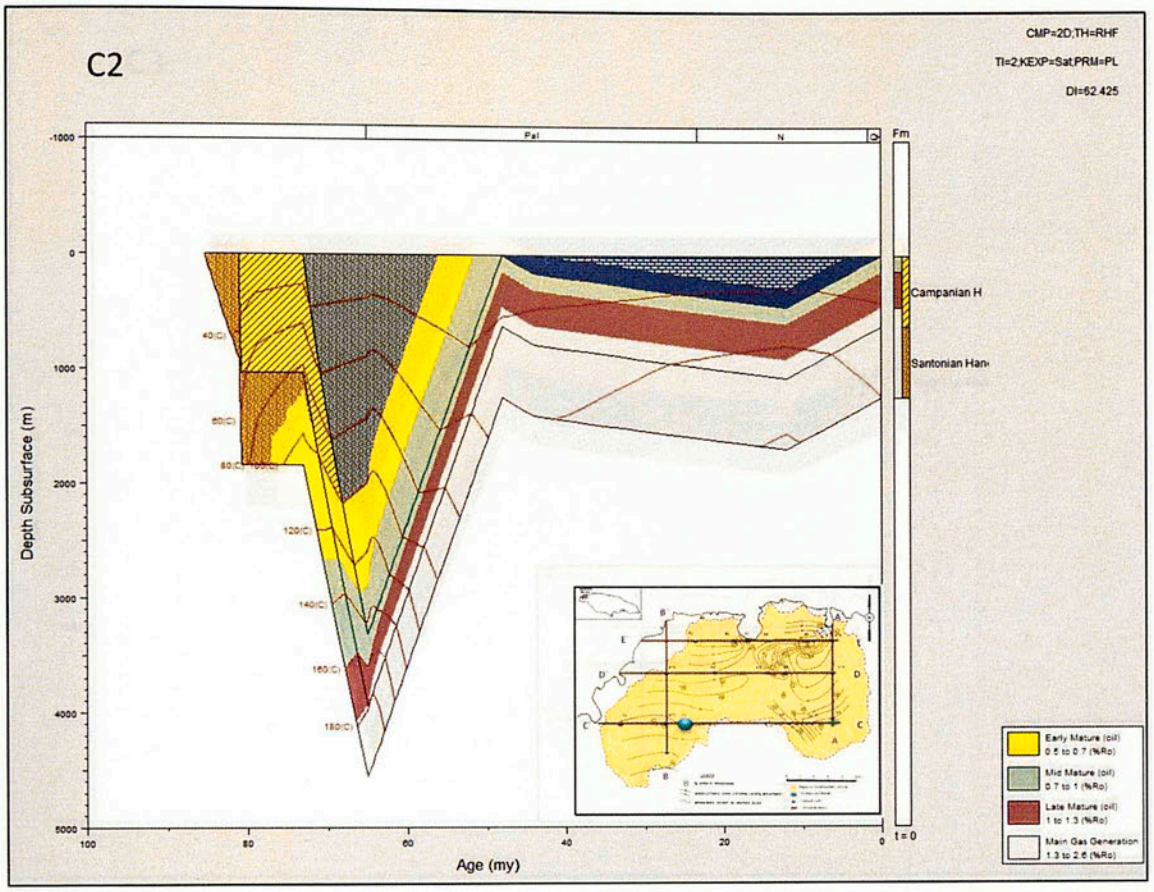


**Figure 8.17** Burial History of Virtual Well C2 with rifting heat flow and related oil windows. Blue dot indicates position of the well on the inset.

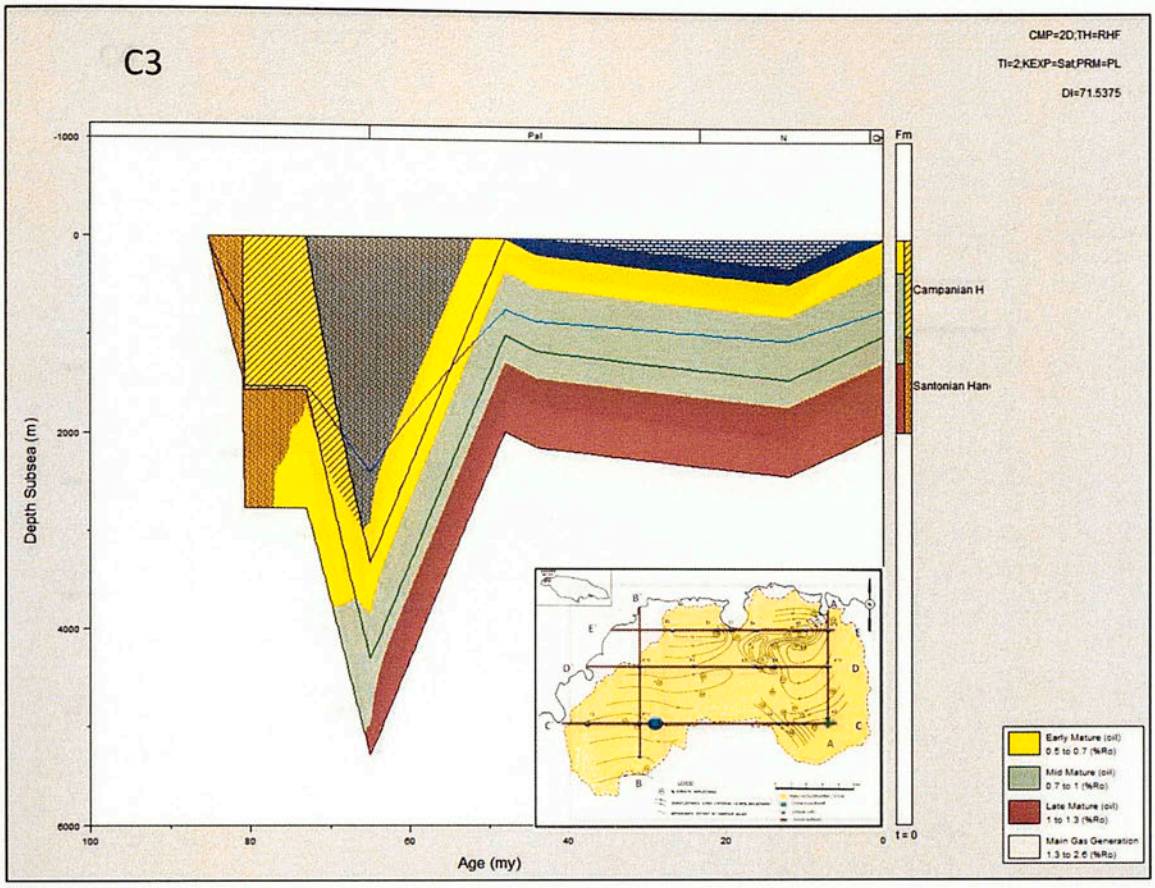


**Figure 8.18** Burial History of Virtual Well C3 with rifting heat flow and related oil windows. Blue dot indicates position of the well on the inset.

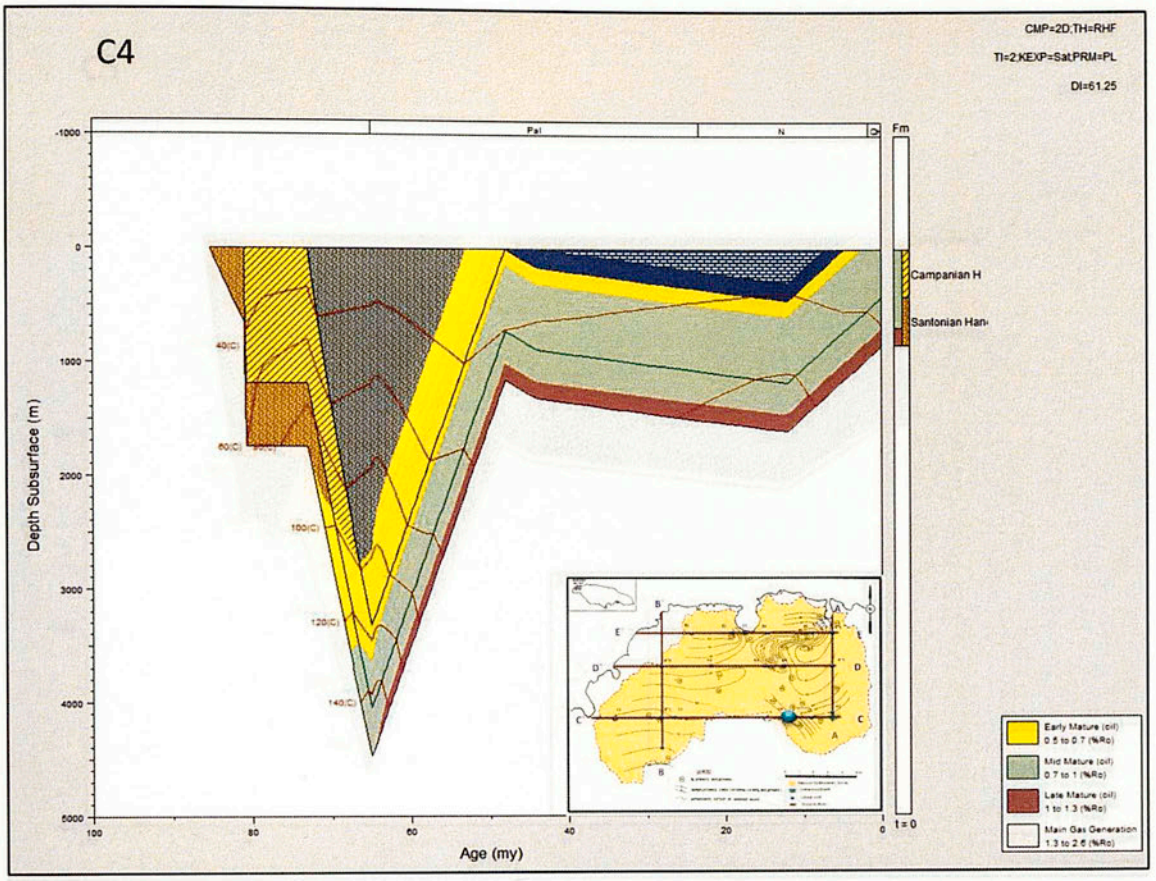


**Figure 8.19** Burial History of Virtual Well C4 with rifting heat flow and related oil windows. Blue dot indicates position of the well on the inset.

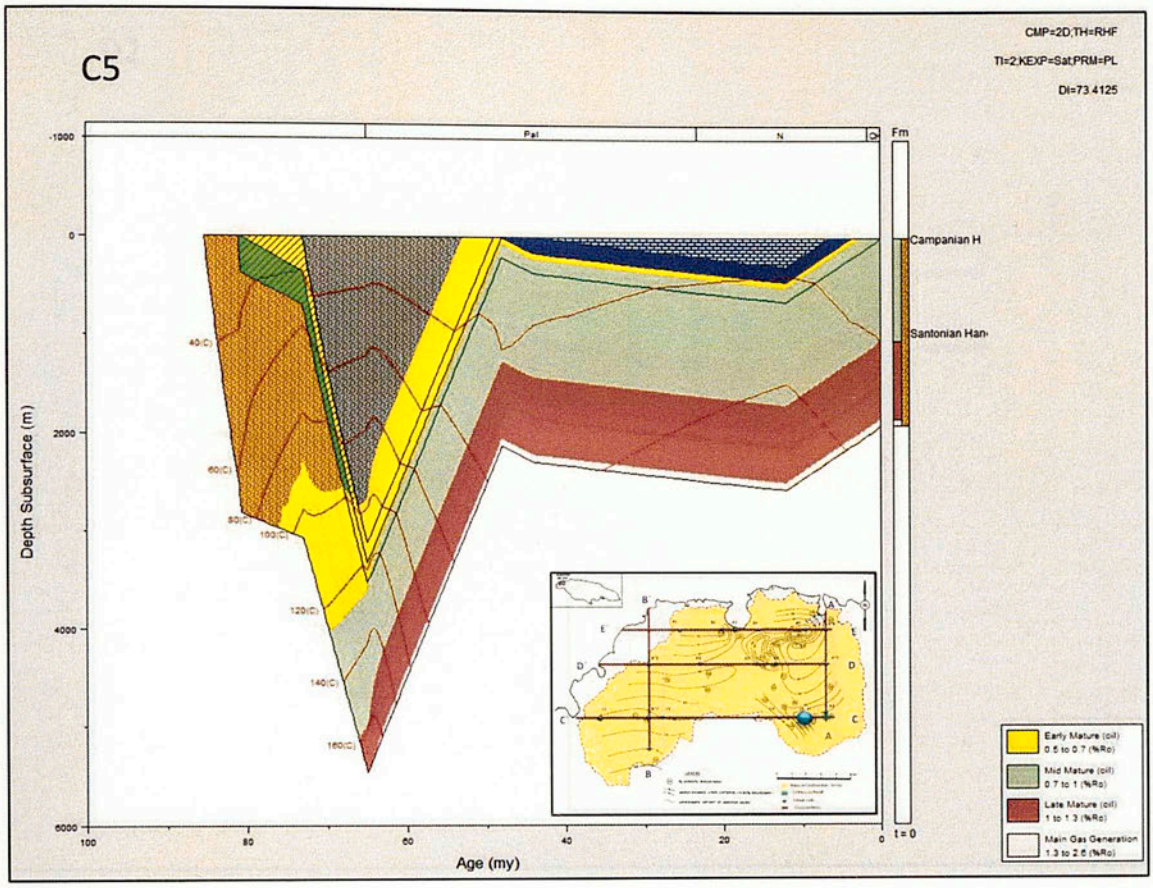


**Figure 8.20** Burial History of Virtual Well C5 with rifting heat flow and related oil windows. Blue dot indicates position of the well on the inset.

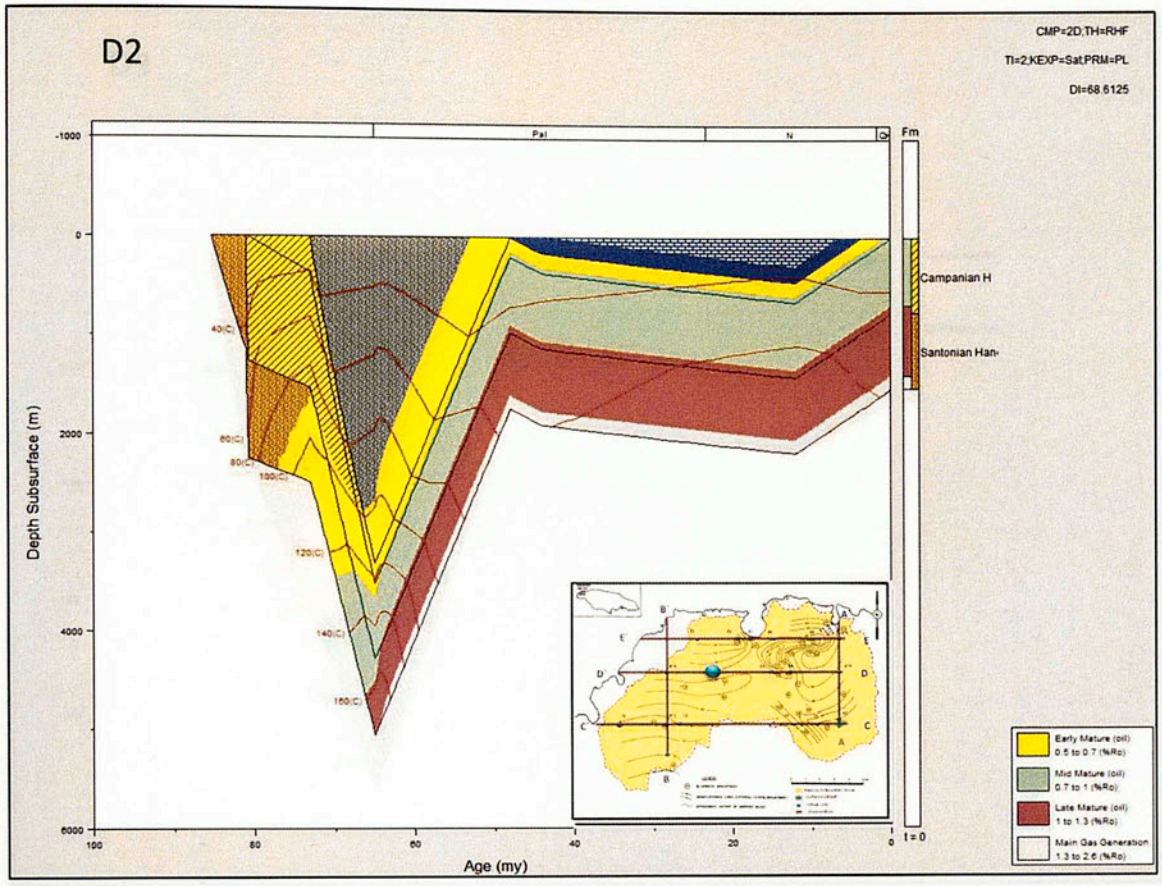


**Figure 8.21** Burial History of Virtual Well D2 with rifting heat flow and related oil windows. Blue dot indicates position of the well on the inset.

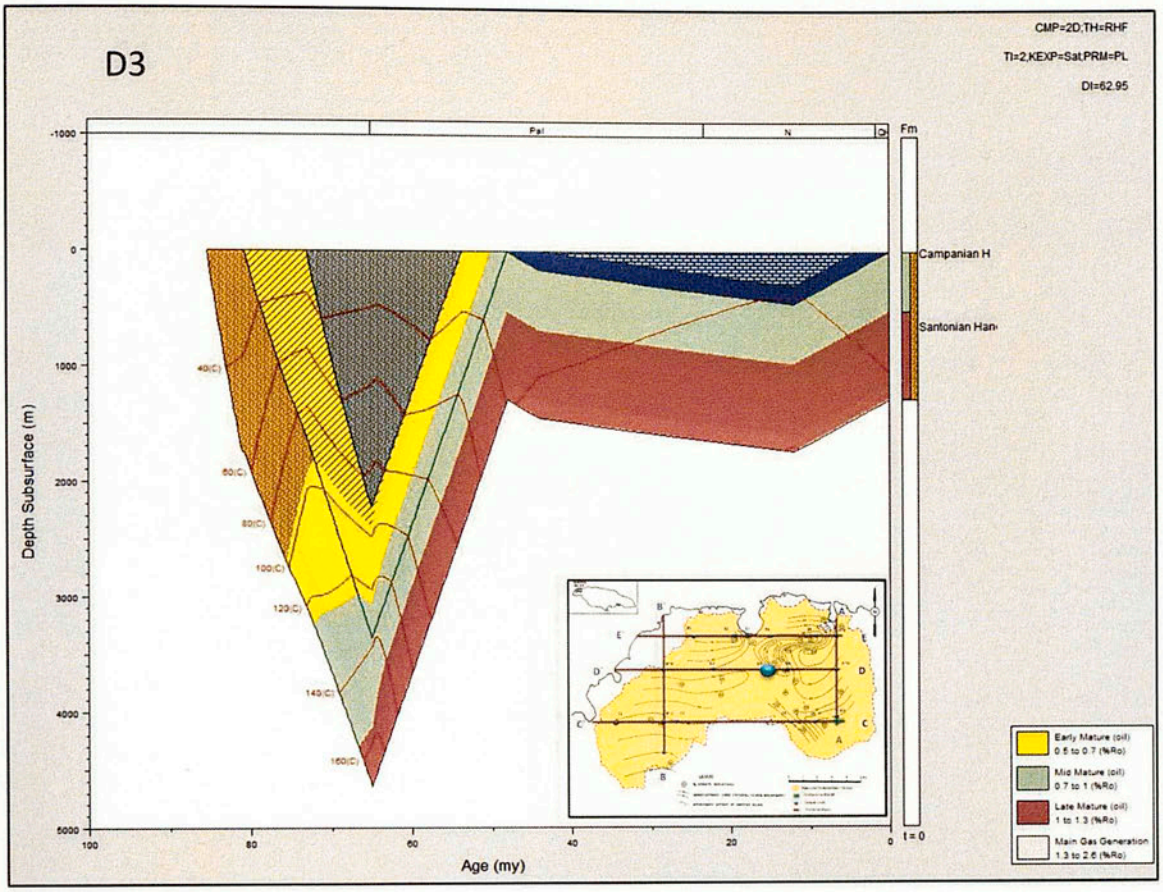


**Figure 8.22** Burial History of Virtual Well D3 with rifting heat flow and related oil windows. Blue dot indicates position of the well on the inset.

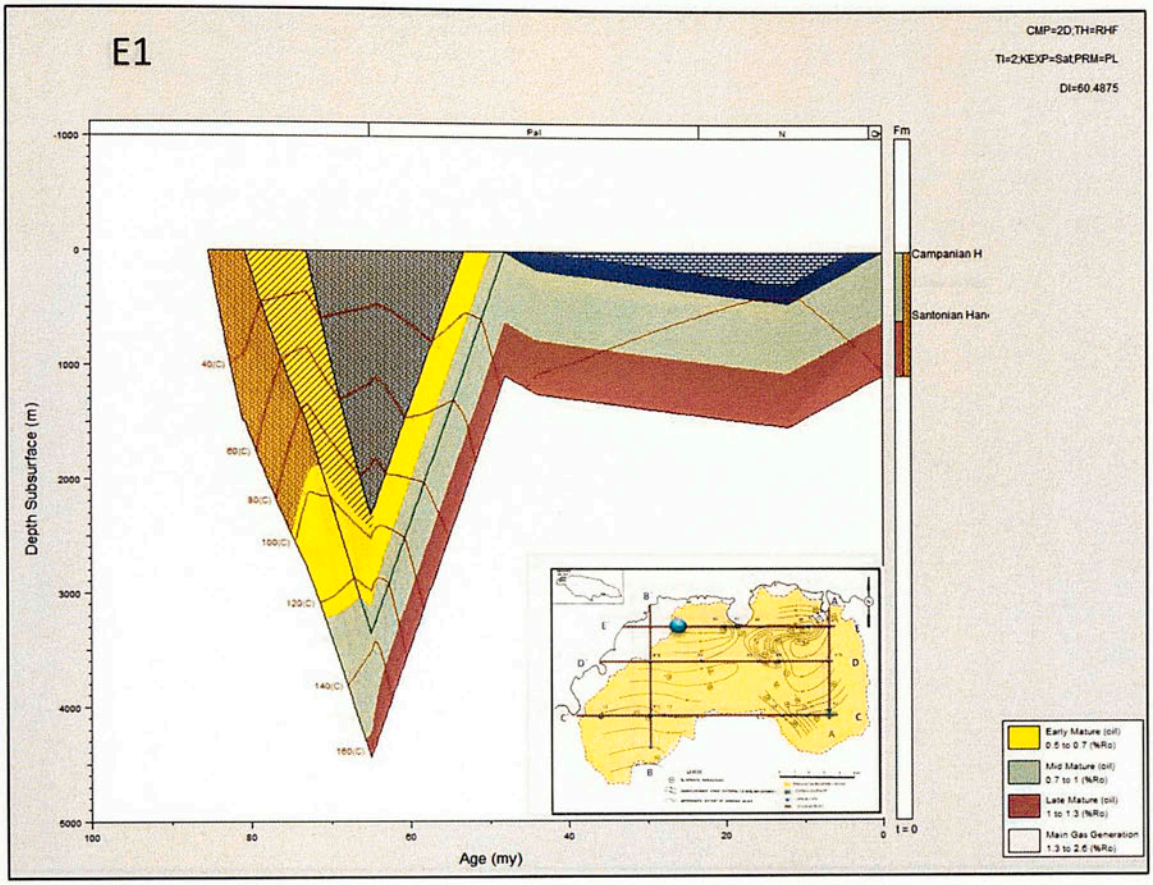


**Figure 8.23** Burial History of Virtual Well E1 with rifting heat flow and related oil windows. Blue dot indicates position of the well on the inset.

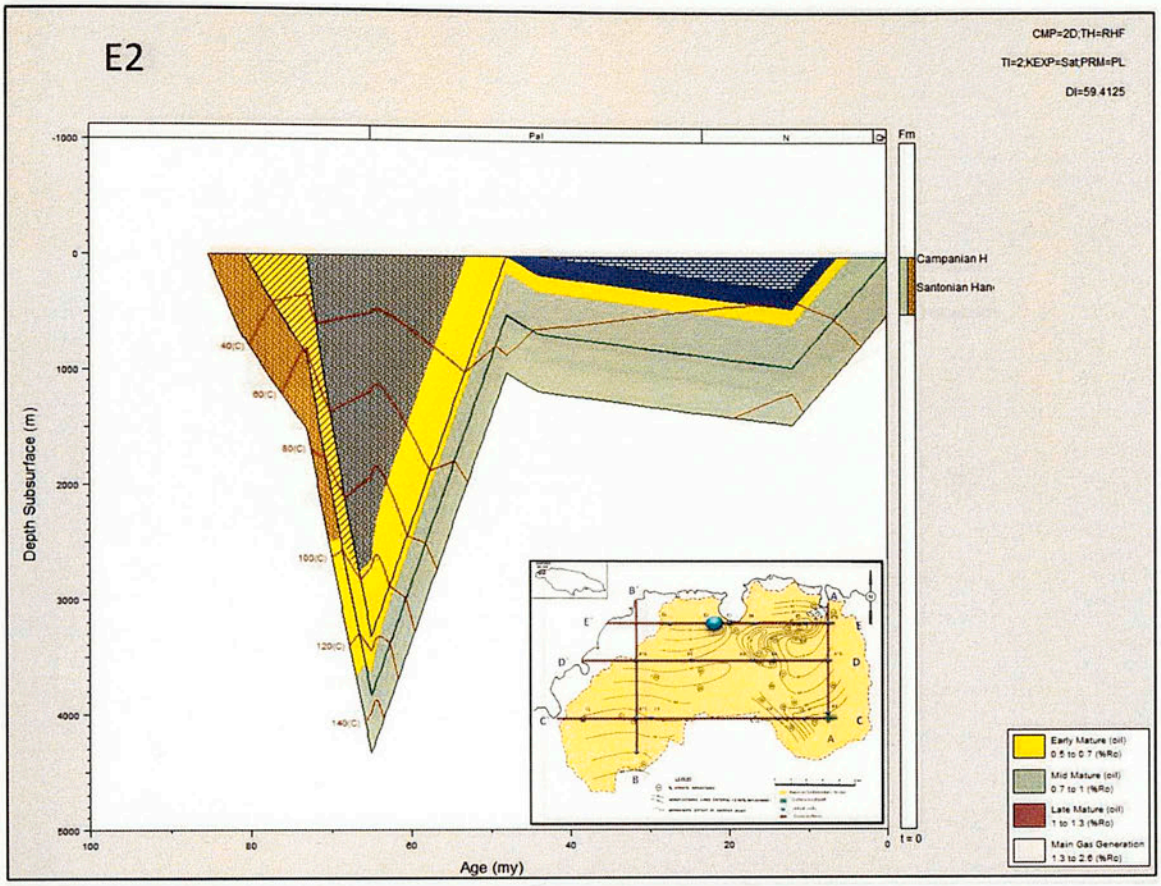


**Figure 8.24** Burial History of Virtual Well E2 with rifting heat flow and related oil windows. Blue dot indicates position of the well on the inset.

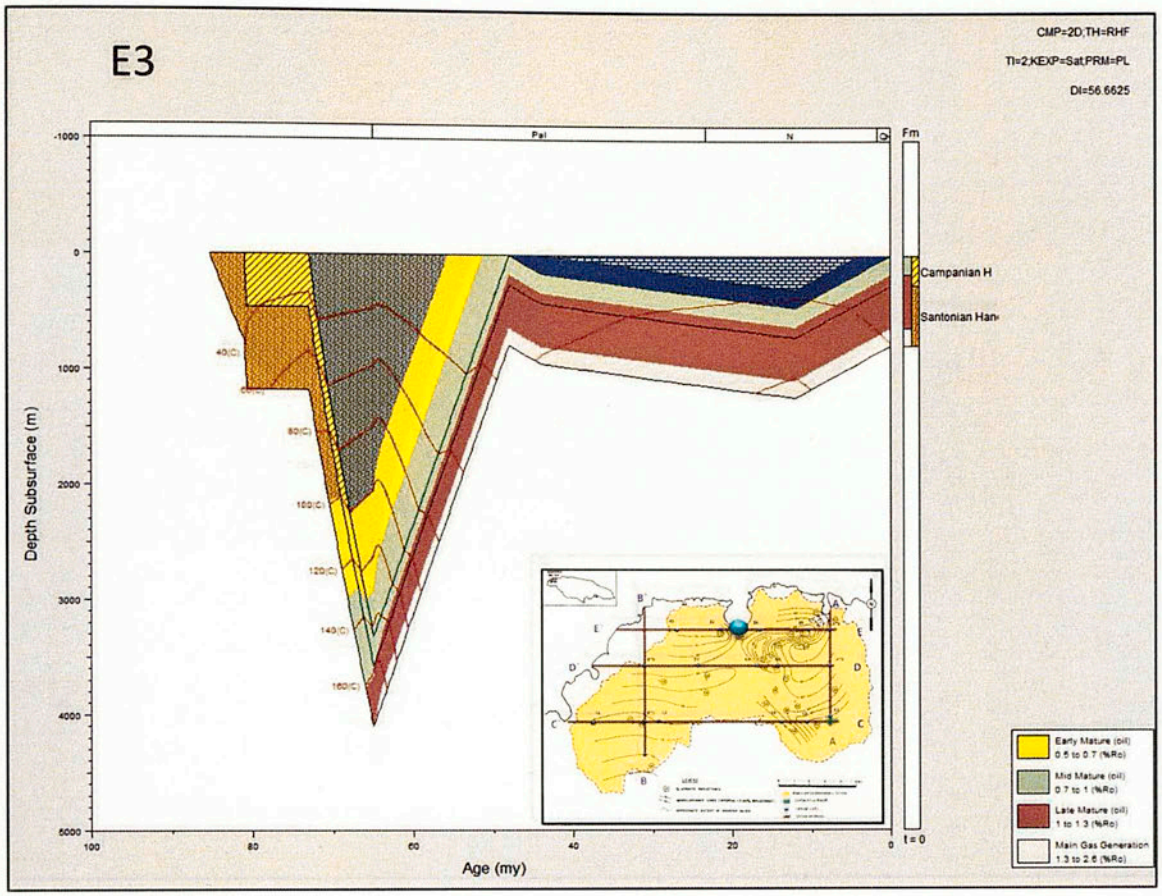


**Figure 8.25** Burial History of Virtual Well E3 with rifting heat flow and related oil windows. Blue dot indicates position of the well on the inset.

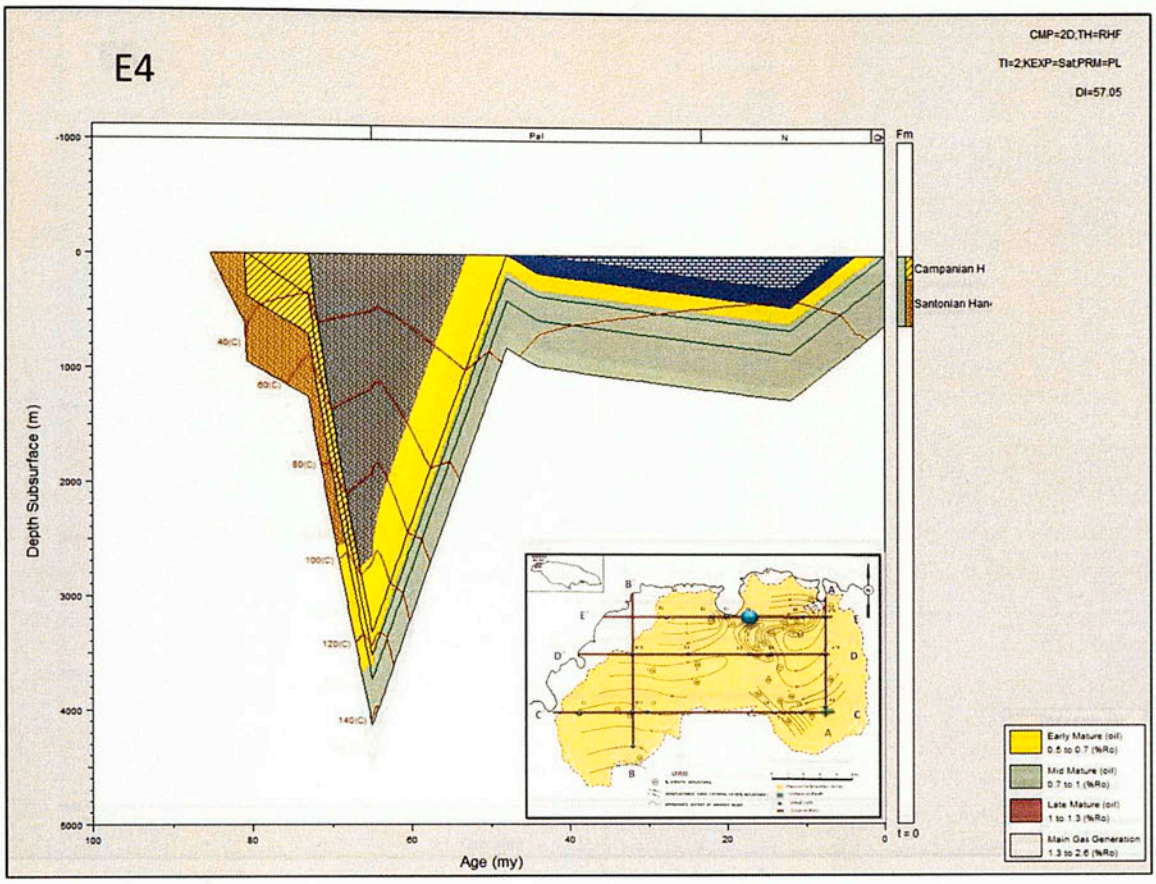


**Figure 8.26** Burial History of Virtual Well E4 with rifting heat flow and related oil windows. Blue dot indicates position of the well on the inset.

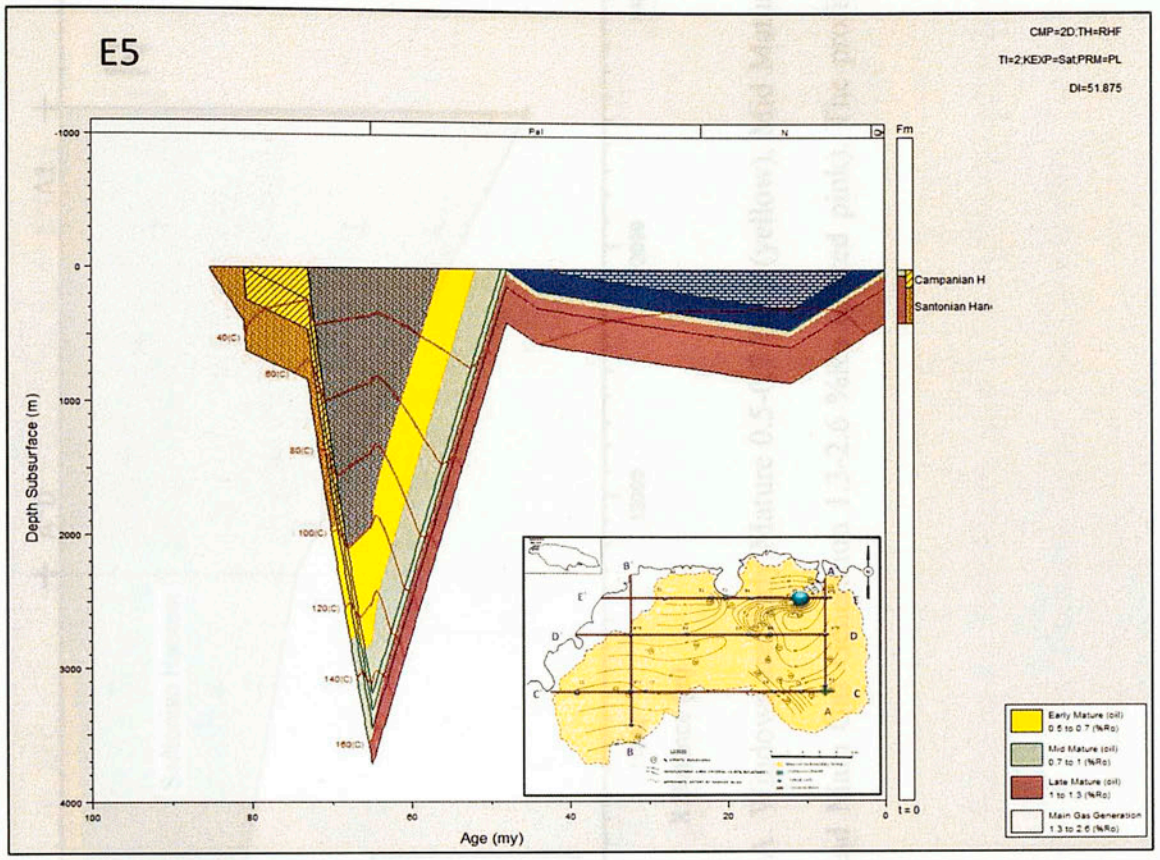


**Figure 8.27** Burial History of Virtual Well E5 with rifting heat flow and related oil windows. Blue dot indicates position of the well on the inset.

### 8.5.2 2-D Maturity

As the Hanover Inlier has gone through similar tectonic events (consequently with the same thermal conditions) as the Hanover Block, one may assume little lateral change of heat flow outside the proximity of the volcanic intrusion. Although the depth section changes throughout the inlier, if lithospheric thickness is invariant and contributions from sediments radioactivity is minimal, one may assume heat flow is not a function of vertical depth. Then, applying like thermal conditions for the 2-D model as the 1-D model resulted in the following present day maturity cross-sections in Hanover Block (Fig. 8.28 to Fig. 8.32).

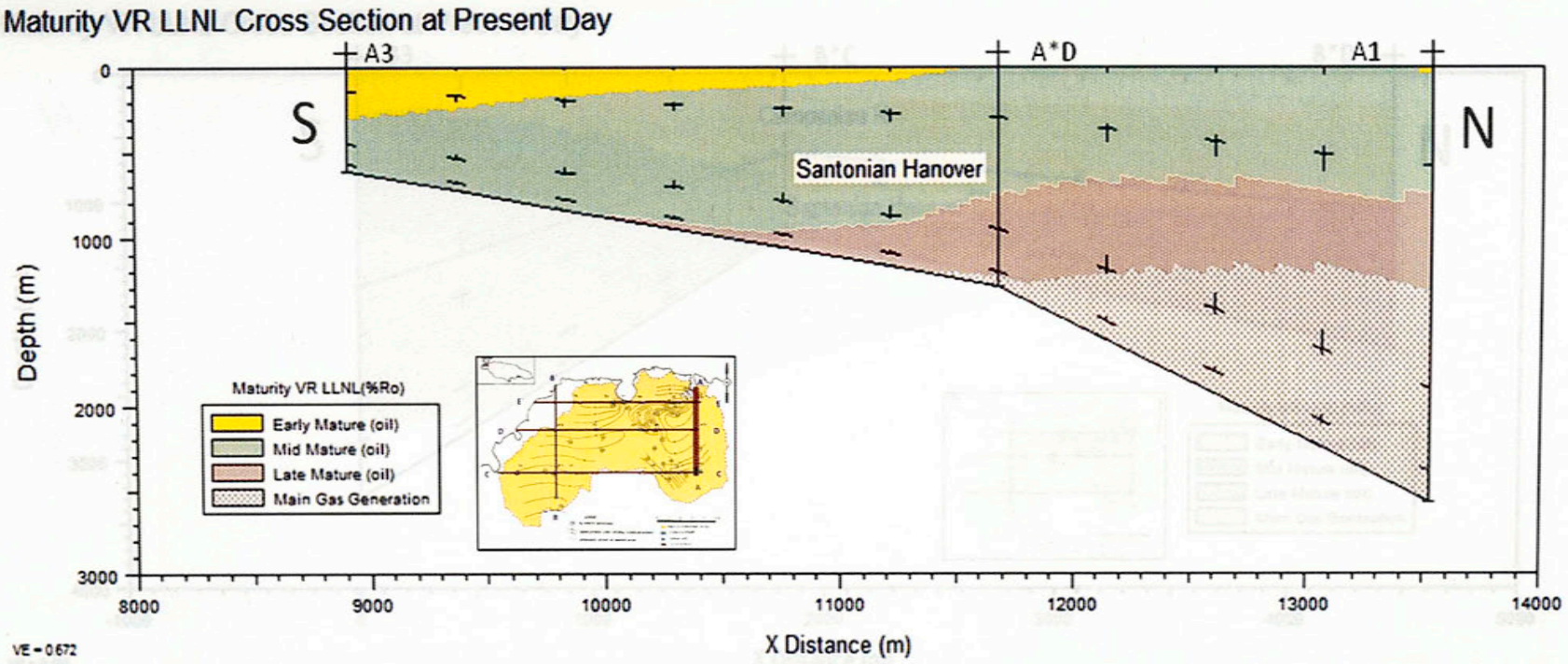


**Figure 8.28** The present day maturity in cross-section A`-A. Windows are Early Mature 0.5-0.7 %Ro (yellow), Mid Mature 0.7-1.0 %Ro (green), Late Mature 1.0-1.3 %Ro (pink), and Main Gas Generation 1.3-2.6 %Ro (dotted pink). The profile location is shown on the inset map as a red line.

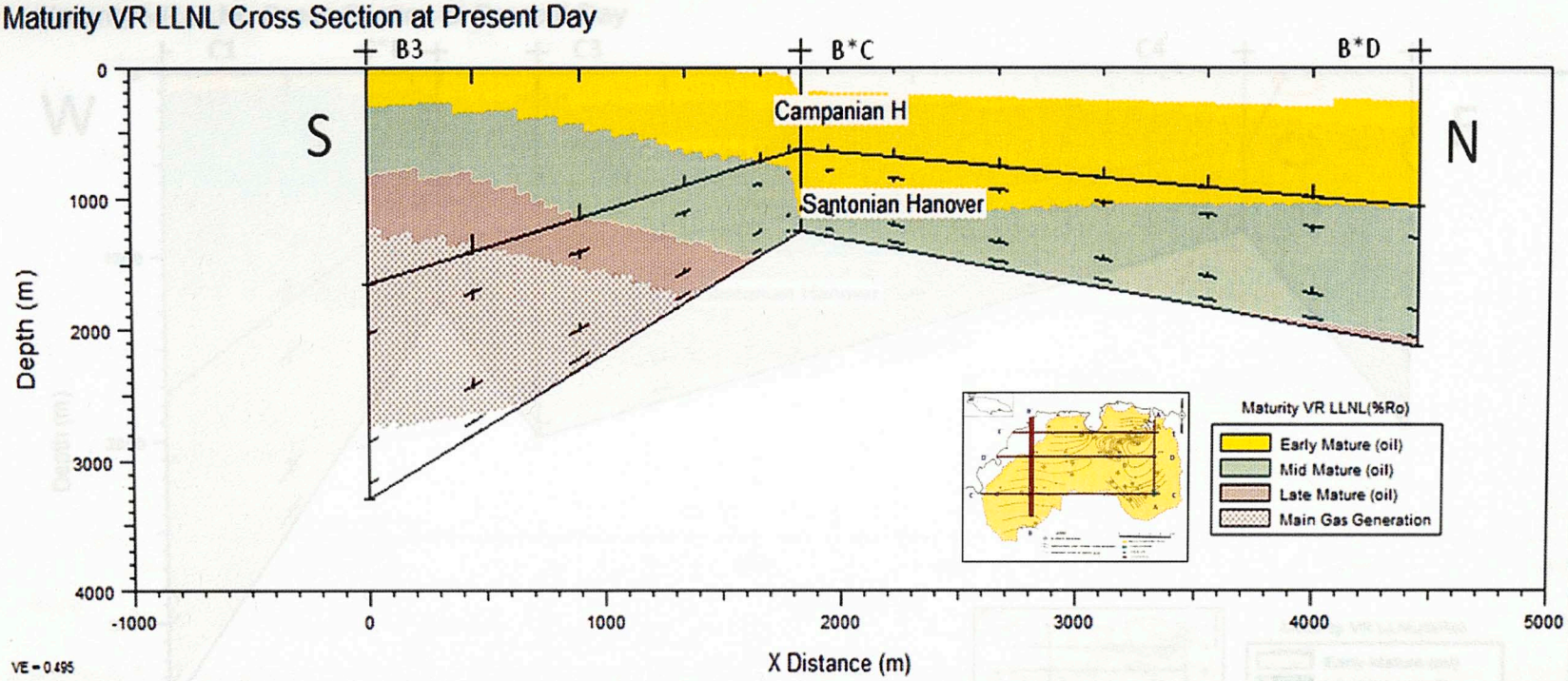


**Figure 8.29** The present day maturity in cross-section B`-B. Windows are Early Mature 0.5-0.7 %Ro (yellow), Mid Mature 0.7-1.0 %Ro (green), Late Mature 1.0-1.3 %Ro (pink), and Main Gas Generation 1.3-2.6 %Ro (dotted pink). The profile location is shown on the inset map as a red line.

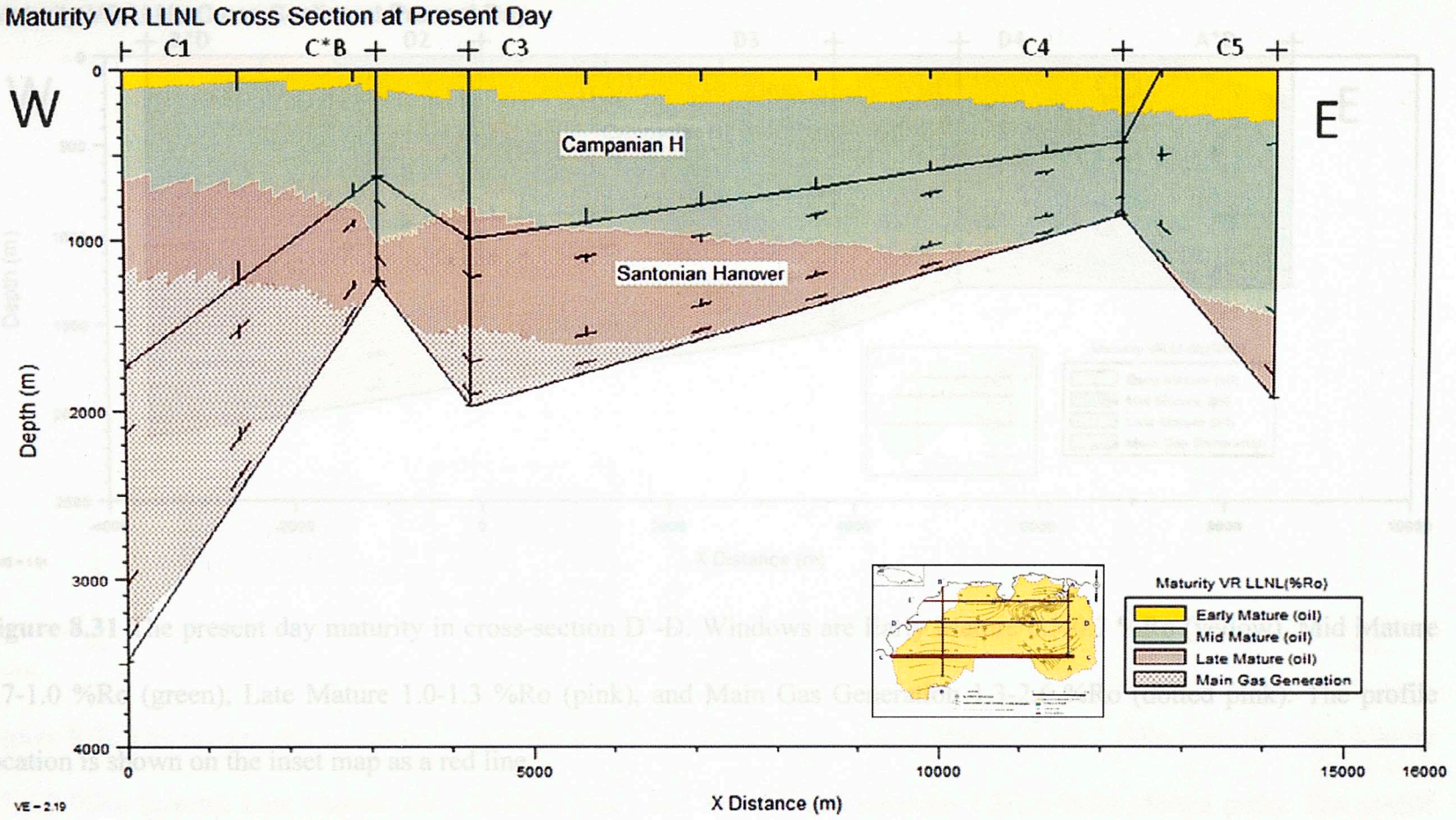


**Figure 8.30** The present day maturity in cross-section C`-C. Windows are Early Mature 0.5-0.7 %Ro (yellow), Mid Mature 0.7-1.0 %Ro (green), Late Mature 1.0-1.3 %Ro (pink), and Main Gas Generation 1.3-2.6 %Ro (dotted pink). The profile location is shown on the inset map as a red line.

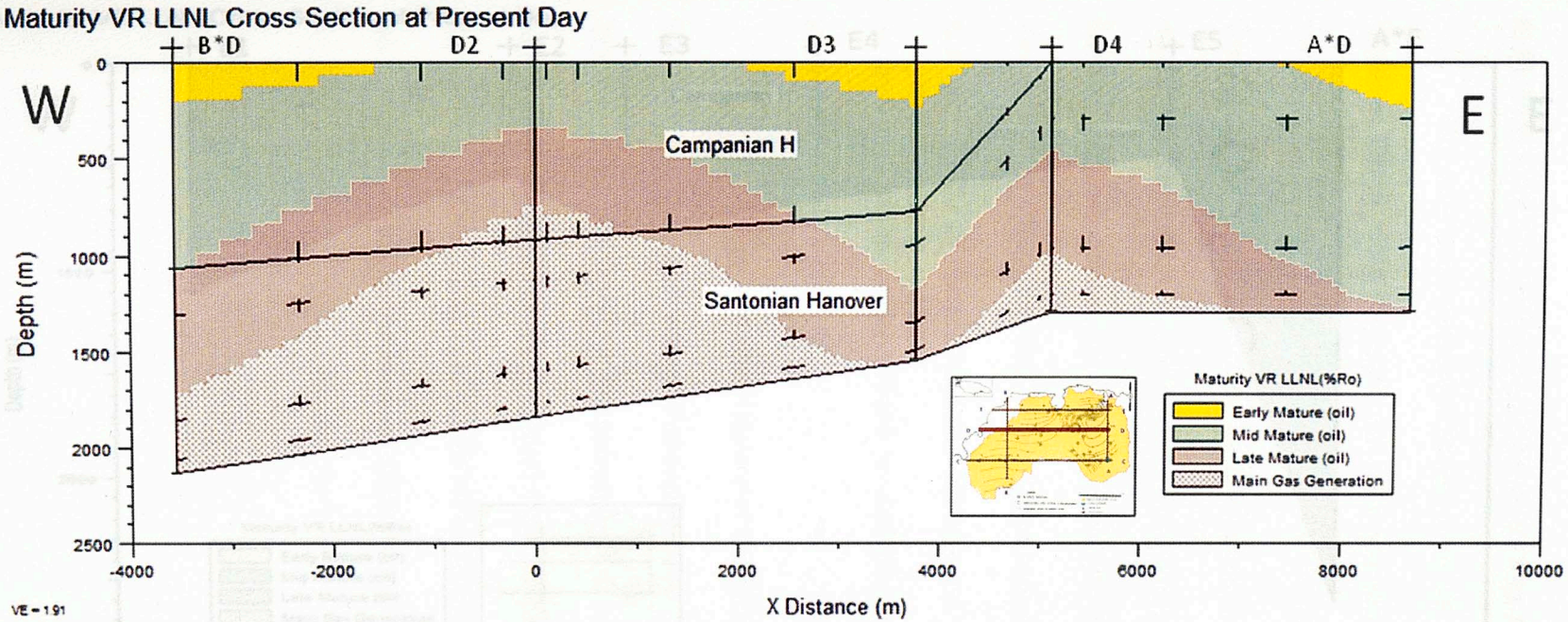


**Figure 8.31** The present day maturity in cross-section D`-D. Windows are Early Mature 0.5-0.7 %Ro (yellow), Mid Mature 0.7-1.0 %Ro (green), Late Mature 1.0-1.3 %Ro (pink), and Main Gas Generation 1.3-2.6 %Ro (dotted pink). The profile location is shown on the inset map as a red line.

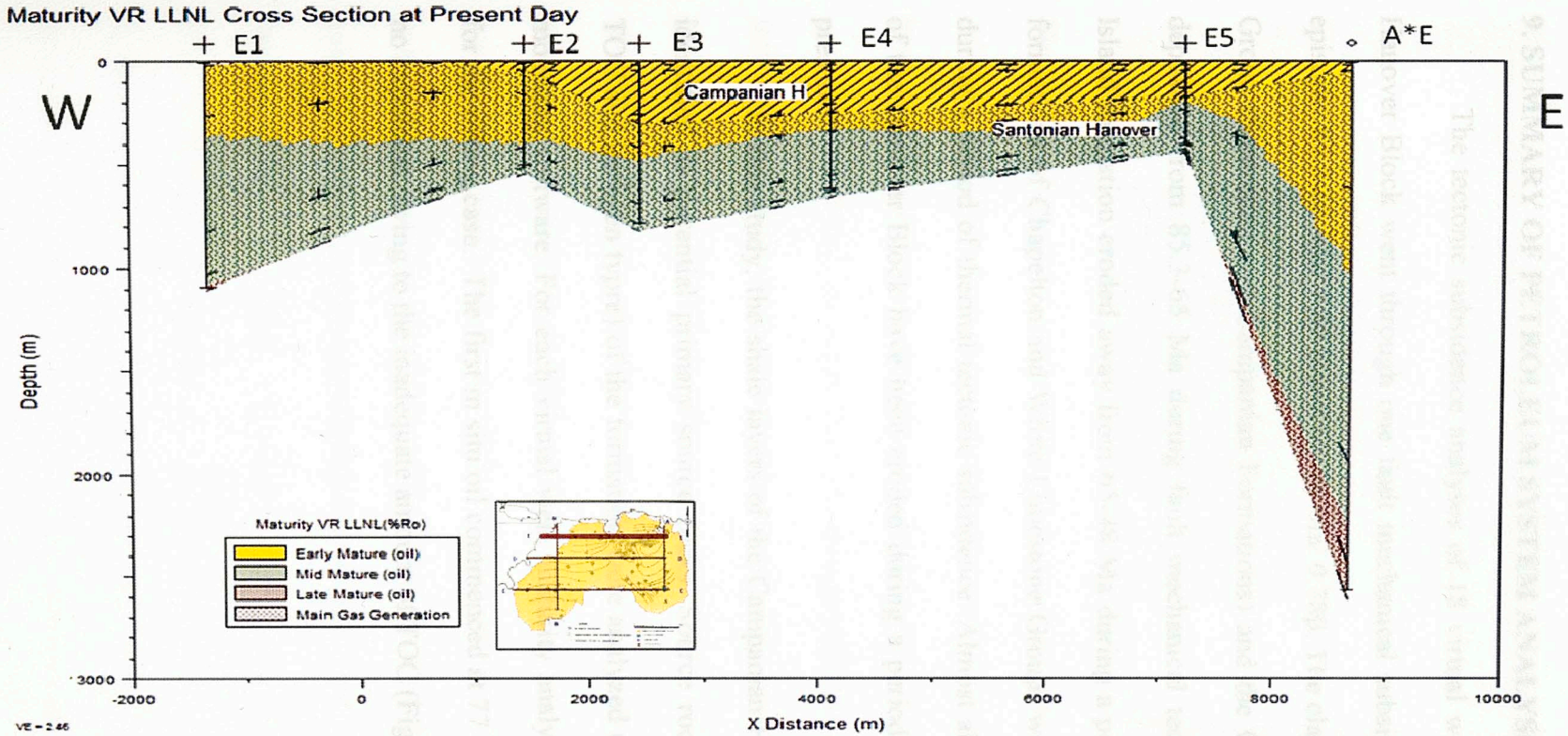


**Figure 8.32** The present day maturity in cross-section E`-E. Windows are Early Mature 0.5-0.7 %Ro (yellow), Mid Mature 0.7-1.0 %Ro (green), Late Mature 1.0-1.3 %Ro (pink), and Main Gas Generation 1.3-2.6 %Ro (dotted pink). The profile location is shown on the inset map as a red line.

## 9. SUMMARY OF PETROLEUM SYSTEM ANALYSIS

The tectonic subsidence analyses of 18 virtual wells onshore showed that the Hanover Block went through one fault mechanical subsidence episode and one uplift episode: 85.3-65 Ma/ 1.85 β and 65-48 Ma/ 0.78β. The clastic sediments of the Hanover Group (Santonian and Campanian Formations) and the Green Island Formation were deposited from 85.3-65 Ma during fault mechanical tectonic subsidence. All Green Island formation eroded away from 65-48 Ma during a period of uplift. The carbonate formations of Chapelton and White Limestone Groups were deposited from 48-12 Ma during a period of thermal tectonic subsidence. Almost all of the carbonate formations of the Hanover Block have been eroded during a period of uplift from 12 Ma to the present.

In this study, the shale layers of the Campanian Hanover Formation have been identified as potential primary source rocks. Source rock volume and quantity (e.g. TOC and kerogen typre) of the formation were analyzed using both 1-D and 2-D basin modeling software. For each virtual well, maturity analysis was conducted separately for the rifting case. The first in situ oil commenced at 77 Ma. However, there would be no expulsion owing to the inadequate amount of TOC (Fig. 9.1).




**Figure 9.1** Cumulative Hydrocarbon/TOC vs. Time graphs for virtual wells C*B and A*D showing the first in-situ hydrocarbon commenced at 77 Ma but there is no hydrocarbon expulsion in the Petroleum System owing to the lack of TOC values.

In summary, no observable effective petroleum system has been developed in this system. Although there is sufficient maturity, owing to thermal conditions with strong calibration of vitrinite reflectance values, lack of TOC (average equal to 0.39%) prevents expulsion migration and the lack of reservoir porosity negates an accumulation. However, if TOC values exceed the average lean number, and if outcrop weathering contributed to the lack of observed porosity through localized calcite cementation, then the possibility of deep surface favorable petroleum system criticals exist. Evaluation of such a possibility would best occur through a combined bore-hole-seismic study.

## 10. CONCLUSIONS

Ten conclusions from this study are:

1. With respect to tectonic subsidence, the Hanover Inlier from western Jamaica exhibits one major fault mechanical tectonic subsidence period (85.3-65 Ma/ 1.85 β) and one major uplift or shortening period (65-48 Ma/ 0.78β).

2. Maturity of the potential source rocks was modeled for rifting heat flow case. Present heat flow is calculated from the measured borehole temperature values. The generated thermal model is geovalidated with published vitrinite reflectance values.

3. The Campanian and/or Santonian formations are in both oil and gas windows, although it is unlikely that they have produced oil or gas due to lack of TOC.

4. The first in-situ oil in the Campanian and/or Santonian formation commenced at 77 Ma. There is no expulsion of hydrocarbon owing to the inadequate amount of TOC (0.39 %).

5. The Petroleum Play for Hanover Group is not present for the following reasons: poor TOC of the source rock, no proven seal and trap, and calcite filling porosity reduction of possible reservoirs.

6. A minimum porosity value for Kc Sandstone is estimated with software assisted petrographic image study as 10 %.

7. Green Island Formation thickness is calculated as 3300 meters with an empirical formula assuming rapid burial.

8. Outcrop macroscopic observations, and SGR reveal distinct deep water architectural elements (channels, crevasse splays, levees, fan lobe deposits and distal fan deposits) were observed in the Claremont (sub) Formation.

9. Synthesis of outcrop macroscopic observations and reservoir architectural element interpretations reveal relative facies positions on the shelf (intra slope, toe-of-slope, and abyssal plain) and its system type (confined, weakly confined, and un-confined).

10. Synthesis of positions of architectural elements in a deep marine system and outcrop macroscopic observations reveal the relative position of deposits on a sea level cycle as several stages of Lowstand System Tract (falling stage, turnaround stage, and early rise stage).

## REFERENCES CITED


Allen, P. and J. Allen, 2005, Basin analysis, principles and applications, second edition: Oxford, Blackwell Publishing, 549 p.

Andrew, E.M., Paterson Grant and Watson Ltd, G. Wadge, S. Brookes, M. Royall, G.

BasinMod 1-D Manual, 2005. Platte River Associates Inc., Boulder, Colorado, 546 p.

BasinMod 1-D Manual, 2005. Platte River Associates Inc., Boulder, Colorado, 603 p.

Bouma, A. H, 1962, Sedimentology of some Flysch deposits: A graphic approach to facies interpretation: Amsterdam, Elsevier, 168 p.

Burke, K., Cooper, C., Dewey, J.F., Mann, P. & Pindell, J.L. (1984) Caribbean tectonics and relative plate motions. Geol. Soc. Am. Mem. 162, 31-63.

Connan, J. and Cassou, A.M., 1980. Properties of gases and petroleum liquids derived from terrestrial kerogen at various levels of maturation. Geochim. et Cosmochim. Acta. 44, 1-24.

Dow, W.G. 1977. Kerogen studies and geological interpretations. Journal of Geochemical Exploration, 7, 79-99.

Draper, and E. Robinson, 1992, Bouguer Gravity: Kingston, Ministry og Production, Mining and Commerce, Jamaica Geological Survey Division, map number: 92-106, scale 1:250000, 1 sheet.

Fowler, C.M.R., 1990, The solid earth, an introduction to global geophysics: Cambridge, University Press, 472 p.

Grippi, J. 1980. Geology of the Lucea Inlier, western Jamaica. Journal of the Geological Society of Jamaica, 19, 1-24.

Hedberg, H.D., 1968. Significance of high-wax oils with respect to genesis of petroleum. AAPG Bull., 52, 736-750.

Hegarty, K.A., Weissel, J.K., and Mutter, J.C., 1988. Subsidence history of Australia's southern margin: constraints on basin models. AAPG Bull., 72:615–633.

Hunt, J.M., 1979. Petroleum geochemistry and geology. W.H. Freeman and Co., San Francisco.

Jackson, T.A. & Smith, T.E. 1979. The tectonic significance of basalts and dacites in the Wagwater Belt, Jamaica. Geological Magazine, 116, 365-374.

Jordan, D.W., D.R. Lowe, R.M. Slatt, C.G. Stone, A. D'Agostino, M.H. Scheihing, and R.H. Gillespie, 1993, Scales of geological heterogeneity of Pennsylvanian Jackfork Group, Ouachita Mountains, Arkansas: Applications to Field Development and Exploration for Deep-Water Sandstones, Arkansas Geological Commission Field Guidebook 93-1, 141 p.

Loutit, T. S., J. Hardenbol, P. R. Vail, and G. R. Baum, 1988, Condensed sections: the key to age determination and correlation of continental margin sequences, in C. K. Wilgus, B. S. Hastings, C. A. Ross, H. W. Posamentier, J. Van Wagoner, and C. G. St. C. Kendall, eds., Sea-level changes: an integrated approach: SEPM Special Publication No. 42, p. 183–213.

Magoon, L.B. and Dow, W.G., 1994. The petroleum system. In: The Petroleum System-From Source to Trap (eds. L.B. Magoon and W.G. Dow). American Association Petroleum Geologists Memoir.

Mahaffie, M. J., 1994, reservoir classification for turbidite intervals at the Mars discovery, Mississippi canyon 807, Gulf of Mexico, in P. Weimer, A.H. Bouma, and B.F. Perkins, eds., Submarine fans and turbidite systems: Gulf Coast Section–SEPM Foundation 15th Annual Research Conference, p. 233–244.

Mann, P., G. Draper, and K. Burke, 1985, Neotectonics of a strike-slip restraining bend system, Jamaica: Strike-slip Deformation, Basin Formation and Sedimentation: SEPM Special Publication, p. 211-226.

Metwalli, F.I., Pigott, J.D., 2005. Analysis of petroleum system critical of the Matruh-Shushan Basin, Western Desert, Egypt: Petroleum Goescience, v.11, p.157-178.

Meyerhoff, A.A. & Krieg, E.A. 1977. Petroleum potential of Jamaica. Special publication, Ministry of Mining and Natural Resources, Jamaica.

Mines and Geology Division, 1984, Lucea Geological Sheet: Ministry of Mining and Telecommunications, Jamaica, map number 1, scale: 1:50000, 20 sheets.

Ministry of Production, Mining and Commerce, 1992, Bouguer Gravity Map of Jamaica, CIDA Metallic Mineral Project 504/12713

Mitchell, S. F., 2003, Sedimentology and tectonic evolution of the Cretaceous rocks of central Jamaica: Relationships to the platetectonic evolution of the Caribbean, in C. Bartolini, R. T. Buffler, and J. Blickwede, eds., The Circum-Gulf of Mexico and the Caribbean:Hydrocarbon habitats, basin formation, and plate tectonics: AAPG Memoir 79, p. 605– 623.

Mutti, E. and W. R. Normark, 1987, Comparing examples of modern and ancient turbidite systems: problems and concepts, in J. K. Leggett and G. G. Zuffa, eds., Marine clastic sedimentology: London, Graham and Trotman, p. 1–38.

Mutti, E. and W. R. Normark, 1991, An integrated approach to the study of turbidite systems, in P. Weimer and M. H. Link, eds, Seismic facies and sedimentary processes of submarine fans and turbidite systems: New York, Springer-Verlag, 75–106.

Pigott, J.D., G. Teferra, Y. A. Abdelhady, 1996. Late Cenezoic paleo-heatflow of the Red Sea: Regional Implications for Tectonic and Hydrocarbon Exploration: Proceedings 13th Petroleum Conference, Cairo, Egypt, Vol.1, p. 313-339.

Pigott, P., and N. Sattayarak, 1993. Aspects of sedimentary basin evolution assessed through tectonic subsidence analysis. Example: Northern Gulf of Thailand: Journal of Southeast Asia Earth Sciences, v. 8, p. 407-420.

Pigott, J.D., 2009, Written Communication.

Pigott, J.D. and Ru Ke., 1994. Basin superposition on the northern margin of the South China Sea: Tectonophysics, 235, 27-50.

Pindell, J., 1994, Evolution of the Gulf of Mexico and Caribbean: Donovan, S.K. and T.A. Jackson, Caribbean Geology: an Introduction, Kingston, Jamaica, University of the West Indies Publishers` Association, p. 13-40.

Pindell, J., and L. Kennan, in press 2009, Tectonic evolution of the Gulf of Mexico, Caribbean and northern South America in the mantle reference frame: an update, PREPRINT, p. 1-60.

Radiation Solution Inc., RS-230 BGO Spectrometer. User manual.

Rai, C., 2011. Formation Evaluation Using Well Logs PE 3813, Lecture notes.

Rodrigues, K., 1991, Organic Geochemistry and Petroleum Potential of Jamaica, Journal of Petroleum Geology, v. 14, p. 309-322.

Rodrigues, K., 1991, Constraining burial history from vitrinite reflectance, Hanover Block, western Jamaica, Journal of the Geological Society of Jamaica, v. 28, p. 9-18.

Schmidt, W., 1987. Stratigraphy, depositional environment of the Lucea Inlier, western Jamaica. Journal of the Geological Society of Jamaica, 24, 15-35.

Scott, W.F., 1967. Geology of the Green Island Quadrangle. Unpublished report, Mines and Geology Division, Kingston.

Slatt, R.M., 2006, Stratigraphic reservoir characterization for petroleum geologists, geophysicists, and engineers, Elsevier Publ. Co. 492p.

Slatt, R.M., 2009, Petroleum Geology of Deepwater Depositional Systems, lecture notes.

Sohl, N.F., 1976. Cretaceous geology of the Jamaican inliers. Unpublished report, Mines and Geology Division, Kingston.

Tissot, B. & Welte, D.H., 1978. Petroleum formation and occurrence. Springer-Verlag, New York.

Wadge, G., Draper, G. and Robinson, E., 1983. Gravity anomalies in the Blue Mountains, Eastern Jamaica. Trans. 9th. Caribb. Geol. Conf. Dominican Repub., 1980, 467-474.

Walker, R.G., 1978, Deep-water sandstone facies and ancient submarine fans: Models for exploration for stratigraphic traps: AAPG Bulletin, v. 62, p. 932–966.

Ward, T.P., 2009, 3-D Basin Analysis of the Cenozoic Wagwater Trough, Jamaica. M.S. Thesis, OU.

Wescott, W.A., and Ethridge, F.G., 1983, Eocene fan delta-submarine fan deposition in the Wagwater Trough, east-central Jamaica: Sedimentology, v. 30, p. 235-247.

## APPENDICES

Appendix A – Field Stops.....135
Appendix B – Virtual Wells.....146
Appendix C – Porosity Quantification.....152

**APPENDIX A**

## FIELD STOPS

**Format:**

I. Location of Stations on the outcrop

II. Lithologic and Outcrop description superposed on Outcrop photo on each station

**STOP 1**

I.

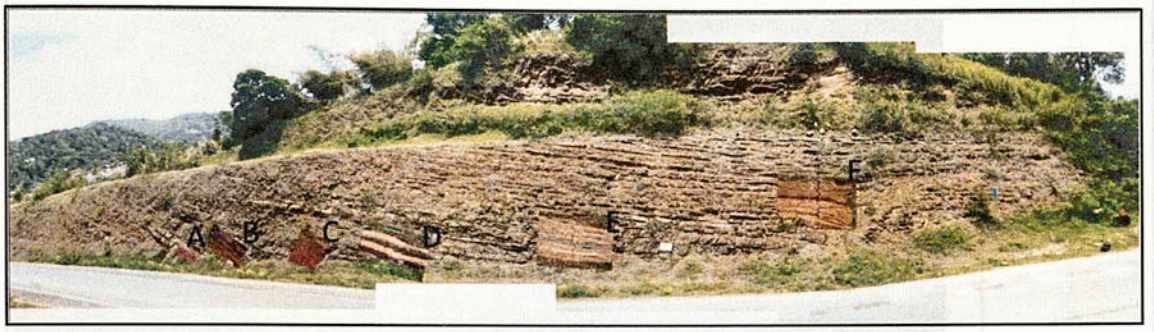


II.

Station A

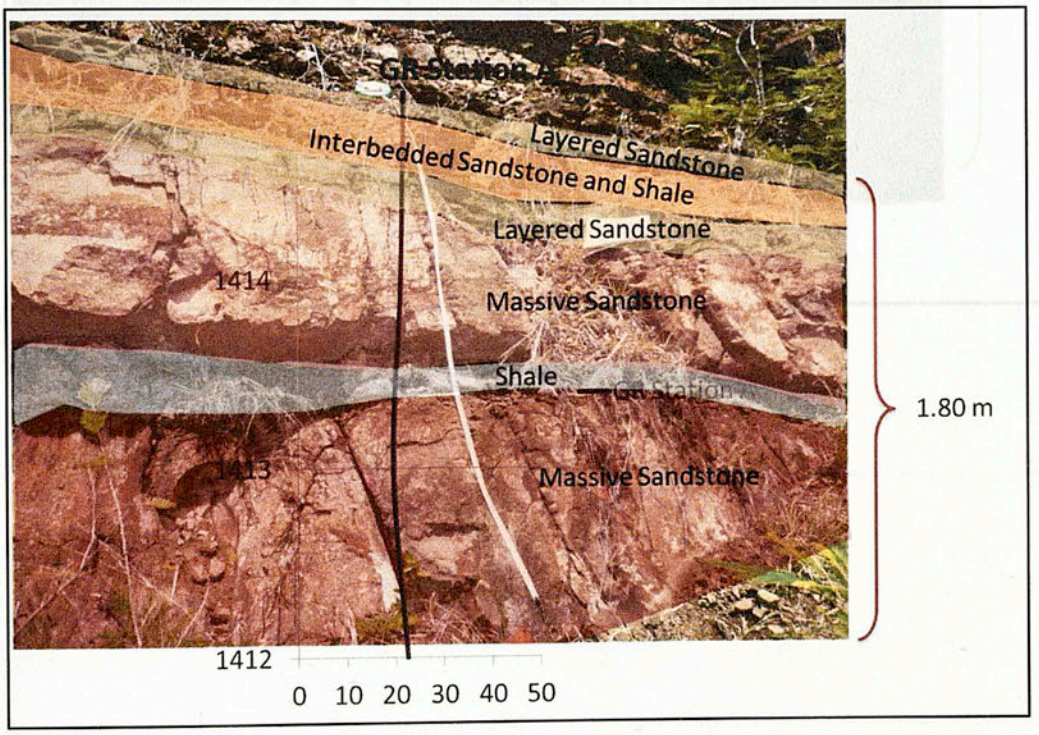

Station B

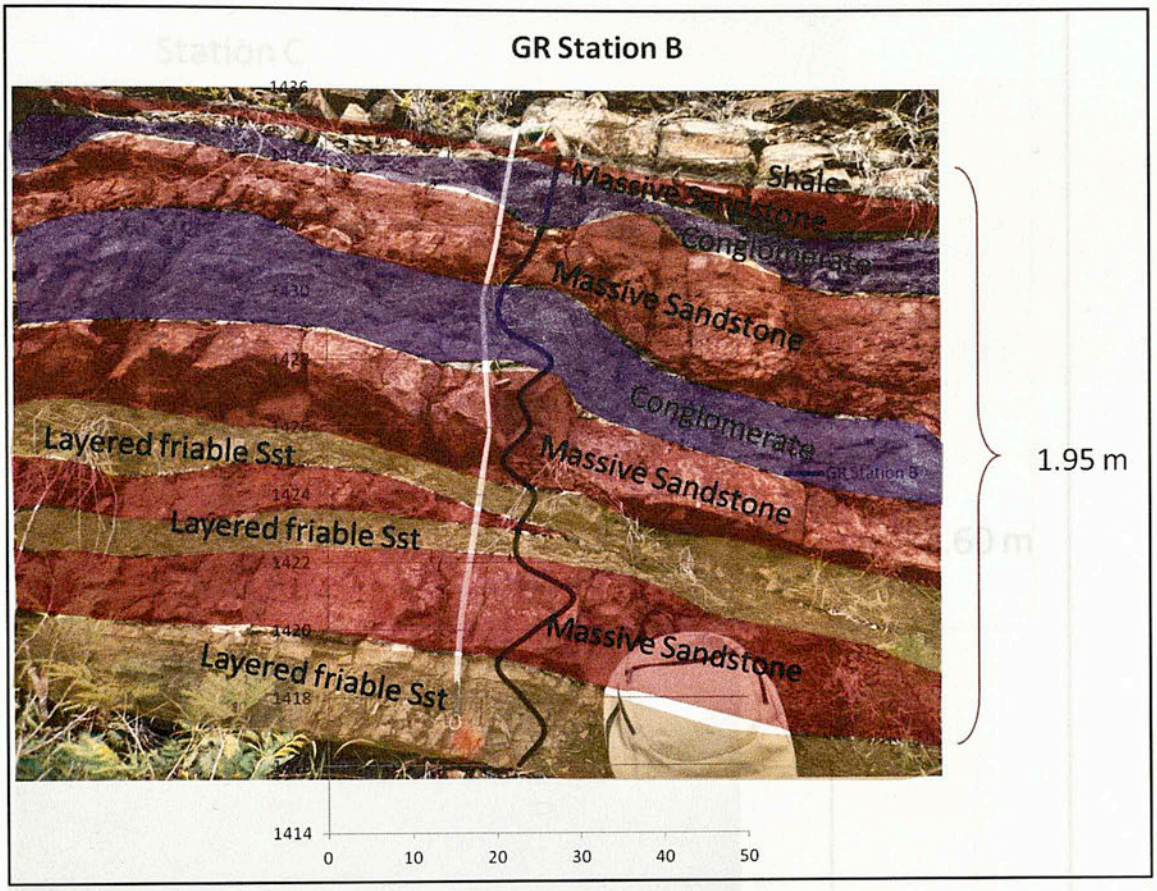
GR Station B
Shale
Massive Sandstone
Conglomerate
Massive Sandstone
Conglomerate
Massive Sandstone
Massive Sandstone
Layered friable Sst
Layered friable Sst
Layered friable Sst
1.95 m
1436
1434
1432
1430
1428
1426
1424
1422
1420
1418
1414
0
10
20
30
40
50

Station C

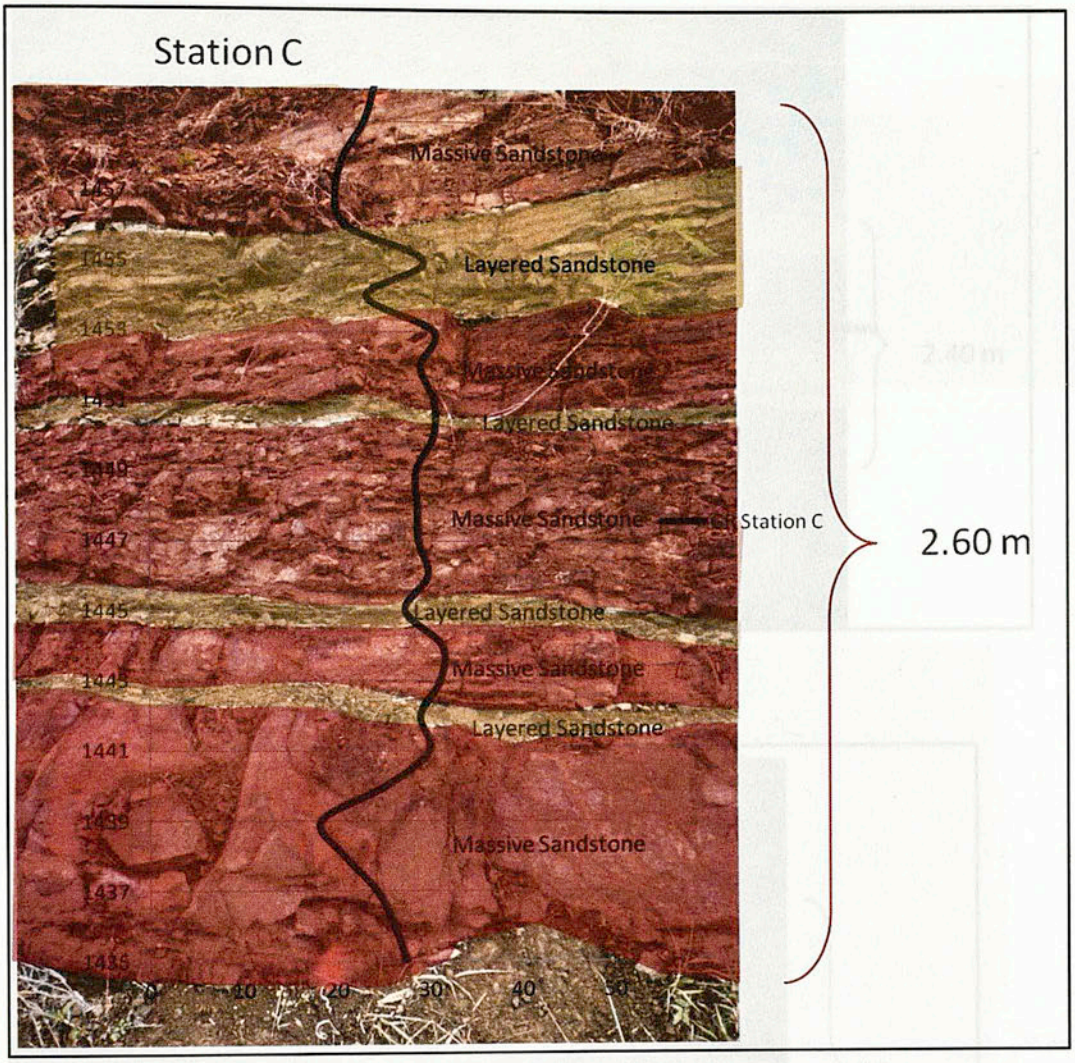
Station C
Massive Sandstone
Layered Sandstone
Massive Sandstone
Layered Sandstone
Massive Sandstone
Station C
Layered Sandstone
Massive Sandstone
Layered Sandstone
Massive Sandstone
1457
1455
1453
1451
1449
1447
1445
1443
1441
1439
1437
1435
0
10
20
30
40
50
2.60 m

Station D

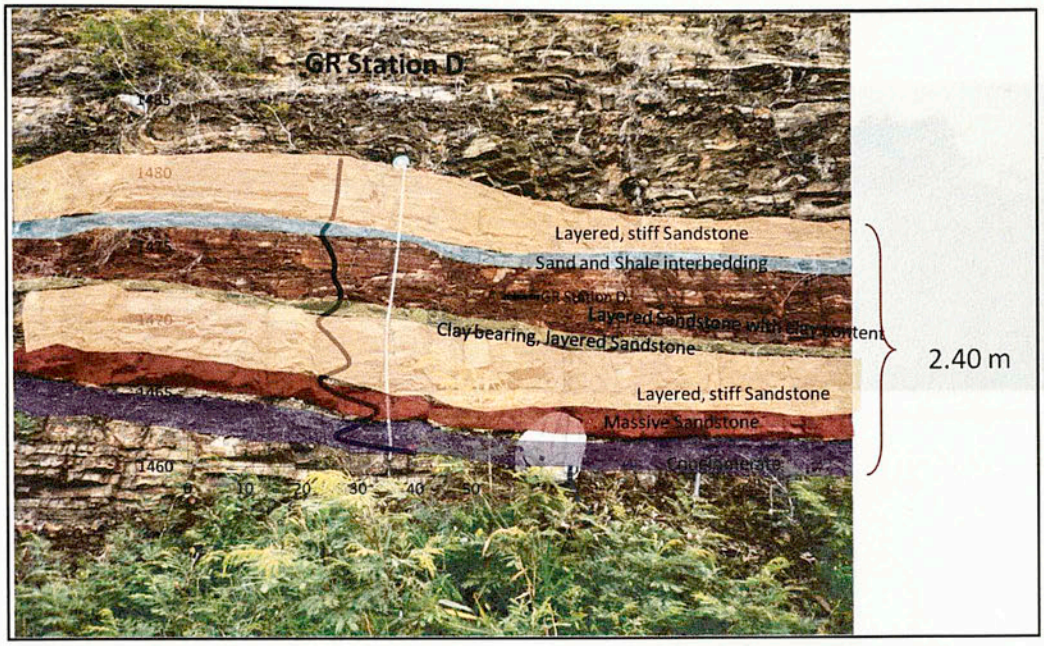


Station E

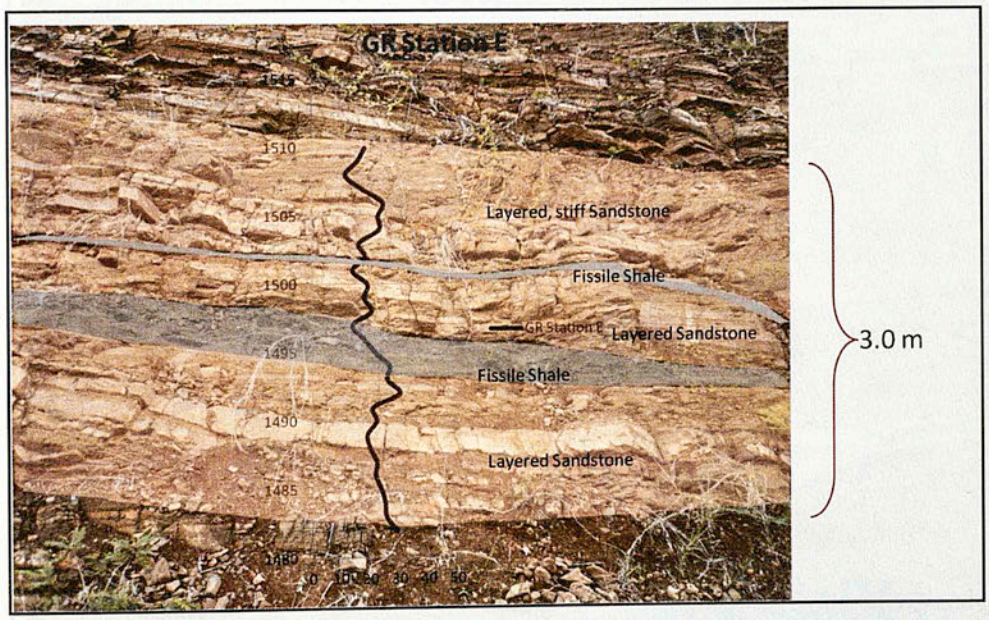

## STOP 2

**I.**


A
LAU-1

**II.**

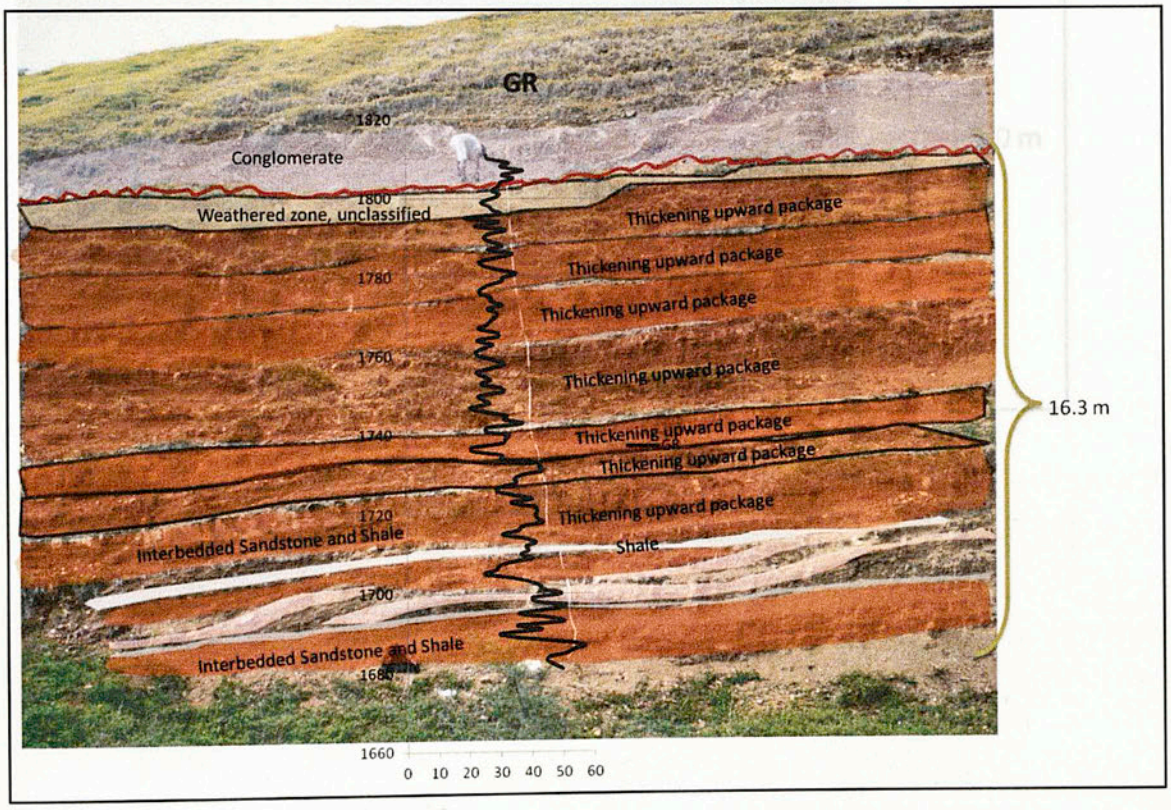
GR
1820
Conglomerate
1800
Weathered zone, unclassified
1780
1760
1740
1720
Interbedded Sandstone and Shale
1700
Interbedded Sandstone and Shale
1680
1660
0 10 20 30 40 50 60
Thickening upward package
Thickening upward package
Thickening upward package
Thickening upward package
Thickening upward package
Thickening upward package
Shale
16.3 m

**STOP 3**

**I.**




**II.**

**Station A**

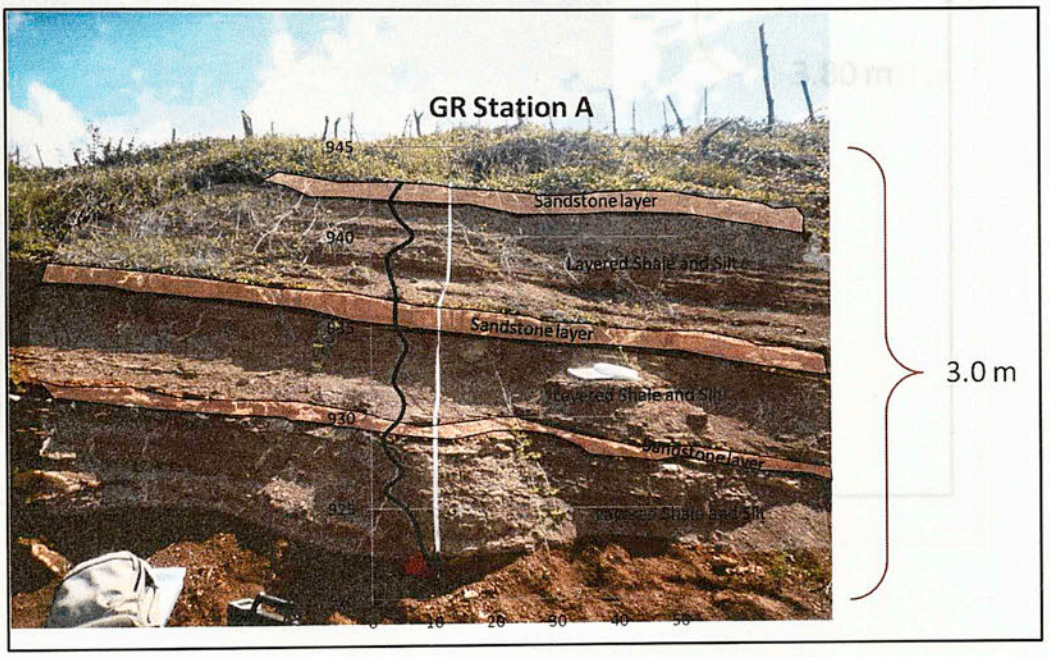

**Station B**

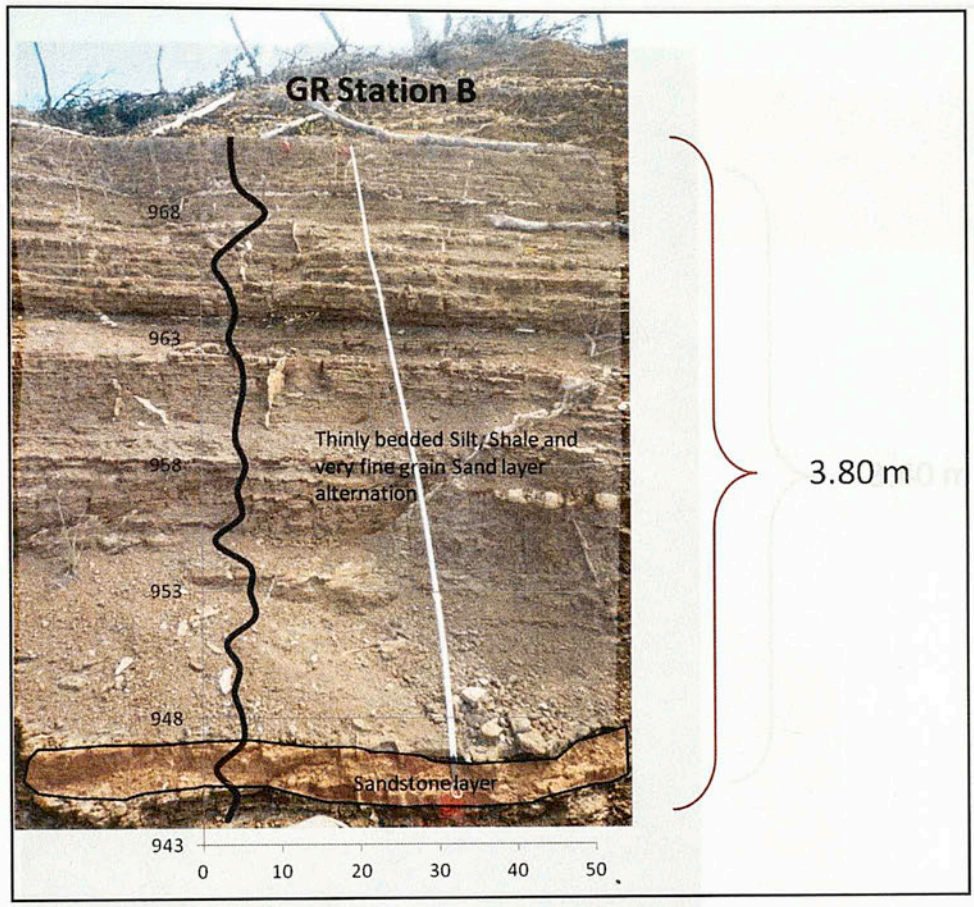
GR Station B
968
963
958
953
948
943
0
10
20
30
40
50
Thinly bedded Silt/Shale and very fine grain Sand layer alternation
Sandstone layer
3.80 m

**Station C**

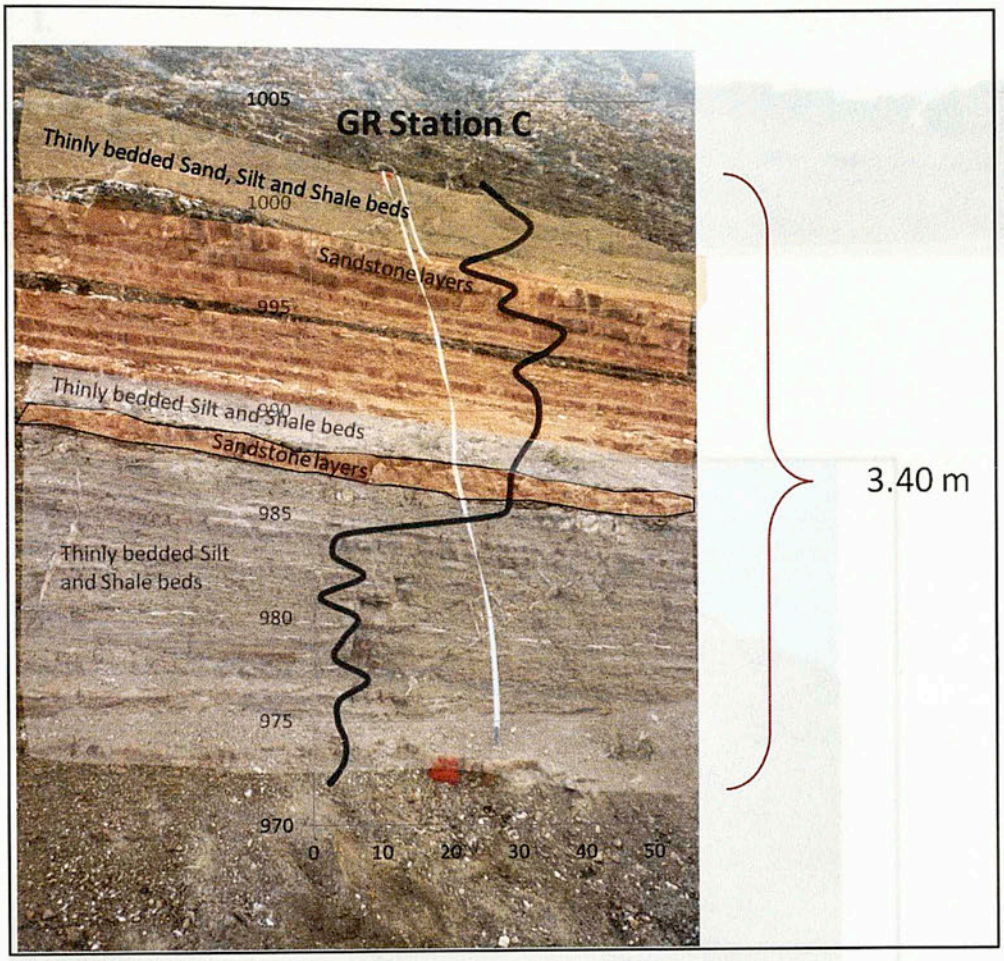
GR Station C
1005
1000
995
990
985
980
975
970
0
10
20
30
40
50
Thinly bedded Sand, Silt and Shale beds
Sandstone layers
Thinly bedded Silt and Shale beds
Sandstone layers
Thinly bedded Silt and Shale beds
3.40 m

**STOP 4**

**I.**




**II.**

**Station A**

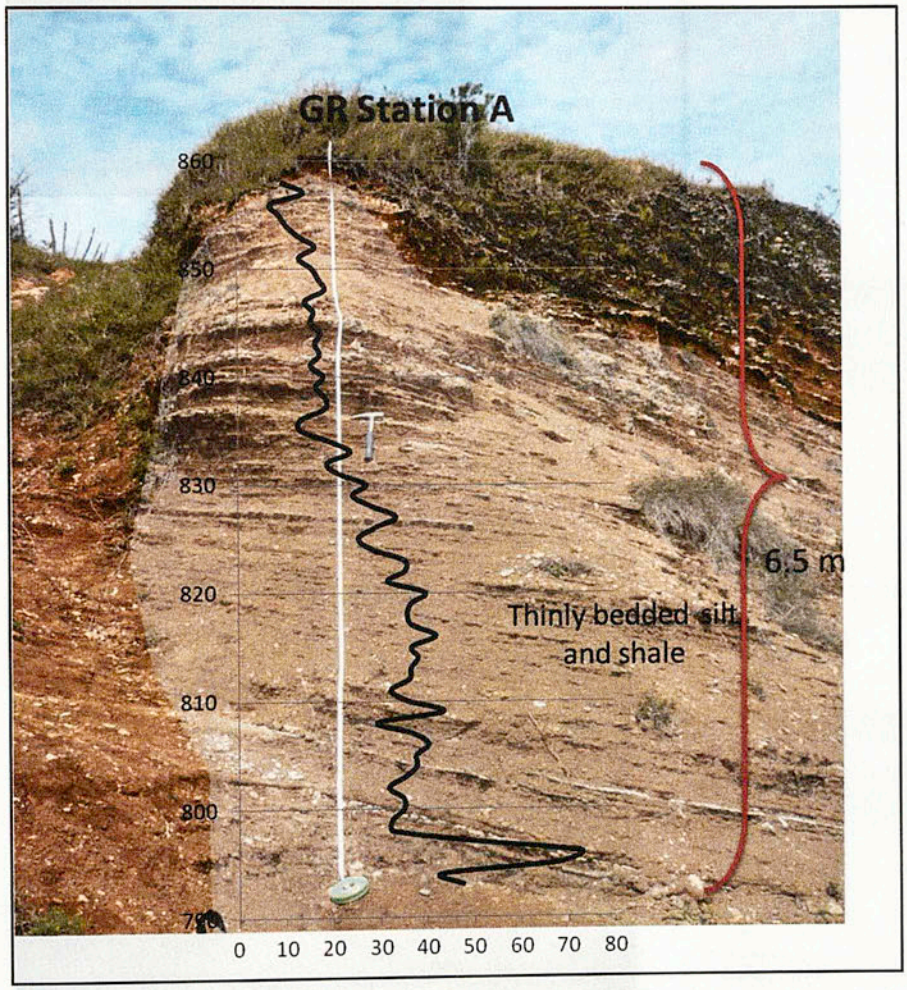

**Station B**

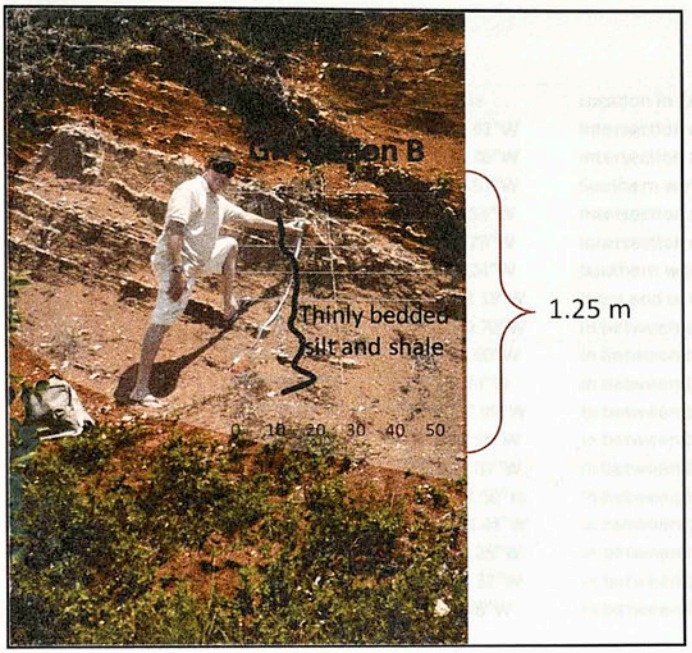


**Station C**

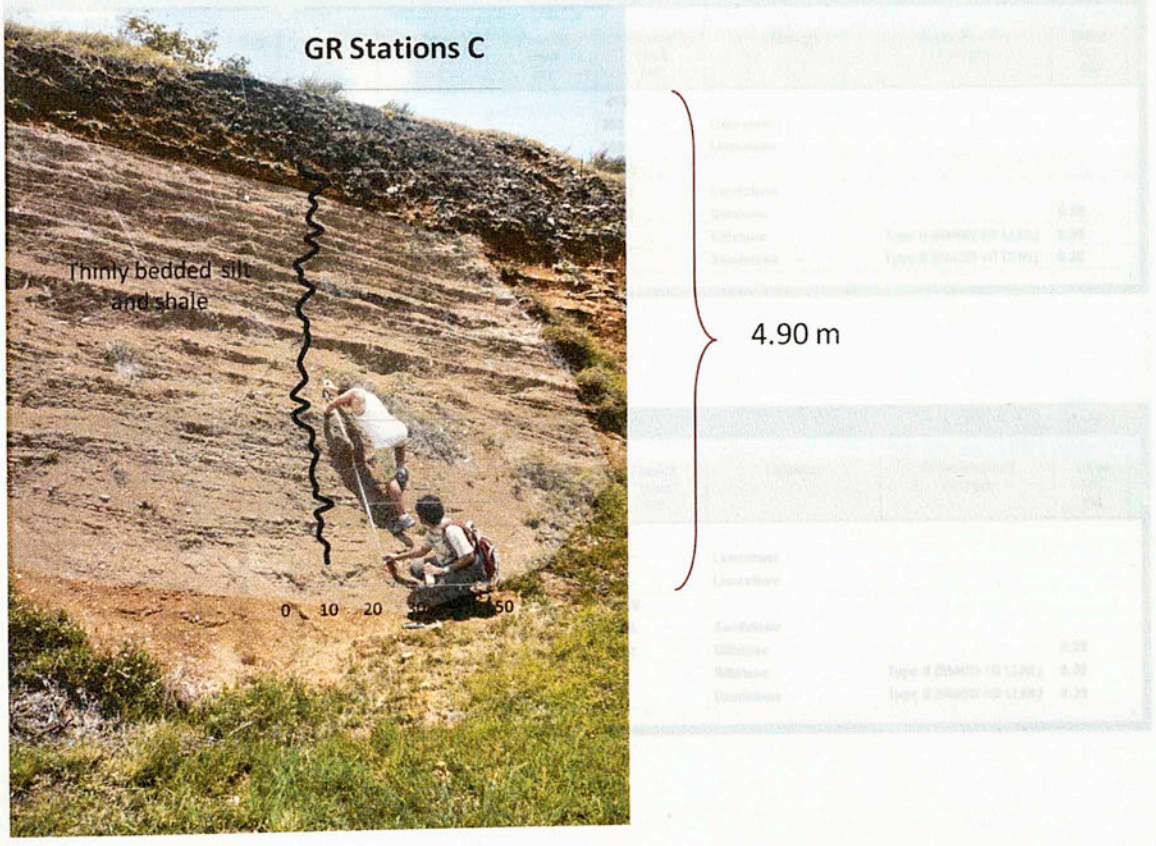

# APPENDIX B

## VIRTUAL WELLS

| Virtual Well Name | Lattitude | Longitude | Location in Cross-sections | Approx. Elevation in meters |
|---|---|---|---|---|
| A1 & E6(A*E) | 18°26'10.65"N | 78° 6'23.41"W | Intersection of A`-A and E`-E | 150 |
| A2 & D5( A*D) | 18°25'34.70"N | 78° 6'24.36"W | Intersection of A`-A and D`-D | 100 |
| A3 | 18°24'39.53"N | 78° 6'25.57"W | Southern well on A`-A line | 400 |
| B1 & D1(B*D) | 18°25'36.00"N | 78°13'9.53"W | Intersection of B`-B and D`-D | 125 |
| B2 & C2 (B*C) | 18°24'40.96"N | 78°13'9.23"W | Intersection of B`-B and C`-C | 200 |
| B3 | 18°23'35.65"N | 78°13'8.24"W | Southern well on B`-B line | 200 |
| C1 | 18°24'41.46"N | 78°14'32.18"W | West end of C`-C line | 80 |
| C3 | 18°24'40.51"N | 78°12'40.70"W | in between b and a lines on c-line | 200 |
| C4 | 18°24'37.32"N | 78° 8'11.60"W | in between b and a lines on c-line | 200 |
| C5 | 18°24'36.97"N | 78° 7'5.74"W | in between b and a lines on c-line | 200 |
| D2 | 18°25'35.02"N | 78°11'27.99"W | in between b and a lines on d-line | 120 |
| D3 | 18°25'35.01"N | 78° 9'12.95"W | in between b and a lines on d-line | 100 |
| D4 | 18°25'34.80"N | 78° 8'22.81"W | in between b and a lines on d-line | 90 |
| E1 | 18°26'16.15"N | 78°12'13.50"W | in between b and a lines on e-line | 150 |
| E2 | 18°26'15.04"N | 78°10'28.44"W | in between b and a lines on e-line | 50 |
| E3 | 18°26'14.70"N | 78° 9'53.25"W | in between b and a lines on e-line | 20 |
| E4 | 18°26'13.39"N | 78° 8'46.32"W | in between b and a lines on e-line | 100 |
| E5 | 18°26'12.30"N | 78° 7'6.76"W | in between b and a lines on e-line | 70 |

## A1

Stratigraphy

File Edit Help

| Formation or Event Name | Type | Begin Age (my) | Top Depth (m) | Present Thick (m) | Eroded Thick (m) | Lithology | Organofacies / Kerogen | Initial TOC (%) |
|---|---|---|---|---|---|---|---|---|
| Post Miocene-Eocene Upl | E | 12 | | | -450 | | | |
| White Lst | D | 44 | | | 300 | Limestone | | |
| Chapelton Formation | D | 48 | | | 150 | Limestone | | |
| Paleocene-Eocene Uplift | E | 65 | | | -3300 | | | |
| Green Island Fm Hiatus | D | 73 | | | 1100 | Sandstone | | |
| Campanian Hanover | D | 80.7 | | | 2200 | Siltstone | | 0.39 |
| Campanian H | F | 81 | 0 | 1 | | Siltstone | Type II (BMOD-1D LLNL) | 0.39 |
| Santonian Hanover | F | 85.3 | 1 | 2567 | | Sandstone | Type II (BMOD-1D LLNL) | 0.39 |

## A2

Stratigraphy

File Edit Help

| Formation or Event Name | Type | Begin Age (my) | Top Depth (m) | Present Thick (m) | Eroded Thick (m) | Lithology | Organofacies / Kerogen | Initial TOC (%) |
|---|---|---|---|---|---|---|---|---|
| Post Miocene-Eocene Upl | E | 12 | | | -450 | | | |
| White Lst | D | 44 | | | 300 | Limestone | | |
| Chapelton Formation | D | 48 | | | 150 | Limestone | | |
| Paleocene-Eocene Uplift | E | 65 | | | -3300 | | | |
| Green Island Fm Hiatus | D | 73 | | | 2198 | Sandstone | | |
| Campanian Hanover | D | 80.7 | | | 1102 | Siltstone | | 0.39 |
| Campanian H | F | 81 | 0 | 1 | | Siltstone | Type II (BMOD-1D LLNL) | 0.39 |
| Santonian Hanover | F | 85.3 | 1 | 1286 | | Sandstone | Type II (BMOD-1D LLNL) | 0.39 |

## A3

Stratigraphy

File Edit Help

| | Formation or Event Name | Type | Begin Age (my) | Top Depth (m) | Present Thick (m) | Eroded Thick (m) | Lithology | Organofacies / Kerogen | Initial TOC (%) |
|---|---|---|---|---|---|---|---|---|---|
| | Post Miocene-Eocene Upli | E | 12 | | | -450 | | | |
| | White Lst | D | 44 | | | 300 | Limestone | | |
| | Chapelton Formation | D | 48 | | | 150 | Limestone | | |
| | Paleocene-Eocene Uplift | E | 65 | | | -3300 | | | |
| | Green Island Fm Hiatus | D | 73 | | | 2779 | Sandstone | | |
| | Campanian Hanover | D | 80.7 | | | 521 | Siltstone | | 0.39 |
| | Campanian H | F | 81 | 0 | 1 | | Siltstone | Type I (BMOD-1D LLNL) | 0.39 |
| | Santonian Hanover | F | 85.3 | 1 | 608 | | Sandstone | Type II (BMOD-1D LLNL) | 0.39 |

## B1

Stratigraphy

File Edit Help

| | Formation or Event Name | Type | Begin Age (my) | Top Depth (m) | Present Thick (m) | Eroded Thick (m) | Lithology | Organofacies / Kerogen | Initial TOC (%) |
|---|---|---|---|---|---|---|---|---|---|
| | Post Miocene-Eocene Upli | E | 12 | | | -451 | | | |
| | White Lst | D | 44 | | | 300 | Limestone | | |
| | Chapelton Formation | D | 48 | | | 150 | Limestone | | |
| | Paleocene-Eocene Uplift | E | 65 | | | -3300 | | | |
| | Green Island Fm Hiatus | D | 73 | | | 3300 | Sandstone | | |
| | Campanian Hanover | D | 80.7 | | | 1 | Siltstone | | 0.39 |
| | Campanian H | F | 81 | 0 | 1060 | | Siltstone | Type II (BMOD-1D LLNL) | 0.39 |
| | Santonian Hanover | F | 85.3 | 1060 | 1067 | | Sandstone | Type II (BMOD-1D LLNL) | 0.39 |

## B2

Stratigraphy

File Edit Help

| | Formation or Event Name | Type | Begin Age (my) | Top Depth (m) | Present Thick (m) | Eroded Thick (m) | Lithology | Organofacies / Kerogen | Initial TOC (%) |
|---|---|---|---|---|---|---|---|---|---|
| | Post Miocene-Eocene Upli | E | 12 | | | -451 | | | |
| | White Lst | D | 44 | | | 300 | Limestone | | |
| | Chapelton Formation | D | 48 | | | 150 | Limestone | | |
| | Paleocene-Eocene Uplift | E | 65 | | | -3300 | | | |
| | Green Island Fm Hiatus | D | 73 | | | 3300 | Sandstone | | |
| | Campanian Hanover | D | 80.7 | | | 1 | Siltstone | | 0.39 |
| | Campanian H | F | 81 | 0 | 620 | | Siltstone | Type II (BMOD-1D LLNL) | 0.39 |
| | Santonian Hanover | F | 85.3 | 620 | 623 | | Sandstone | Type II (BMOD-1D LLNL) | 0.39 |

## B3

Stratigraphy

File Edit Help

| | Formation or Event Name | Type | Top Depth (m) | Present Thick (m) | Eroded Thick (m) | Lithology | Organofacies / Kerogen | Initial TOC (%) | Initial HI (mg/gTOC) | Sc |
|---|---|---|---|---|---|---|---|---|---|---|
| | Post Miocene-Eocene Upli | E | | | -451 | | | | | |
| | White Lst | D | | | 300 | Limestone | | | | |
| | Chapelton Formation | D | | | 150 | Limestone | | | | |
| | Paleocene-Eocene Uplift | E | | | -3300 | | | | | |
| | Green Island Fm Hiatus | D | | | 3300 | Sandstone | | | | |
| | Campanian Hanover | D | | | 1 | Siltstone | | 0.39 | | |
| | Campanian H | F | 0 | 1650 | | Siltstone | Type II (BMOD-1D LLNL) | 0.39 | | |
| | Santonian Hanover | F | 1650 | 1648 | | Sandstone | Type II (BMOD-1D LLNL) | 0.39 | | |

## C1

Stratigraphy

File Edit Help

| | Formation or Event Name | Type | Top Depth (m) | Present Thick (m) | Eroded Thick (m) | Lithology | Organofacies / Kerogen | Initial TOC (%) | Initial HI (mg/gTOC) | Sc |
|---|---|---|---|---|---|---|---|---|---|---|
| | Post Miocene-Eocene Upli | E | | | -451 | | | | | |
| | White Lst | D | | | 300 | Limestone | | | | |
| | Chapelton Formation | D | | | 150 | Limestone | | | | |
| | Paleocene-Eocene Uplift | E | | | -3300 | | | | | |
| | Green Island Fm Hiatus | D | | | 3300 | Sandstone | | | | |
| | Campanian Hanover | D | | | 1 | Siltstone | | 0.39 | | |
| | Campanian H | F | 0 | 1740 | | Siltstone | Type I (BMOD-1D LLNL) | 0.39 | | |
| | Santonian Hanover | F | 1740 | 1745 | | Sandstone | Type II (BMOD-1D LLNL) | 0.39 | | |

## C3

Stratigraphy

File Edit Help

| | Formation or Event Name | Type | Begin Age (my) | Top Depth (m) | Present Thick (m) | Eroded Thick (m) | Lithology | Organofacies / Kerogen | Initial TOC (%) |
|---|---|---|---|---|---|---|---|---|---|
| | Post Miocene-Eocene Upli | E | 12 | | | -451 | | | |
| | White Lst | D | 44 | | | 300 | Limestone | | |
| | Chapelton Formation | D | 48 | | | 150 | Limestone | | |
| | Paleocene-Eocene Uplift | E | 65 | | | -3300 | | | |
| | Green Island Fm Hiatus | D | 73 | | | 3300 | Sandstone | | |
| | Campanian Hanover | D | 80.7 | | | 1 | Siltstone | | 0.39 |
| | Campanian H | F | 81 | 0 | 986 | | Siltstone | Type II (BMOD-1D LLNL) | 0.39 |
| | Santonian Hanover | F | 85.3 | 986 | 986 | | Sandstone | Type II (BMOD-1D LLNL) | 0.39 |

## C4

Stratigraphy

File Edit Help

| | Formation or Event Name | Type | Begin Age (my) | Top Depth (m) | Present Thick (m) | Eroded Thick (m) | Lithology | Organofacies / Kerogen | Initial TOC (%) |
|---|---|---|---|---|---|---|---|---|---|
| | Post Miocene-Eocene Upli | E | 12 | | | -451 | | | |
| | White Lst | D | 44 | | | 300 | Limestone | | |
| | Chapelton Formation | D | 48 | | | 150 | Limestone | | |
| | Paleocene-Eocene Uplift | E | 65 | | | -3300 | | | |
| | Green Island Fm Hiatus | D | 73 | | | 3300 | Sandstone | | |
| | Campanian Hanover | D | 80.7 | | | 1 | Siltstone | | 0.39 |
| | Campanian H | F | 81 | 0 | 420 | | Siltstone | Type II (BMOD-1D LLNL) | 0.39 |
| | Santonian Hanover | F | 85.3 | 420 | 430 | | Sandstone | Type II (BMOD-1D LLNL) | 0.39 |

## C5

Stratigraphy

File Edit Help

| | Formation or Event Name | Type | Begin Age (my) | Top Depth (m) | Present Thick (m) | Eroded Thick (m) | Lithology | Organofacies / Kerogen | Initial TOC (%) |
|---|---|---|---|---|---|---|---|---|---|
| | Post Miocene-Eocene Upli | E | 12 | | | -650 | | | |
| | White Lst | D | 44 | | | 300 | Limestone | | |
| | Chapelton Formation | D | 48 | | | 150 | Limestone | | |
| | Paleocene-Eocene Uplift | E | 65 | | | -3300 | | | |
| | Green Island Fm Hiatus | D | 73 | | | 3100 | Sandstone | | |
| | Campanian Hanover | D | 80.7 | | | 200 | Siltstone | | 0.39 |
| | Campanian H | F | 81 | 0 | 1 | | Siltstone | Type II (BMOD-1D LLNL) | 0.39 |
| | Santonian Hanover | F | 85.3 | 1 | 1922 | | Sandstone | Type II (BMOD-1D LLNL) | 0.39 |

## D2

Stratigraphy

File Edit Help

| | Formation or Event Name | Type | Begin Age (my) | Top Depth (m) | Present Thick (m) | Eroded Thick (m) | Lithology | Organofacies / Kerogen | Initial TOC (%) |
|---|---|---|---|---|---|---|---|---|---|
| | Post Miocene-Eocene Upli | E | 12 | | | -651 | | | |
| | White Lst | D | 44 | | | 300 | Limestone | | |
| | Chapelton Formation | D | 48 | | | 150 | Limestone | | |
| | Paleocene-Eocene Uplift | E | 65 | | | -3300 | | | |
| | Green Island Fm Hiatus | D | 73 | | | 3300 | Sandstone | | |
| | Campanian Hanover | D | 80.7 | | | 200 | Siltstone | | 0.39 |
| | Campanian H | F | 81 | 0 | 765 | | Siltstone | Type II (BMOD-1D LLNL) | 0.39 |
| | Santonian Hanover | F | 85.3 | 765 | 773 | | Sandstone | Type II (BMOD-1D LLNL) | 0.39 |

## D3

Stratigraphy

File Edit Help

| | Formation or Event Name | Type | Begin Age (my) | Top Depth (m) | Present Thick (m) | Eroded Thick (m) | Lithology | Organofacies / Kerogen | Initial TOC (%) |
|---|---|---|---|---|---|---|---|---|---|
| | Post Miocene-Eocene Upli | E | 12 | | | -450 | | | |
| | White Lst | D | 44 | | | 300 | Limestone | | |
| | Chapelton Formation | D | 48 | | | 150 | Limestone | | |
| | Paleocene-Eocene Uplift | E | 65 | | | -3300 | | | |
| | Green Island Fm Hiatus | D | 73 | | | 2200 | Sandstone | | |
| | Campanian Hanover | D | 80.7 | | | 1100 | Siltstone | | 0.39 |
| | Campanian H | F | 81 | 0 | 1 | | Siltstone | Type II (BMOD-1D LLNL) | 0.39 |
| | Santonian Hanover | F | 85.3 | 1 | 1285 | | Sandstone | Type II (BMOD-1D LLNL) | 0.39 |

## E1

Stratigraphy

File Edit Help

| | Formation or Event Name | Type | Begin Age (my) | Top Depth (m) | Present Thick (m) | Eroded Thick (m) | Lithology | Organofacies / Kerogen | Initial TOC (%) |
|---|---|---|---|---|---|---|---|---|---|
| | Post Miocene-Eocene Upli | E | 12 | | | -450 | | | |
| | White Lst | D | 44 | | | 300 | Limestone | | |
| | Chapelton Formation | D | 48 | | | 150 | Limestone | | |
| | Paleocene-Eocene Uplift | E | 65 | | | -3300 | | | |
| | Green Island Fm Hiatus | D | 73 | | | 2300 | Sandstone | | |
| | Campanian Hanover | D | 80.7 | | | 1000 | Siltstone | | 0.39 |
| | Campanian H | F | 81 | 0 | 1 | | Siltstone | Type II (BMOD-1D LLNL) | 0.39 |
| | Santonian Hanover | F | 85.3 | 1 | 1088 | | Sandstone | Type II (BMOD-1D LLNL) | 0.39 |

## E2

Stratigraphy

File Edit Help

| | Formation or Event Name | Type | Begin Age (my) | Top Depth (m) | Present Thick (m) | Eroded Thick (m) | Lithology | Organofacies / Kerogen | Initial TOC (%) |
|---|---|---|---|---|---|---|---|---|---|
| | Post Miocene-Eocene Upli | E | 12 | | | -951 | | | |
| | White Lst | D | 44 | | | 300 | Limestone | | |
| | Chapelton Formation | D | 48 | | | 150 | Limestone | | |
| | Paleocene-Eocene Uplift | E | 65 | | | -3300 | | | |
| | Green Island Fm Hiatus | D | 73 | | | 3300 | Sandstone | | |
| | Campanian Hanover | D | 80.7 | | | 500 | Siltstone | | 0.39 |
| | Campanian H | F | 81 | 0 | 1 | | Siltstone | Type II (BMOD-1D LLNL) | 0.39 |
| | Santonian Hanover | F | 85.3 | 1 | 501 | | Sandstone | Type II (BMOD-1D LLNL) | 0.39 |

## E3

Stratigraphy

File Edit Help

| | Formation or Event Name | Type | Begin Age (my) | Top Depth (m) | Present Thick (m) | Eroded Thick (m) | Lithology | Organofacies / Kerogen | Initial TOC [%] |
|---|---|---|---|---|---|---|---|---|---|
| | Post Miocene-Eocene Upli | E | 12 | | | -451 | | | |
| | White Lst | D | 44 | | | 300 | Limestone | | |
| | Chapelton Formation | D | 48 | | | 150 | Limestone | | |
| | Paleocene-Eocene Uplift | E | 65 | | | -3300 | | | |
| | Green Island Fm Hiatus | D | 73 | | | 3300 | Sandstone | | |
| | Campanian Hanover | D | 80.7 | | | 1 | Siltstone | | 0.39 |
| | Campanian H | F | 81 | 0 | 260 | | Siltstone | Type II (BMOD-1D LLNL) | 0.39 |
| | Santonian Hanover | F | 85.3 | 260 | 522 | | Sandstone | Type II (BMOD-1D LLNL) | 0.39 |

## E4

Stratigraphy

File Edit Help

| | Formation or Event Name | Type | Begin Age (my) | Top Depth (m) | Present Thick (m) | Eroded Thick (m) | Lithology | Organofacies / Kerogen | Initial TOC [%] |
|---|---|---|---|---|---|---|---|---|---|
| | Post Miocene-Eocene Upli | E | 12 | | | -651 | | | |
| | White Lst | D | 44 | | | 300 | Limestone | | |
| | Chapelton Formation | D | 48 | | | 150 | Limestone | | |
| | Paleocene-Eocene Uplift | E | 65 | | | -3300 | | | |
| | Green Island Fm Hiatus | D | 73 | | | 3300 | Sandstone | | |
| | Campanian Hanover | D | 80.7 | | | 200 | Siltstone | | 0.39 |
| | Campanian H | F | 81 | 0 | 204 | | Siltstone | Type II (BMOD-1D LLNL) | 0.39 |
| | Santonian Hanover | F | 85.3 | 204 | 409 | | Sandstone | Type II (BMOD-1D LLNL) | 0.39 |

## E5

Stratigraphy

File Edit Help

| | Formation or Event Name | Type | Top Depth (m) | Present Thick (m) | Eroded Thick (m) | Lithology | Organofacies / Kerogen | Initial TOC [%] | Initial HI (mg/gTOC) | Sc |
|---|---|---|---|---|---|---|---|---|---|---|
| | Post Miocene-Eocene Upli | E | | | -450 | | | | | |
| | White Lst | D | | | 300 | Limestone | | | | |
| | Chapelton Formation | D | | | 150 | Limestone | | | | |
| | Paleocene-Eocene Uplift | E | | | -3300 | | | | | |
| | Green Island Fm Hiatus | D | | | 3170 | Sandstone | | | | |
| | Campanian Hanover | D | | | 130 | Siltstone | | 0.39 | | |
| | Campanian H | F | 0 | 130 | | Siltstone | Type II (BMOD-1D LLNL) | 0.39 | | |
| | Santonian Hanover | F | 130 | 270 | | Sandstone | Type II (BMOD-1D LLNL) | 0.39 | | |

## APPENDIX C

## POROSITY QUANTIFICATION

Image 1: Calcite filled porosity calculated as 9.67 %

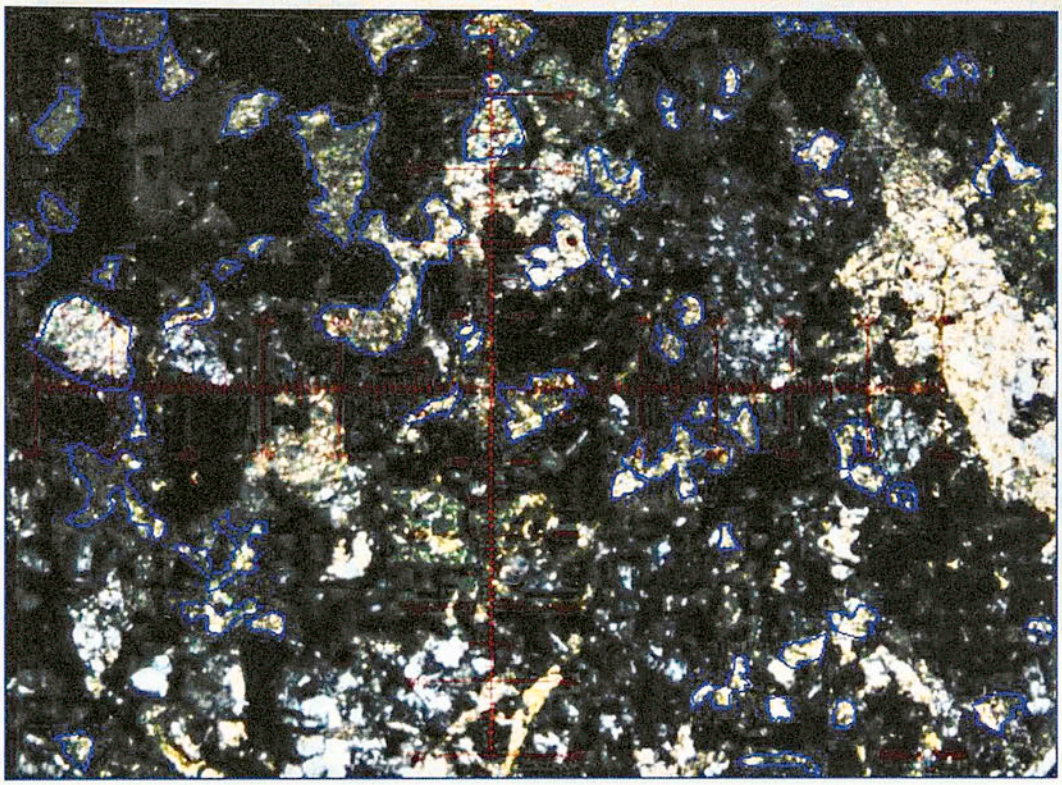

Image 2: Calcite filled porosity calculated as 14.03 %

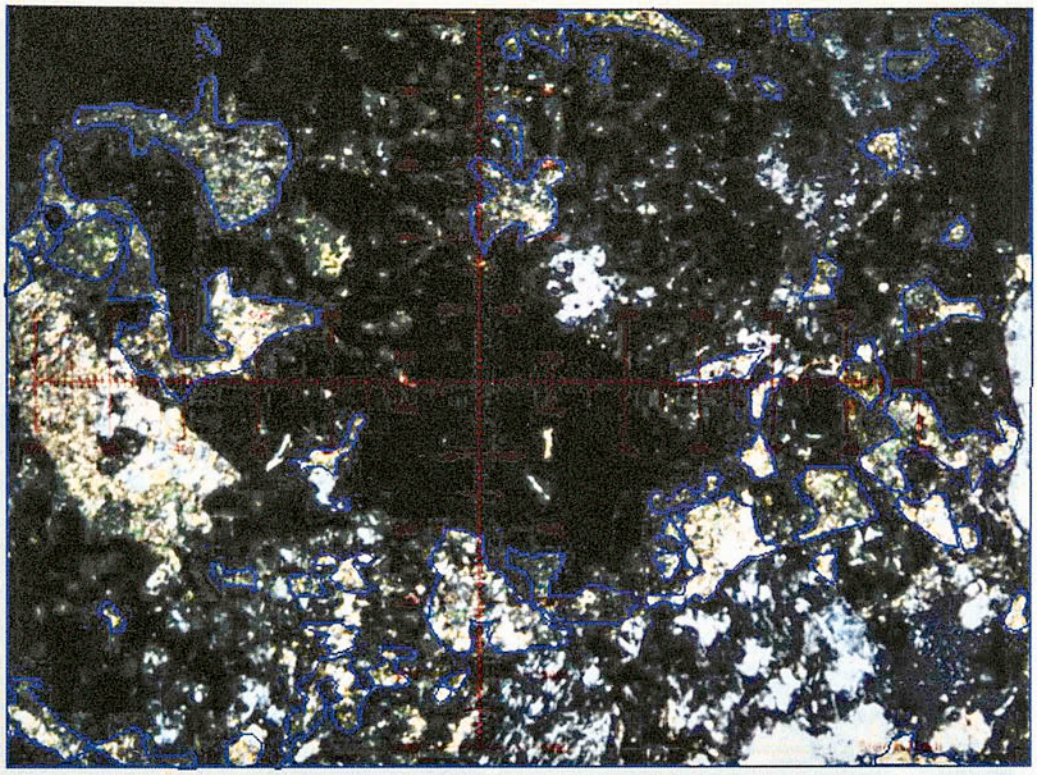

Image 3: Calcite filled porosity calculated as 8.58 %

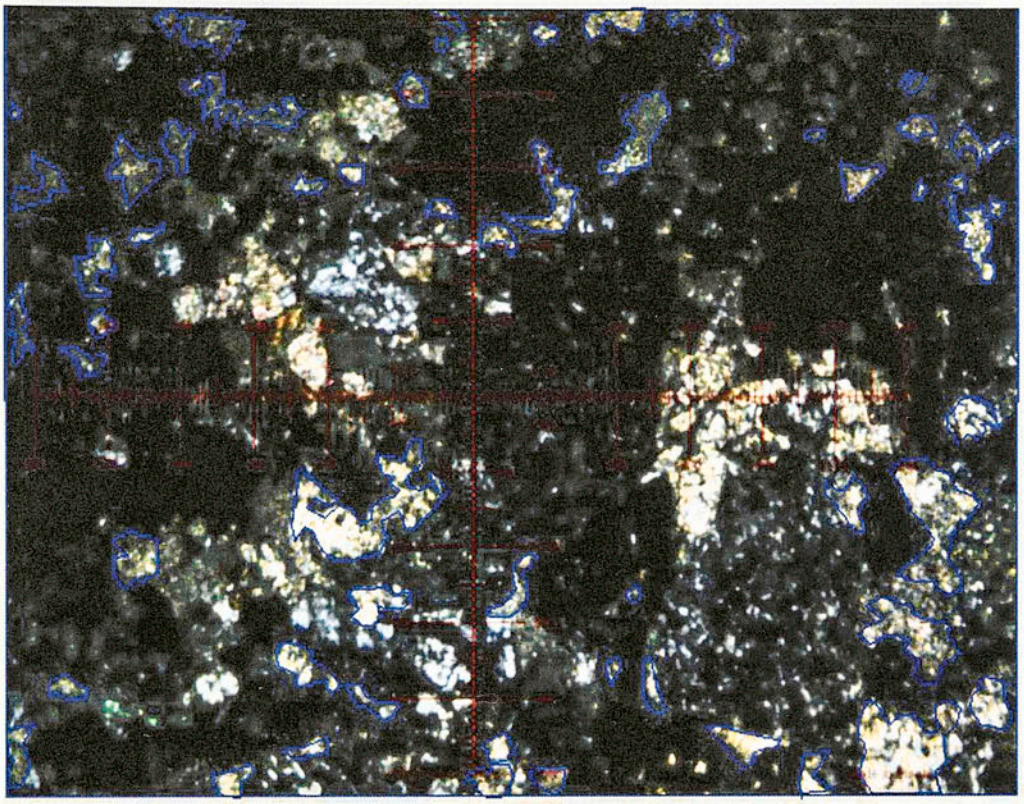

Image 4: Calcite filled porosity calculated as 7.65 %

